Resummation of Next-to-Leading Non-Global Logarithms

Inaugural dissertation
at the Faculty of Science,
University of Bern

presented by

Nicolas François Schalch

from Schaffhausen SH

Supervisor of the doctoral thesis
Prof. Dr. Thomas Becher

Albert Einstein Center for Fundamental Physics
Institute for Theoretical Physics, University of Bern

Resummation of Next-to-Leading Non-Global Logarithms

Inaugural dissertation
at the Faculty of Science,
University of Bern

presented by

Nicolas François Schalch

from Schaffhausen SH

Supervisor of the doctoral thesis
Prof. Dr. Thomas Becher

Albert Einstein Center for Fundamental Physics
Institute for Theoretical Physics, University of Bern

Accepted by the Faculty of Science.

Bern, 02.09.2024

The Dean
Prof. Dr. Jean-Louis Reymond

Abstract

An intricate pattern of enhanced higher-order corrections known as non-global logarithms arises in cross sections with angular cuts. While the leading logarithmic terms have been calculated numerically more than two decades ago, the resummation of subleading non-global logarithms remained an open problem. In this monograph, we present a solution to this challenge using effective field theory techniques. Starting from a factorization theorem, we develop a dedicated parton shower framework in the Veneziano limit where the number of colors N_c becomes large, but the ratio of N_c to the number of fermion flavors n_F remains fixed. We solve the associated renormalization-group equations using our Monte-Carlo framework, thereby resumming the subleading non-global logarithms. Combined with matching corrections, we obtain, for the first time, the complete set of next-to-leading logarithmic corrections for a non-global observable at a hadron collider.

Declaration

This thesis is based on the following work to which the author contributed to directly

[1] T. Becher, N. Schalch and X. Xu, *Resummation of Next-to-Leading Non-Global Logarithms at the LHC*, *Phys. Rev. Lett.* **132**, no.8, 081602 (2024) [arXiv:2307.02283].

Hence, text may be directly copied without reference. The work presented in this thesis has been supported by the Albert Einstein Center for Fundamental Physics (AEC).

Contents

Chapter 1

Introduction

Particle physics seeks to describe and uncover the fundamental building blocks of nature and the complex interactions governing their behavior. The underlying theoretical framework is quantum field theory (QFT), which merges principles of quantum mechanics with special relativity. The Standard Model (SM) of particle physics [2–5] is a prime example of a QFT, successfully unifying electromagnetic, weak, and strong forces. These forces are mediated through the exchange of gauge bosons among elementary particles. Central to QFTs is the concept of symmetries, which are crucial in formulating gauge theories such as the SM. These symmetries dictate the interactions between elementary particles that are represented as fields interacting over space and time.

The foundation of the SM is the gauge group $SU(3)_C \times SU(2)_L \times U(1)_Y$, which is typically divided into two sectors. The symmetry group $SU(2)_L \times U(1)_Y$ describes the electroweak sector which is spontaneously broken down to $U(1)_{\text{em}}$ by the Higgs-Brout-Englert mechanism [6–11] at the electroweak scale (~ 100 GeV). This symmetry-breaking mechanism gives rise to all elementary particle masses within the SM. The strong sector carries an $SU(3)_C$ gauge symmetry and describes the strong nuclear interaction between the elementary constituents of hadrons, such as nucleons. This sector is known as Quantum Chromodynamics, or QCD for short. While the SM has been extraordinarily successful, there are many open questions in particle physics it cannot answer, such as the origin of the matter-antimatter asymmetry or the nature of dark matter. Moreover, the SM suffers from several theoretical pathologies, the most prominent examples being the hierarchy problem or the strong CP problem. In addition, several tensions between theoretical predictions and experimental results challenge the SM as well [12–14]. These issues all point towards the existence of a broader and more general theory, of which the SM is merely an effective low-energy description. As a consequence, the search for new physics beyond the SM is among the main endeavors of particle physics today. The prerequisite to identify new physics is a firm handle on the SM theoretical predictions. Due to its associated dynamics and uncertainties, the QCD sector is both particularly important and challenging, representing the main focus of this thesis.

Experimentally, high-energy colliders such as the Large Hadron Collider (LHC) at CERN have made significant contributions to the discoveries of fundamental particles, thus consolidating our understanding of the smallest building blocks of matter. These machines provide the necessary environment to probe predictions of the SM and pave the way to the potential observation of hitherto unknown particles and interactions. The growing volume of experimental data currently being collected at the LHC increases the demand for percent-level precision on QCD calculations. QFTs are typically not exactly solvable, but due to the phenomenon of asymptotic freedom [15,16], the strength of QCD interactions decreases with energy, and already at a few GeV (and certainly at energies reached at the LHC) the strong coupling $\alpha_s \sim 0.1$ is small, thus enabling perturbation

theory to serve as the essential tool for obtaining theoretical predictions. Specifically, sufficiently inclusive cross sections σ can be systematically expanded as a power series in α_s. By including more terms in the expansion, the precision of theoretical predictions is improved.

Despite the impressive ability of fixed-order calculations to describe processes involving a small number of partons, for numerous applications at the LHC, contributions beyond fixed perturbative order are necessary to reach the aforementioned percent-level accuracy. Many cross sections describing hard scattering processes associated with a scale Q, also have sensitivity to a soft scale Q_0. For large hierarchies between Q and Q_0, such cross sections develop large logarithms in the scale ratio $L = \ln(Q/Q_0)$. The logarithmic contributions arise in specific regions of the phase space and degrade the perturbative expansion. Consider the following example as an illustration. If a very energetic lepton pair is produced with an energy of $Q = 1$ TeV alongside soft radiation $Q_0 = 5$ GeV, then the product $\alpha_s L$ is $\mathcal{O}(1)$.

We conclude that large scale hierarchies induce logarithms which may overpower the suppression by the coupling α_s in the perturbative expansion. For $\alpha_s L \sim \mathcal{O}(1)$, we should account for the entire tower of $(\alpha_s L)^n$ for any n and assign these enhanced contributions to the leading contribution of the expansion in α_s. This reorganization of the perturbative expansion restores the suppression by the coupling. In general, to obtain reliable predictions these enhanced logarithmic contributions need to be captured to all orders, which is referred to as resummation.

Apart from soft logarithms L, another common source of logarithmic enhancement is related to collinear effects. For cross sections sensitive to both types of logarithmic sources, the leading contribution is a double-logarithm of the form $\left(\alpha_s L^2\right)^n$ whereas the leading logarithm scales as $(\alpha_s L)^n$ for observables involving only single logarithms. In general, most observables – more precisely, the ones satisfying recursive infrared and collinear safety [17] – have the property that their resummation is characterized by the following exponentiated structure [18]

$$\Sigma(v) = \int dv \, \frac{d\sigma}{dv} = \left(1 + \sum_n C_n \, \alpha_s^n\right) e^{L g_1(\alpha_s L) + g_2(\alpha_s L) + \alpha_s \, g_3(\alpha_s L) + \cdots} + D(v) \,, \tag{1.1}$$

where $v = e^{-L}$, C_n are constants, and $D(v)$ goes to zero as $v \to 0$. At the differential level $\frac{d\sigma}{dv}$ is studied. The knowledge of the function $L g_1(\alpha_s L)$ corresponds to the resummation of the leading logarithms (LL), while the next-to-leading-logarithmic (NLL) terms are resummed through $g_2(\alpha_s L)$ and next-to-next-to-leading logarithms (NNLL) with $\alpha_s g_3(\alpha_s L)$ respectively. In (1.1) a double-logarithmic behavior was assumed. The leading term $L g_1(\alpha_s L)$ vanishes for single logarithmic observables. In these cases, we use the notation LL to denote $(\alpha_s L)^n$, despite this being a potentially confusing notation. Similarly, terms proportional to next-to-single-logarithmic corrections are identified as next-to-leading logarithms NLL $\sim \alpha_s \, (\alpha_s L)^n$.

Starting from factorization theorems that disentangle the physics associated with different scales present in a given cross section, resummation can then be performed using different techniques. Over the past couple of decades, the methods and techniques behind resummed calculations have seen substantial development. The state-of-the-art evolved from NLL accuracy for a very restricted class of inclusive observables during the 90's to the automation of NNLL results for global event shapes [19–21]. Event shapes classify final states according to their geometric properties. Furthermore, for certain inclusive observables, impressive accuracy has been achieved [19–81]. Although analytical resummation is systematic and exact, its application is still limited to observables which can be understood very precisely in specific limits.

On the other hand, the observables currently studied at the LHC typically involve fiducial cuts. These experimental cuts are usually required to model aspects of the detector as closely as possible

or to distinguish between signal and background for tagging purposes. As a result, enhanced logarithmic contributions depending on the cut variable may arise, which need to be resumed, but the phase-space restrictions render analytic approaches unviable. In addition, an extensive class of observables involves final state jets of collimated particles. These jets are produced in high-energy collisions and are omnipresent in various measurements and searches. However, the presence of jets introduces additional complexities. The dense QCD environment within jets makes it challenging to model radiation accurately to resolve the underlying interactions, making the resummation of logarithmic contributions for jet observables particularly challenging to achieve analytically. Given the limitations of analytical resummation, the development of numerical techniques is of paramount importance to capture enhanced contributions that are currently out of reach.

A generic set of observables involving scale hierarchies are cross sections where hard radiation is vetoed in specific angular regions. Prime examples are exclusive jet cross sections which require a veto on additional hard jets. While ubiquitous, the all-order resummation of such observables is challenging since they involve a complicated pattern of enhanced higher-order corrections known as non-global logarithms (NGLs), which arise due to secondary emissions off hard partons [82–84]. In Chapter 2, we provide a detailed comparison between global and non-global observables in an attempt to demystify the source of the non-global nature. At LL $\sim (\alpha_s L)^n$ accuracy[1], resummed results both at large [82–84] and finite N_c [85–88] are available. Despite continued progress in the understanding of non-global observables over the past 20 years [89–116], a full resummation of NLL $\sim \alpha_s (\alpha_s L)^n$ corrections remained elusive.

In this thesis, we present a solution to that particular problem based on a factorization theorem [94, 95] obtained in Soft-Collinear Effective Theory (SCET) [117–122]. The factorization theorem splits the cross section into hard and soft functions, each depending on their natural scale and carrying a residual renormalization scale, μ, dependence. To resum the large logarithms, one utilizes the residual renormalization scale dependence to set up renormalization group (RG) equations. The solution of these RG equations evolves the hard functions from their natural scale $\mu \sim Q$ down to $\mu \sim Q_0$, thereby generating the large logarithms. Since the associated anomalous dimension governing the evolution is a matrix in the (infinite) space of particle multiplicities, we resort to Monte Carlo (MC) methods to solve the RG equations. A key ingredient for NLL resummation is the recently extracted two-loop anomalous dimension [123] that we implement into the parton shower framework Marzili (Monte-cArlo for the RenormaliZation group Improved calculation of non-global LogarIthms), which iteratively generates additional emissions during the RG evolution.

A complementary approach to resummation is followed in general-purpose parton showers which resum logarithms numerically. The most common general-purpose ones are Pythia [124], Sherpa [125] and Herwig [126]. Typically, collinear enhancements factorize exactly such that the associated logarithms are captured correctly. Soft enhancements, on the other hand, are usually not resummed accurately. While these general-purpose parton showers are very versatile tools and, at least in principle, applicable to a wide range of SM processes, their accuracy is generally limited to the leading double-logarithms in the large-N_c limit. As a result, the precision is relatively poor and usually insufficient for percent-level predictions needed in the precision era. In principle, most of the ingredients necessary to achieve subleading accuracy are already contained within these showers. Indeed, some power corrections and parts of the higher logarithmic terms are also included, but a systematic understanding of the shower accuracy beyond LL was missing. Recently, there has been renewed interest to systematically increase the accuracy of parton showers beyond LL [127–132], notably by the PanScales collaboration [111–115,133–146]. A set of tests [112] have been established

[1] We focus on soft NGLs which are single-logarithmic.

to demonstrate that a shower achieves subleading accuracy. However, the precise procedure to isolate a pure subleading contribution is numerically delicate. Among other things, our semi-numerical parton shower framework MARZILI provides results that can serve as a benchmark at higher logarithmic accuracy, offering valuable tests for general-purpose parton showers.

This thesis is structured in the following way. In Chapter 2, we introduce the necessary analytical tools, such as the factorization theorem for dijet cross sections from which we derive RG equations. Most importantly, we present the one- and two-loop anomalous dimensions which govern the evolution. Chapter 3 provides details about the implementation of the RG evolution in MARZILI. We compare numerically with PanScales [142] and GNOLE [147,148] to validate our implementation. We then present our results for the energy flow into a rapidity slice at NLL accuracy matched to fixed order. In Chapter 4, we apply our framework to a gap-between-jets observable at hadron colliders. Finally, we summarize the main findings of this work in Chapter 5 and indicate future directions.

Chapter 2

Methodology

The accurate description of jet cross sections is fundamental to the investigation of high-energy processes because they offer a direct window into the underlying hard-scattering processes, thus providing invaluable insights into fundamental particle interactions. In the pioneering work [149] Sterman and Weinberg introduced (di)jet cross sections in e^+e^- collisions. In order for a jet event to be valid, they imposed that all the energy must be confined within oppositely directed narrow cones with half-opening angle δ, with the exception of a small fraction $\beta/2$ of the center-of-mass energy Q. For small δ and β the corresponding cross section reads

$$\frac{\sigma(\beta,\delta)}{\sigma_0} = 1 + \frac{\alpha_s C_F}{4\pi}\left(-16\ln\delta\ln\beta - 12\ln\delta + c_0\right), \tag{2.1}$$

with σ_0 the leading-order cross section and $c_0 = 10 - 8\zeta_2$ a constant depending on the definition of the jet axis. From (2.1) it is obvious that the higher-order contributions, in this case the next-to-leading-order (NLO) corrections, suffer from large logarithms both in β and δ. In addition, it is a priori unclear to what value the scale μ present in $\alpha_s = \alpha_s(\mu)$ should be set, since $\mu = Q, Q\delta, Q\beta$ or even $\mu = Q\delta\beta$ seem inappropriate because the presence of these scales lead to large logarithms in at least one part of phase space. This twofold issue arises in any perturbative calculation involving multiple scales. The natural solution to both difficulties is to factorize the cross section into various objects, each capturing the physics of their associated scale. In other words, once factorization is achieved, one can evaluate each contribution at its appropriate scale, which solves the ambiguity of the scale setting, and use RG equations to resum the large logarithms to all orders.

Relatively recently, first factorization theorems [94, 95] achieving complete scale separation for jet processes have been obtained using SCET [117–122]. The seminal works [94, 95] have paved the way for the resummation of jet observables using effective field theory techniques and are especially well suited for higher-logarithmic resummations. One of the main challenges to achieve factorization is the non-global nature of jet cross sections. Indeed, as mentioned in Chapter 1, every cross section where hard radiation is restricted to a specific angular region of the phase space is by construction non-global. Obviously, this is also the case for the cross section in (2.1). Specifically, NGLs arise because only a small amount of radiation is allowed outside the jet cones, while no restriction is imposed on the radiation inside.

This chapter starts with a comparison between global and non-global observables. Section 2.2 motivates a factorization theorem for wide-angle jet cross sections involving NGLs. Subsequently, we will calculate all the ingredients up to NLO accuracy in Sections 2.3 and 2.4. We then show that all the divergences of the individual ingredients cancel in Section 2.5. Additionally, we will also demonstrate how to obtain (2.1) from the factorization theorem. In Section 2.6, we present the one-

and two-loop anomalous dimension matrices that govern the resummation up to NLL accuracy. These anomalous dimensions represent the main analytical ingredients for the evolution equations.

2.1 Global versus non-global observables

In this section, we give an overview of the differences between global and non-global observables. In simple cases, an observable which is sensitive to radiation anywhere in the phase space is referred to as global. The simplest observables beyond hadronically inclusive cross sections are event shapes. Famous examples include thrust, heavy jet mass or the C-parameter [150]. On the other hand, observables which are only sensitive to radiation in a restricted region of the phase space are non-global. Since exclusive jet cross sections only constrain soft radiation to be within a certain corner of phase space, NGLs are ubiquitous at the LHC. Therefore, an important task of theoretical work is to resum these specific logarithms to guarantee reliable predictions across large scale hierarchies.

To illustrate more precisely the difference between global and non-global observables, we focus on Figure 2.1. The left of Figure 2.1a shows the NLO corrections to the total cross section for dijet production in $e^+e^- \to \gamma^* \to X_{had}$ with a center-of-mass energy Q. The integral over the gluon momentum p_g indicates that for the total cross section we integrate inclusively over p_g. In this case, we do not obtain any large logarithms. The situation is different for event shapes such as the jet broadening b_T [151, 152] which measures the transverse momentum with respect to the thrust axis. The thrust axis $\vec{n}_T$ is given by the direction with maximum momentum flow. The eye and the looking glass on the right of Figure 2.1a indicate that the transverse momentum of the gluon w.r.t the thrust axis is studied. Three-particle events involving two almost back-to-back jets develop large logarithms $\ln \frac{Q}{b_T}$ because the transverse momentum of the recoiling gluon is very small. The variable b_T is global, meaning that the gluon is constrained independently of its direction.

The situation is very different for non-global observables, the canonical example being the interjet energy flow. Here, the hard radiation is restricted to be within the cones as depicted in Figure 2.1b. To be precise, we impose that the (transverse) energy of particles in the gap, i.e. the region outside of the cones, is below Q_0. It turns out that a twofold pattern of logarithms arises. According to (2.1), the cross section is both sensitive to logarithms w.r.t the opening angle of the jet-cones $\ln \delta$ as well as on $\ln \frac{Q}{Q_0}$. The main difference with the former situation on the right of Figure 2.1a is shown on the left of 2.1c. Hard radiation cannot enter the rapidity slice because it is constrained to be within the (jet-)cones, whereas in the global case, the emission was not constrained to be in any particular region of the phase space. In fact, the first non-global contribution arises at two loops from a secondary emission, as depicted on the right of Figure 2.1c. We elaborate further on the different sources of single logarithmic corrections in Figure 2.2. Primary emissions from the initial hard partons directly entering the gap lead to an incomplete cancellation between real and virtual corrections. As a consequence, we obtain a global contribution, see uppermost Figure in 2.2. These logarithms exponentiate at the level of the cross section. A second source of single logarithms is also present, see middle illustration in Figure 2.2. Here, the first emission is inside the cone and is considered to be hard. This primary hard emission further radiates into the veto region, leading to a logarithmically enhanced contribution $(\alpha_s L)^2$. Taking into account further soft emissions into the veto region, radiated from arbitrary ensembles of soft (but more energetic) gluons inside the jet cones, builds up an entire tower of single logarithms $(\alpha_s L)^n$. For the sake of simplicity, we refer to this type of emissions collectively as secondary emissions. We point out that this is merely a figure of speech since the final emission entering the veto region is coherently radiated from external ensembles which may consist of primary, secondary, tertiary, and higher-

order configurations. In general, we associate all contributions arising from secondary emissions with NGLs.

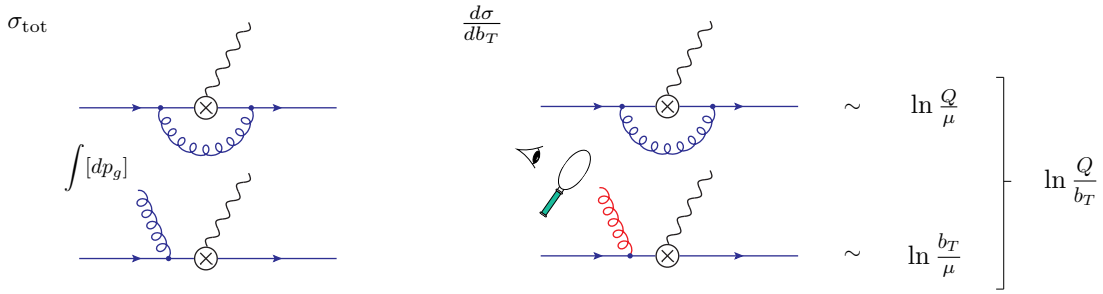

(a) Inclusive and differential cross sections in dijet production [153].

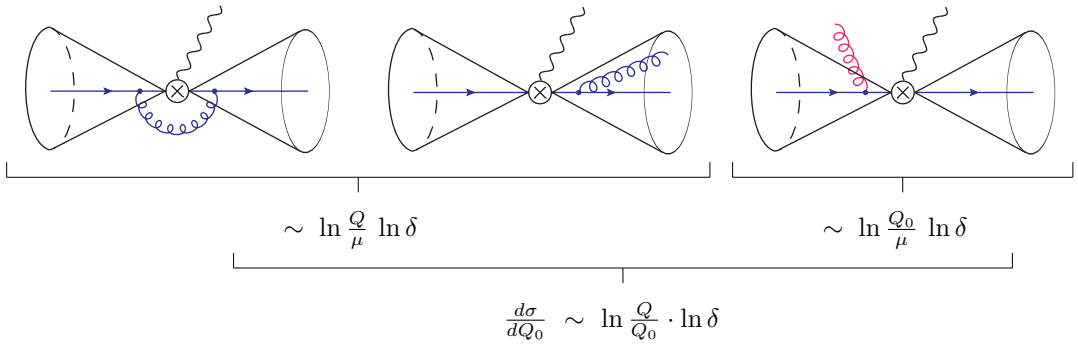

(b) Two-jet event with a veto region outside of the two cones.

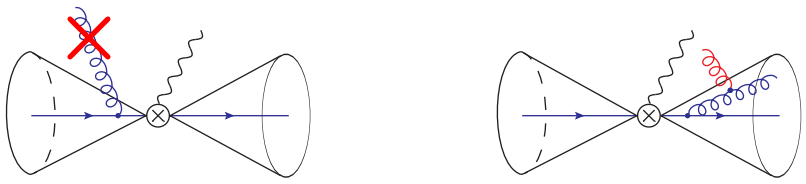

(c) Emissions into the veto region. The red cross indicates that the unconstrained emission on the left cannot enter the veto region, while a soft emission can.

Figure 2.1: Comparison of different observables in dijet production. Blue indicates unconstrained contributions while red illustrates soft corrections. The quantity δ is related to the opening angle of the cone.

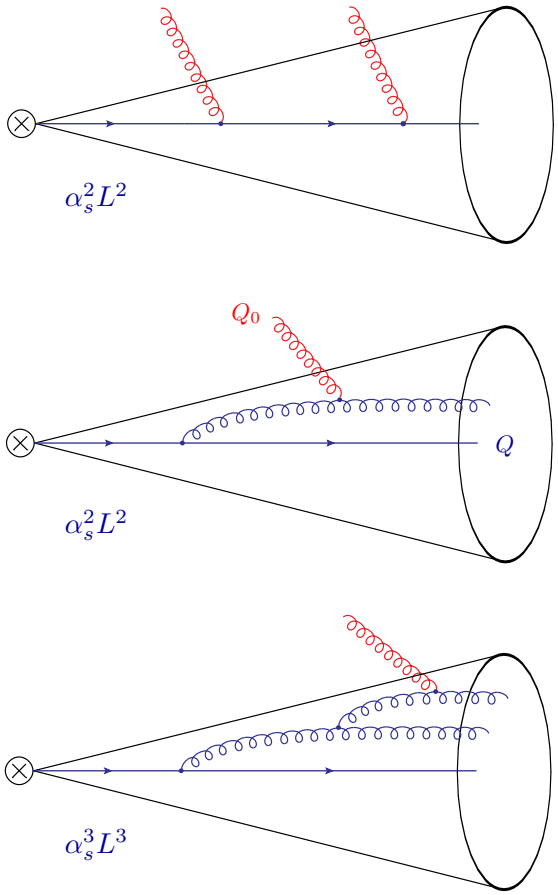

Figure 2.2: Different sources of single logarithms. Blue indicates hard contributions while red illustrates soft corrections. The uppermost picture represents a global logarithm while the two lower ones represent NGLs.

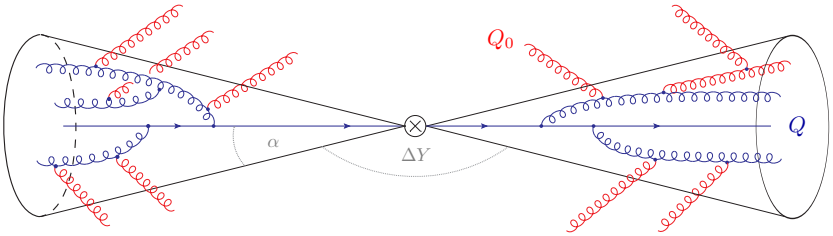

Figure 2.3: Representation of the factorization formula (2.11). The blue lines depict hard radiation associated with the energy scale Q, which is constrained inside the jet cones, while the red lines represent the soft radiation at lower energies Q_0. The soft radiation covers the entire phase space.

2.2 Factorization for jet production in e^+e^- annihilation

The basis for our resummation are factorization theorems for jet production in the presence of a veto on radiation in certain angular regions of the phase space. The simplest case is two-jet production in e^+e^- collisions, i.e. $e^+e^- \to 2\,\text{jets}$ at center-of-mass energy $\sqrt{s} = Q$, which we will focus on throughout this section. We use the jet axis as the thrust axis, which is defined as the unit-vector $\vec{n}$ in the direction of the maximum momentum flow. This is different from common clustering algorithms such as k_t [154, 155], anti-k_t [156] or Cambridge-Aachen [157, 158] which are typically used at hadron colliders to define jets. However, it turns out that the angular constraints, e.g. the gap in Figure 2.3, differ order-by-order. It has recently been shown how to take clustering into account in the factorization framework [159], but for simplicity, we restrict the discussion in this section to a fixed jet axis. We orient the two final-state jets along two light-like vectors $n^\mu = (1, \vec{n})$ and $\bar{n}^\mu = (1, -\vec{n})$ such that $n \cdot \bar{n} = 2$ and $n^2 = \bar{n}^2 = 0$. Using these vectors, we can decompose any four-momentum p^μ into a component proportional to n, another component proportional to $\bar{n}$, and two residual components perpendicular to both

$$p^\mu = \bar{n} \cdot p \, \frac{n^\mu}{2} + n \cdot p \, \frac{\bar{n}^\mu}{2} + p_\perp^\mu \,. \tag{2.2}$$

The cone jets have an opening angle α, and a particle (or radiation) is considered inside the jet if and only if the absolute value of its rapidity Y lies within

$$|Y| \geq \frac{1}{2} \log\left(\frac{1+\cos\alpha}{1-\cos\alpha}\right), \tag{2.3}$$

as depicted in Figure 2.3. We also introduce the abbreviation $\delta = \tan\left(\frac{\alpha}{2}\right)$ which is related to the opening angle α. The cross section is defined by imposing a veto on the energy E_{out} of the particles inside the gap. In other words, we require that the total energy emitted outside of the jet cones is below Q_0. The full dijet cross section including m hard and l soft partons with momenta $\{\underline{\hat{p}}\} \equiv \{p_1, p_2, \ldots, p_m, \ldots, p_{m+l}\}$ can then be written in $d = 4 - 2\epsilon$ as

$$\begin{aligned}\sigma(Q, Q_0) = \frac{1}{2Q^2} \sum_{m=2}^{\infty} \prod_{i=1}^{m+l} \int \frac{d^{d-1}p_i}{(2\pi)^{d-1} 2E_i} \, \langle \mathcal{M}_m^{\text{full}}(\{\underline{\hat{p}}\}) | \mathcal{M}_m^{\text{full}}(\{\underline{\hat{p}}\}) \rangle \\ \times (2\pi)^d \, \delta(Q - \hat{E}_{\text{tot}}) \, \delta^{(d-1)}(\vec{\hat{p}}_{\,\text{tot}}) \, \Theta_{\text{in}}\big(\{\underline{p}\}\big) \, \theta(Q_0 - E_{\text{out}}) \,,\end{aligned} \tag{2.4}$$

where $|\mathcal{M}_m^{\text{full}}(\{\underline{\hat{p}}\})\rangle$ is the full QCD matrix element, $\hat{E}_{\text{tot}} = \sum_{i=1}^{m+l} E_i$ is the total energy and $\vec{\hat{p}}_{\,\text{tot}} = \sum_{i=1}^{m+l} \vec{p}_i$ is the total momentum. The m hard particles must lie inside the jet cones, as imposed by $\Theta_{\text{in}}\big(\{\underline{p}\}\big)$. The list $\{\underline{p}\} \equiv \{p_1, p_2, \ldots, p_m\}$ refers to the hard particles only while $\{\underline{\hat{p}}\}$

collects all particles present. At this point, we may already anticipate that by performing the phase-space integral in (2.4) using the full theory, the result will depend on logarithms of the ratio between the different energy scales $L = \log(Q/Q_0)$ which yield enhanced contributions for disparate scales.

To separate the different scales that contribute to this problem, we investigate which momentum regions contribute. It turns out that for wide-angle jets with $\delta \sim 1$, exactly two momentum regions are relevant, with respective scaling $(n \cdot p, \bar{n} \cdot p, p_\perp)$

$$\begin{aligned} \text{hard:} \quad & p_h \sim Q\,(1,1,1)\,, \\ \text{soft:} \quad & p_s \sim Q_0\,(1,1,1)\,. \end{aligned} \tag{2.5}$$

The hard region describes the highly energetic particles that must be inside the jet cones, whereas soft partons can populate the entire phase space, i.e. they may be inside or outside of the jet cones. Since there is no collinear momentum region for sizable cones, this observable is single-logarithmic. In the following, we will carefully analyze the hard and soft contributions to (2.4) in order to render each of them explicit to eventually obtain the relevant factorization formula. Each hard particle may emit soft radiation, which we describe through a Wilson line $\boldsymbol{S}_i(n_i)$ along the corresponding direction $n_i = \frac{p_i^\mu}{E_i}$

$$\boldsymbol{S}_i(n_i) = \mathbf{P} \exp\left(i g_s \int_0^\infty ds\, n_i \cdot A_s^a(s n_i)\, \boldsymbol{T}_i^a \right), \tag{2.6}$$

where $\boldsymbol{T}_i^a$ is a matrix in the color-space formalism [160, 161] and $\mathbf{P}$ is a path ordering operator, ensuring that fields at different spacetime points are correctly ordered. Dressing each hard particle with such a Wilson line operator, we can make the soft factorization at the amplitude level manifest

$$|\mathcal{M}_m^{\text{full}}(\{\hat{p}\})\rangle = \boldsymbol{S}_1(n_1)\, \boldsymbol{S}_2(n_2)\, \ldots\, \boldsymbol{S}_m(n_m)\, |\mathcal{M}_m(\{\underline{p}\})\rangle + \mathcal{O}(\text{NLP}). \tag{2.7}$$

The $\mathcal{O}(\text{NLP})$ indicates that this factorization holds up to power corrections in $\frac{Q_0}{Q}$. To derive equation (2.7) from the effective field theory, one would match onto SCET. This means that it is necessary to introduce a collinear field along each hard direction. It turns out that for our case, there are exactly two operators which can be related to the usual quark and gluon field [162]. Upon performing the decoupling transformation [163] we obtain (2.7).

To isolate the pure soft contribution of an arbitrary number of soft partons to the jet cross section, we define the soft function $\boldsymbol{\mathcal{S}}_m$ as the vacuum matrix element squared of these soft Wilson lines

$$\boldsymbol{\mathcal{S}}_m(\{\underline{n}\}, Q_0) = \sum\!\!\!\!\!\!\int_{X_s} \langle 0|\, \boldsymbol{S}_1^\dagger(n_1)\, \ldots\, \boldsymbol{S}_m^\dagger(n_m)\, |X_s\rangle\langle X_s|\, \boldsymbol{S}_1(n_1)\, \ldots\, \boldsymbol{S}_m(n_m)\, |0\rangle\, \theta(Q_0 - E_{\text{out}}), \tag{2.8}$$

where the constraint is imposed on the total energy E_{out} in the veto region outside the jets. This means that the soft function depends on the cone size δ since it is sensitive to the outside energy. Using equation (2.8) we can disentangle the soft from the hard contributions in (2.4) and make them explicit by writing

$$\begin{aligned} \sigma(Q, Q_0) = \frac{1}{2Q^2} \sum_{m=2}^{\infty} \prod_{i=1}^{m} \int \frac{d^{d-1}p_i}{(2\pi)^{d-1} 2E_i}\, \langle \mathcal{M}_m(\{\underline{p}\})|\, \boldsymbol{\mathcal{S}}_m(\{\underline{n}\})\, |\mathcal{M}_m(\{\underline{p}\})\rangle \\ \times (2\pi)^d\, \delta(Q - E_{\text{tot}})\, \delta^{(d-1)}(\vec{p}_{\text{tot}})\, \Theta_{\text{in}}\big(\{\underline{p}\}\big) + \mathcal{O}(\text{NLP}), \end{aligned} \tag{2.9}$$

here the list of momenta $\{\underline{p}\} = \{p_1, p_2, \ldots, p_m\}$ specifies the hard partons which are restricted inside the jet cones. The symbol $\vec{p}_{\text{tot}} = \sum_{i=1}^m p_i$ is the total momentum of the hard final state

particles and the total momentum $\vec{p}_{\,\rm tot}$ does not involve any soft radiation because its contribution is power suppressed and can be expanded away. The integration is over the m-dimensional phase space of the hard partons which we treat as massless. To make the factorization of the cross section (2.9) evident, we introduce hard functions $\boldsymbol{\mathcal{H}}_m$ which describe m hard partons inside the jet cones. To obtain $\boldsymbol{\mathcal{H}}_m$, one integrates standard QCD amplitudes squared over the energies of the m hard partons while keeping their directions $\{\underline{n}\} = \{n_1, \dots, n_m\}$ fixed. The bare hard functions are defined as

$$\boldsymbol{\mathcal{H}}_m(\{\underline{n}\}, Q) = \frac{1}{2Q^2} \prod_{i=1}^{m} \int \frac{dE_i\, E_i^{d-3}}{\tilde{c}^\epsilon\, (2\pi)^2}\, |\mathcal{M}_m(\{\underline{p}\})\rangle\langle\mathcal{M}_m(\{\underline{p}\})| \\ \times (2\pi)^d\, \delta\Big(Q - \sum_{i=1}^{m} E_i\Big)\, \delta^{(d-1)}(\vec{p}_{\,\rm tot})\, \Theta_{\rm in}(\{\underline{n}\})\,. \tag{2.10}$$

The constraint $\Theta_{\rm in}\,(\{\underline{n}\})$ prevents the hard radiation from entering the veto region, i.e., it forces the hard partons to be inside the jet region. The constant $\tilde{c} = e^{\gamma_E}/\pi$ was introduced in [123]. These hard functions can be seen as matching coefficients to the soft operators from an effective field theory perspective. Using the definitions of hard and soft functions, we directly obtain the factorization theorem

$$\sigma(Q, Q_0) = \sum_{m=2}^{\infty} \big\langle \boldsymbol{\mathcal{H}}_m(\{\underline{n}\}, Q, \mu) \otimes \boldsymbol{\mathcal{S}}_m(\{\underline{n}\}, Q_0, \mu) \big\rangle\,, \tag{2.11}$$

valid at leading power in Q_0/Q expansion, μ is the renormalization scale. Both hard and soft functions are matrices in the color space [164] of the m partons, such that it is necessary to take the color trace, as indicated by $\langle \cdots \rangle$. The trace is normalized in such a way that $\langle \boldsymbol{\mathcal{H}}_2^{(0)} \otimes \mathbf{1} \rangle = \mathbf{1}$. Eventually, in order to obtain the cross section, we integrate over all directions $\{\underline{n}\}$ which is indicated by the symbol $\otimes$

$$\boldsymbol{\mathcal{H}}_m(\{\underline{n}\}, Q, \mu) \otimes \boldsymbol{\mathcal{S}}_m(\{\underline{n}\}, Q_0, \mu) = \prod_{i=2}^{m} \int \frac{d\Omega(n_i)}{4\pi}\, \boldsymbol{\mathcal{H}}_m(\{\underline{n}\}, Q, \mu)\, \boldsymbol{\mathcal{S}}_m(\{\underline{n}\}, Q_0, \mu)\,. \tag{2.12}$$

We would like to point out that our problem does not involve any collinear scale because $\delta \sim 1$, and we consider massless particles. In practice, we do not have access to the hard and soft functions to all orders. As usual, we make a perturbative expansion in α_s, e.g. up to NLO, the following matching corrections are necessary

$$\boldsymbol{\mathcal{H}}_2 = \sigma_0 \left(\boldsymbol{\mathcal{H}}_2^{(0)} + \frac{\alpha_s}{4\pi} \boldsymbol{\mathcal{H}}_2^{(1)} + \cdots \right), \tag{2.13}$$

$$\boldsymbol{\mathcal{H}}_3 = \sigma_0 \left(\frac{\alpha_s}{4\pi} \boldsymbol{\mathcal{H}}_3^{(1)} + \cdots \right), \tag{2.14}$$

$$\boldsymbol{\mathcal{S}}_m = \mathbf{1} + \frac{\alpha_s}{4\pi} \boldsymbol{\mathcal{S}}_m^{(1)} + \cdots, \tag{2.15}$$

where σ_0 is the leading-order cross section. The superscript (n) indicates the order of the correction in α_s, while the subscript i denotes the amount of hard final state particles. For instance, $\boldsymbol{\mathcal{H}}_2^{(1)}$ is the virtual contribution and $\boldsymbol{\mathcal{H}}_3^{(1)}$ is the corresponding real correction. The bare hard functions contain infrared divergences which are in one-to-one correspondence with the ultraviolet divergences of the soft functions. Once combined, these divergences cancel and we obtain a finite cross section. Inserting the expansions (2.13) - (2.15) into (2.11), we can expand the cross section $\sigma(Q, Q_0)$ and extract its NLO coefficient $\sigma_{\rm NLO}$

$$\frac{\sigma(Q, Q_0)}{\sigma_0} = 1 + \frac{\alpha_s}{4\pi}\, \sigma_{\rm NLO} + \mathcal{O}(\alpha_s^2) \\ = 1 + \frac{\alpha_s}{4\pi} \big\langle \boldsymbol{\mathcal{H}}_2^{(1)} \otimes \mathbf{1} + \boldsymbol{\mathcal{H}}_2^{(0)} \otimes \boldsymbol{\mathcal{S}}_2^{(1)} + \boldsymbol{\mathcal{H}}_3^{(1)} \otimes \mathbf{1} \big\rangle + \mathcal{O}(\alpha_s^2)\,. \tag{2.16}$$

In the following, we will calculate $\boldsymbol{\mathcal{H}}_2^{(1)}, \boldsymbol{\mathcal{H}}_3^{(1)}$ as well as $\boldsymbol{\mathcal{S}}_m^{(1)}$ using standard methods in perturbative quantum field theories.

To conclude this section, we would like to emphasize that the main result presented here is the factorization formula (2.11), which was obtained by analyzing the factorization properties of the full QCD amplitudes. However, this result can also be obtained within SCET using collinear fields along the directions of the energetic on-shell particles [95].

2.3 Hard functions

Starting from the abstract operator definition given in (2.10), we can extract the contributions to the hard functions $\boldsymbol{\mathcal{H}}_m$ from the full QCD matrix element for the process

$$\gamma^* \to q(p_1)\,\bar{q}(p_2). \tag{2.17}$$

The contribution is straightforward at leading order because we normalize the hard functions with the born cross section σ_0. Since we eventually want to reproduce (2.1) up to and including α_s corrections, we need to calculate the NLO corrections to the hard function $\boldsymbol{\mathcal{H}}$ which are in one-to-one correspondence with real and virtual corrections to (2.17). We will carry out this extraction in the following sections.

2.3.1 Real emission contributions

The real corrections start at $\mathcal{O}(\alpha_s)$ and the procedure to calculate them is similar to a fixed-order calculation for $\gamma^*(q) \to q(p_1)\,\bar{q}(p_2)\,g(p_3)$. In the notation of (2.10) the hard function $\boldsymbol{\mathcal{H}}_3^{(1)}$ is given by

$$\begin{aligned}\frac{\alpha_0}{4\pi}\,\sigma_0\,\boldsymbol{\mathcal{H}}_3^{(1)} =& \frac{1}{2Q^2(2\pi)^{2-4\epsilon}}\prod_{i=1}^{3}\int dE_i\,E_i^{1-2\epsilon}\,|\mathcal{M}_3(\{p_1,p_2,p_3\})\rangle\langle\mathcal{M}_3(\{p_1,p_2,p_3\})| \\ &\times\delta(Q-E_1-E_2-E_3)\,\delta^{(3-2\epsilon)}(\vec{p}_1+\vec{p}_2+\vec{p}_3)\;\Theta_{\text{in}}(\{p_1,p_2,p_3\})\,.\end{aligned} \tag{2.18}$$

As mentioned before, the integration is over the energies of the three particles in the final state while their directions are fixed. In other words, this means that to calculate (2.18), we need to calculate the matrix element for $\gamma^*(q) \to q(p_1)\,\bar{q}(p_2)\,g(p_3)$, then parameterize the corresponding phase space in such a way that we can integrate over the energies while keeping the directions fixed. This means that the final result will only depend on the angular information of the partons. The matrix element is given by the squared amplitude and takes the form

$$\big|\mathcal{M}_3\big|^2 = \big|\mathcal{M}_2^{(0)}\big|^2\,\frac{2C_F\,g_s^2\,\tilde{\mu}^{2\epsilon}}{Q^2}\,\frac{x_1^2+x_2^2-\epsilon\,x_3^2}{(1-x_1)(1-x_2)}\,, \tag{2.19}$$

where the variables $x_i = 2E_i/Q$ denote the energy fractions and $\tilde{\mu}^2 = \frac{\mu^2 e^{\gamma_E}}{4\pi}$ with the renormalisation scale μ. Due to momentum conservation, the three partons must lie within a plane. The most energetic particle is aligned with the thrust axis, and the jet cones are centered around it. We find it most convenient to split the phase-space integration into different regions depending on which particle carries the most energy. This leads to six regions

$$\begin{aligned}&\text{I}: \quad x_1>x_2>x_3\,, \quad \text{II}: \quad x_1>x_3>x_2\,, \quad \text{III}: \quad x_3>x_1>x_2\,, \\ &\text{IV}: \quad x_3>x_2>x_1\,, \quad \text{V}: \quad x_2>x_3>x_1\,, \quad \text{VI}: \quad x_2>x_1>x_3\,,\end{aligned} \tag{2.20}$$

depending on the various energy hierarchies among the three partons. Taking into account the $x_1 \leftrightarrow x_2$ symmetry according to (2.19), we only need to calculate the contributions from regions I,

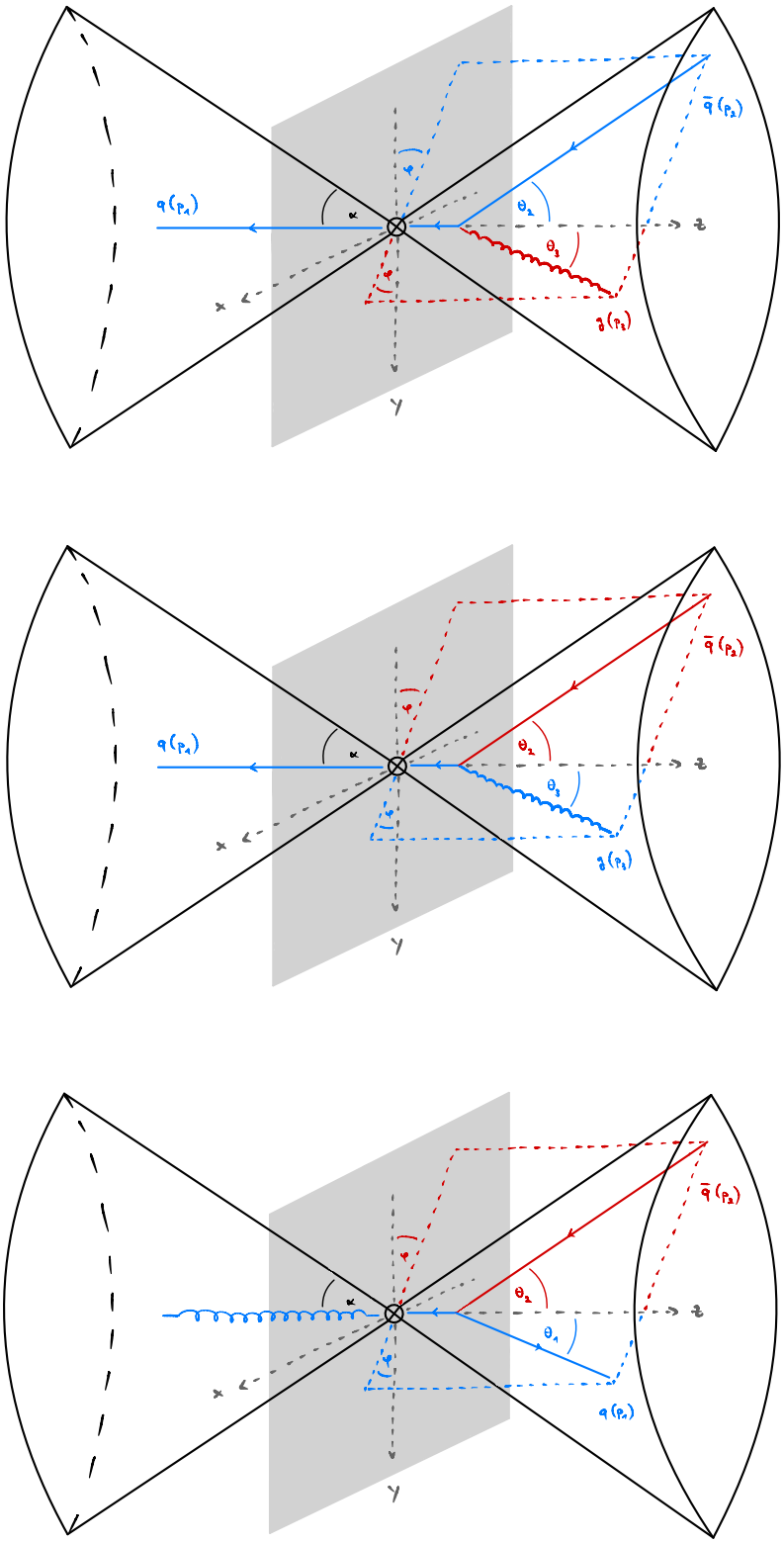

Figure 2.4: Representation of the three different kinematical regions of the three-particle phase space I, II and III as described in equation (2.20). The red color indicates the softest particle in the configuration.

II and III. We will label the hard contributions related to the corresponding region by $\boldsymbol{\mathcal{H}}^{(1)}_{3,\mathrm{I}}$, $\boldsymbol{\mathcal{H}}^{(1)}_{3,\mathrm{II}}$ and $\boldsymbol{\mathcal{H}}^{(1)}_{3,\mathrm{III}}$. In region I, the thrust axis points in the opposite way to p_1 since the quark carries the most energy. We parameterize the final-state particle momenta with polar angles θ_i and an azimuthal angle φ with respect to the thrust axis,

$$\begin{aligned} p_{\gamma^*} &= Q(1,0,\cdots,0), \\ p_1 &= E_1(1,0,\cdots,0,-1), \\ p_2 &= E_2(1,0,\cdots,0,-\sin\varphi\sin\theta_2,-\cos\varphi\sin\theta_2,\cos\theta_2), \\ p_3 &= E_3(1,0,\cdots,0,\sin\varphi\sin\theta_3,\cos\varphi\sin\theta_3,\cos\theta_3), \end{aligned} \tag{2.21}$$

where p_{γ^*} is the momentum of the incoming γ^* in the center-of-mass frame. The situation is shown in Figure 2.4. We point out that since the particles lie in a plane, we could have chosen the azimuthal angle to be zero, however, we keep it as a parameter, such that we may also study distributions in φ. The three-particle phase space only depends on a set of 2 variables due to momentum conservation. We find it convenient to perform the parametrization with the energy fraction of the gluon x_3 and the cosine of the angle between the gluon and the thrust axis θ_3

$$\begin{aligned} \int d\Pi_3 &= \prod_{i=1}^{3}\int \frac{d^{d-1}p_i}{2E_i(2\pi)^{d-1}}\,(2\pi)^d\,\delta^{(d)}(q-p_1-p_2-p_3) \\ &= \int dx_3\,d\varphi\,d(\cos\theta_3)\,\left(\frac{2}{Q}\right)^{6\epsilon}\frac{(2\pi)^{-3+2\epsilon}\,Q^{2+2\epsilon}}{32\,\Gamma\left(\frac{1}{2}-\epsilon\right)\Gamma\left(\frac{3}{2}-\epsilon\right)}\frac{\left(\sin^2\theta_3\right)^{-\epsilon}\,x_1^{1-2\epsilon}\,x_3^{1-2\epsilon}}{2-x_3-x_3\cos\theta_3}\,\left(\sin^2\varphi\right)^{-\epsilon}. \end{aligned} \tag{2.22}$$

We also need to express x_1, x_2 in terms of θ_3 and x_3. We can do this by using the relations

$$x_2 = 2 - x_1 - x_3\,, \tag{2.23}$$

$$x_1 = \frac{2(1-x_3)}{2-x_3-x_3\cos\theta_3}, \tag{2.24}$$

where the first one is obtained by energy conservation and the second one by solving a system of equations to get the minimal set of variables. The next step is to combine (2.19) and (2.22) using equations (2.23) as well as (2.24). To obtain the pure one-loop contribution to the cross section, we factor out the d-dimensional Born-level contribution multiplied by the two-particle phase space

$$\int d\Pi_2\left|\mathcal{M}_2^{(0)}\right|^2 = \left(\frac{2}{Q}\right)^{2\epsilon}\frac{(4\pi)^\epsilon}{16\sqrt{\pi}\,\Gamma\left(\frac{3}{2}-\epsilon\right)}\left|\mathcal{M}_2^{(0)}\right|^2. \tag{2.25}$$

When we evaluate the phase-space integral, we also need to take into account that hard particles must be inside the cone as indicated by $\Theta_{\mathrm{in}}(\{p_1,p_2,p_3\})$. To implement this constraint, we find it convenient to change variables from $x_3 \mapsto \theta_2$ because, in this way, the restriction is manifest. In addition, we introduce the variables

$$\hat{\theta}_2 \equiv \tan\frac{\theta_2}{2}, \qquad\qquad \hat{\theta}_3 \equiv \tan\frac{\theta_3}{2}, \tag{2.26}$$

allowing us to write the bare hard function for region I, i.e. for the case of a quark jet in the left hemisphere

$$\begin{aligned}\boldsymbol{\mathcal{H}}^{(1)}_{3,\mathrm{I}}(\hat{\theta}_2,\hat{\theta}_3,Q,\mu) = \frac{4C_F\sqrt{\pi}\,(4\pi)^\epsilon}{\Gamma\left(\frac{1}{2}-\epsilon\right)}\left(\frac{\tilde{\mu}^2}{Q^2}\right)^\epsilon \int d\hat{\theta}_2 \int d\hat{\theta}_3 \int \frac{d\varphi}{2\pi}\,\left(\sin^2\varphi\right)^{-\epsilon} \\ \times\, \hat{\theta}_2^{-1-2\epsilon}\hat{\theta}_3^{-2\epsilon}\left(\hat{\theta}_2+\hat{\theta}_3\right)^{-3+2\epsilon}\left(1-\hat{\theta}_2\hat{\theta}_3\right)^{-2\epsilon} \\ \times\left[2\hat{\theta}_3\left(1-\hat{\theta}_2^2\right)\left(1-\hat{\theta}_2\hat{\theta}_3\right)\left(\hat{\theta}_2+\hat{\theta}_3\right)+(1-\epsilon)\hat{\theta}_2^2\left(1+\hat{\theta}_3^2\right)^2\right]\Theta_{\mathrm{in}}(\hat{\theta}_2,\hat{\theta}_3)\,\mathbf{1}\,.\end{aligned} \tag{2.27}$$

For a cone opening angle $\alpha > \frac{\pi}{3}$, we need to ensure that the thrust axis does not flip. This issue arises in the limit where both angles θ_2, θ_3 reach $\frac{\pi}{3}$ with respect to the thrust axis. This limit is a symmetric configuration of the three partons, meaning each parton carries one-third of the initial energy, i.e. $Q/3$. If the smaller angle between $\hat{\theta}_2, \hat{\theta}_3$ becomes larger than the threshold of $\frac{\pi}{3}$ then the thrust axis will flip, as it aligns with the direction of the most energetic parton in a three-parton configuration. To prevent this from happening, we use Heaviside functions [98]

$$\Theta_{\mathrm{in}}(\hat{\theta}_2,\hat{\theta}_3) = \Theta\left(\delta-\hat{\theta}_2\right)\Theta\left(\delta-\hat{\theta}_3\right)\Theta\left(\sqrt{1+\hat{\theta}_2^2}-\hat{\theta}_2-\hat{\theta}_3\right)\Theta\left(\sqrt{1+\hat{\theta}_3^2}-\hat{\theta}_2-\hat{\theta}_3\right), \tag{2.28}$$

where δ is related to the opening angle. This means that the smaller angle between $\hat{\theta}_2$ and $\hat{\theta}_3$ must be less than $1/\sqrt{3}$, equivalent to an angle of $\frac{\pi}{3}$ from the thrust axis. To disentangle the soft and collinear divergences present in (2.27), we perform a final change of variables

$$\hat{\theta}_2 \equiv u\,v, \qquad\qquad \hat{\theta}_3 \equiv v, \tag{2.29}$$

where u and v are integrated between 0 and 1. To make the divergences explicit, we expand $\boldsymbol{\mathcal{H}}^{(1)}_{3,\mathrm{I}}$ in terms of distributions

$$u^{-1-2\epsilon} = -\frac{1}{2\epsilon}\delta(u) + \left(\frac{1}{u}\right)_+ - 2\epsilon\left(\frac{\ln u}{u}\right)_+ + \cdots, \tag{2.30}$$

where we introduced the standard $+$-distribution, which is defined according to

$$\left(\frac{1}{u}\right)_+[f] \equiv \int_0^1 du\,\frac{f(u)-f(0)}{u}, \tag{2.31}$$

and consequently for $\left(\frac{\ln u}{u}\right)_+$. The convenience of the variables introduced in (2.29) to parameterize the angles becomes manifest when we use these to express the $\Theta_{\mathrm{in}}(\hat{\theta}_2,\hat{\theta}_3)$ constraint in (2.28). Since the variable v is directly related to $\hat{\theta}_3$ while u represents the relative size of the angles, we can express the constraint that a hard emission must be inside the cone jets using only v. In addition, we can enforce the thrust-axis constraint using one Heaviside function as well, such that we obtain

$$\Theta_{\mathrm{in}}(u,v) = \Theta(\delta-v)\,\Theta\left(\sqrt{1+(uv)^2}-u-v\right), \tag{2.32}$$

for symmetric cone configurations. Eventually, after introducing the appropriate variables and expanding in distributions, we obtain the expression for the bare hard function $\boldsymbol{\mathcal{H}}_3^{(1)}$ in region I

$$\begin{aligned}\boldsymbol{\mathcal{H}}_{3,\mathrm{I}}^{(1)}(u,v,\varphi,Q,\mu) = {}& \frac{2C_F}{\epsilon^2} + \frac{C_F}{\epsilon}\left\{\frac{7}{4} + 4\ln 2 - 4\ln\delta + 4\ln\frac{\mu}{Q}\right\} \\ & + \int_0^1 du \int_0^1 dv \int_0^{2\pi} \frac{d\varphi}{2\pi}\, C_F \Bigg\{ \left[4\ln^2\frac{\mu}{Q} - \frac{\pi^2}{6}\right]\delta(u)\delta(v) + \left[4\ln\left(4\sin^2\varphi\right) - 8\ln\frac{\mu}{Q}\right]\delta(u)\left(\frac{1}{v}\right)_+ \\ & + 8\,\delta(u)\left(\frac{\ln v}{v}\right)_+ + \left[-\ln\frac{\mu}{Q}F(u,0) + \frac{2u^2}{(1+u)^3} - F(u,0)\ln(1+u)\right]\delta(v)\left(\frac{1}{u}\right)_+ \\ & + F(u,0)\delta(v)\left(\frac{\ln u}{u}\right)_+ + F(u,v)\left(\frac{1}{u}\right)_+\left(\frac{1}{v}\right)_+ \Bigg\}\Theta_{\mathrm{in}}(u,v)\,\mathbf{1}, \end{aligned} \tag{2.33}$$

where the integration over u, v and φ has already been carried out for singular parts in (2.33). In principle, we could renormalize the hard function directly in the $\overline{\mathrm{MS}}$ scheme, which is straightforward at the one-loop level because we only need to drop the poles. However, we will keep the poles to verify that all the divergences indeed cancel as they must. The auxiliary function $F(u,v)$ introduced in (2.33) is defined by

$$F(u,v) = \frac{4\left[u\left[-2\left(u^2+u+1\right)v^2 + u\left(2\,u\,(u+1)+1\right)v^4 + u + 2\right] + 2\right]}{(u+1)^3}. \tag{2.34}$$

To obtain the contributions of the hard function to region II, we proceed in close analogy to the discussion above. Recall that in this region the anti-quark $\bar{q}(p_2)$ is the softest particle and not the gluon, as was the case in region I. Hence, in this configuration $\hat{\theta}_2 > \hat{\theta}_3$, while in region I the opposite was true. As a result, we use (2.27), but substitute $\hat{\theta}_2 = v, \hat{\theta}_3 = uv$ before making the divergences explicit upon expanding in terms of distributions. Finally, we get

$$\begin{aligned}\boldsymbol{\mathcal{H}}_{3,\mathrm{II}}^{(1)}(u,v,Q,\mu) = {}& \frac{C_F}{\epsilon}\left\{\frac{5}{4} - 4\ln 2\right\} \\ & + \int_0^1 du \int_0^1 dv \int_0^{2\pi} \frac{d\varphi}{2\pi}\, C_F \Bigg\{ \left[-\ln\frac{\mu}{Q}G(u,0) + \frac{2}{(1+u)^3} + G(u,0)\ln\left(\frac{u}{1+u}\right)\right]\delta(v) \\ & \qquad + G(u,v)\left(\frac{1}{v}\right)_+ \Bigg\}\Theta_{\mathrm{in}}(u,v)\,\mathbf{1}. \end{aligned} \tag{2.35}$$

We point out that $\boldsymbol{\mathcal{H}}_{3,\mathrm{II}}^{(1)}$ is independent of φ, however, we keep the dependence to allow for a differential study in φ. The function $G(u,v)$ is given by

$$G(u,v) = \frac{4\left[u\left[-2\left(u^2+u+1\right)v^2 + u(u(u+2)+2)v^4 + 2(u+1)\right] + 1\right]}{(u+1)^3}. \tag{2.36}$$

In region III, we have a configuration with a gluon jet recoiling against a $q\bar{q}$-pair, which we align with the thrust axis and a hard $q\bar{q}$ pair on the right. Here, we find it most useful to parameterize the phase space with the polar angles of the quark θ_1 and anti-quark θ_2, see Figure 2.4. By using momentum conservation we can perform this change of variables, and after some algebra, we find

that the hard function in terms of $\hat{\theta}_1, \hat{\theta}_2$ reads

$$\begin{aligned}\boldsymbol{\mathcal{H}}^{(1)}_{3,\mathrm{III}}(\hat{\theta}_1,\hat{\theta}_2,Q,\mu) = \frac{4C_F\sqrt{\pi}\,(4\pi)^\epsilon}{\Gamma\left(\frac{1}{2}-\epsilon\right)}\left(\frac{\mu}{Q}\right)^{2\epsilon}\int d\hat{\theta}_1\int d\hat{\theta}_2\int\frac{d\varphi}{2\pi}\,\left(\sin^2\varphi\right)^{-\epsilon}\\ \times\,\hat{\theta}_1^{-2\epsilon}\hat{\theta}_2^{-2\epsilon}\left(\hat{\theta}_1+\hat{\theta}_2\right)^{-2+2\epsilon}\left(1-\hat{\theta}_1\hat{\theta}_2\right)^{-1-2\epsilon}\\ \times\left[\left(1+\hat{\theta}_2^4\right)\hat{\theta}_1^2+\left(1+\hat{\theta}_1^4\right)\hat{\theta}_2^2+4\hat{\theta}_2^2\hat{\theta}_1^2-\epsilon\left(\hat{\theta}_1+\hat{\theta}_2\right)^2\left(1-\hat{\theta}_1\hat{\theta}_2\right)^2\right]\Theta_{\mathrm{in}}(\hat{\theta}_1,\hat{\theta}_2)\,\mathbf{1}\,,\end{aligned} \tag{2.37}$$

where the cone and thrust-axis constraints $\Theta_{\mathrm{in}}(\hat{\theta}_1,\hat{\theta}_2)$ are the same as in (2.28), of course in the appropriate variables. We immediately see that (2.37) is free from collinear or soft divergences. Consequently, we can directly set $\epsilon \to 0$ so that the dependence on φ becomes trivial. We parameterize $\hat{\theta}_1 = u\,v$, $\hat{\theta}_2 = v$ such that we finally obtain

$$\boldsymbol{\mathcal{H}}^{(1)}_{3,\mathrm{III}}(u,v,Q,\mu) = \int_0^1 du\int_0^1 dv\int_0^{2\pi}\frac{d\varphi}{2\pi}\,C_F\,H(u,v)\,\Theta_{\mathrm{in}}(u,v)\,\mathbf{1}, \tag{2.38}$$

with

$$H(u,v) = \frac{4v\left(u^4v^4+u^2v^4+4u^2v^2+u^2+1\right)}{(u+1)^2\,(1-uv^2)}. \tag{2.39}$$

To conclude this section, we summarize the main results. Starting from the full QCD matrix element for $\gamma^*(q) \to q(p_1)\,\bar{q}(p_2)\,g(p_3)$ we extracted the hard functions by integrating over the energies of the hard partons. To perform the energy integrals in d-dimensions, we carefully divided the phase space into three regions, depending on the kinematical configuration. We obtained analytical expressions for the hard functions in (2.33), (2.35) and (2.38), which are distribution-valued in the angles of the particles. These distributions are artifacts of the soft and collinear divergences present.

2.3.2 Virtual contributions

The virtual corrections are in one-to-one correspondence with the ones for the form factor $F_q(q^2)$, which have been calculated up to four loops [165]. However, the first order contribution in α_s is sufficient for our purposes. This contribution is usually referred to as the dijet hard function also arising in global observables [24]

$$\begin{aligned}\boldsymbol{\mathcal{H}}^{(1)}_{2}(u,v,Q,\mu) = &-\frac{4C_F}{\epsilon^2}-\frac{C_F}{\epsilon}\left\{6+8\ln\frac{\mu}{Q}\right\}\\ &+\int_0^1 du\int_0^1 dv\int_0^{2\pi}\frac{d\varphi}{2\pi}\,C_F\left\{-8\ln^2\frac{\mu}{Q}-12\ln\frac{\mu}{Q}-16+\frac{7}{3}\pi^2\right\}\delta(u)\,\delta(v).\end{aligned} \tag{2.40}$$

A priori, there is no dependence on the variables u, v since no emission is present in the virtual correction. However, we choose to introduce a trivial dependence on u, v through delta functions. In this way, we can directly combine finite terms from real and virtual contributions. While collinear singularities cancel once we combine real and virtual contributions, a soft term proportional to the cone-opening angle $\sim \frac{\ln\delta}{\epsilon}$ remains. This residual singularity will eventually cancel when we combine the hard and soft contributions in order to reproduce the cross section at NLO accuracy.

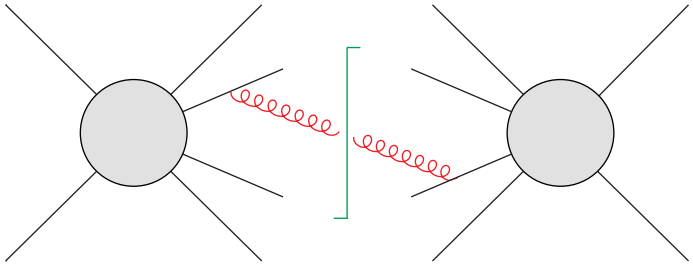

Figure 2.5: Feynman diagram for the one-loop soft contributions $\boldsymbol{\mathcal{S}}_m(\{\underline{n}\}, Q_0, \mu)$. The soft gluon is shown in red and points along the direction n_k.

2.4 Soft functions

The soft function $\boldsymbol{\mathcal{S}}_m$ introduced in (2.8) is defined as the vacuum expectation value squared of m soft Wilson-line operators. At leading order its contribution is trivial $\boldsymbol{\mathcal{S}}_m^{(0)} = \mathbf{1}$, while at one loop it is given as a sum over all dipoles originating from emissions by two Wilson lines, see Figure 2.5. The specific expression in momentum space is

$$\begin{aligned}&\frac{\alpha_s}{4\pi}\boldsymbol{\mathcal{S}}_m^{(1)}(\{\underline{n}\}, Q_0, \mu) = \\ &\quad - g_s^2\,\tilde{\mu}^{2\epsilon}\sum_{(ij)}\boldsymbol{T}_{i,L}\cdot\boldsymbol{T}_{j,R}\int\frac{d^dk}{(2\pi)^{d-1}}\delta(k^2)\theta(k^0)\frac{n_i\cdot n_j}{n_i\cdot k\, n_j\cdot k}\left[\Theta_{\text{in}}(n_k) + \Theta_{\text{out}}(n_k)\theta(Q_0 - E_k)\right] ,\end{aligned} \tag{2.41}$$

where n_k is the light-like direction vector of k and the sum runs over all unordered pairs (ij). In other words this means that we include both contributions $i = 1$, $j = 2$, as well as $i = 2$, $j = 1$. To indicate from which side a color generator acts on the hard functions $\boldsymbol{\mathcal{H}}_m$, we write $\boldsymbol{T}_{i,R}$ and $\boldsymbol{T}_{i,L}$. In principle, we obtain a contribution to the soft function when the n_k is inside the jet cones, however in this case the resulting integral is scaleless since there is no constraint on the soft energy. As a result, the one-loop soft function only receives contributions when the soft emission is inside the veto region, i.e. outside of the jet cones. We point out that the one-loop soft function depends on the radiation being vetoed through $\theta(Q_0 - E_k)$ in the sense that if we decided to restrict not the energy itself, but for instance the transverse energy $E_{t,\text{out}}$, the soft function would change. Indeed, to obtain the soft function for the Sterman-Weinberg jets, we need to use $\theta(Q\beta - 2E_k)$, which specifies that the energy outside of the jet cones E_{out} must be smaller than $\frac{Q\beta}{2}$. We remind the reader that β is the same quantity as in (2.1). For the case where the soft function only contains two Wilson lines $\boldsymbol{\mathcal{S}}_2^{(1)}$, the calculation is straightforward. In this situation, only one dipole with reference vectors n and $\bar{n}$ exists. We parameterize the soft emission in d-dimensions using

$$k^\mu = k^0\,(1, \cdots, \sin\varphi\sin\theta, \cos\varphi\sin\theta, \cos\theta) , \tag{2.42}$$

where φ is the azimuthal angle and θ the polar angle. Next, we expand the measure d^dk in terms of these angles, substitute $v = \tan\frac{\theta}{2}$ and perform the energy integral using the $\theta(Q\beta - 2E_k)$ constraint. After expanding the soft function as a series in ϵ we obtain

$$\begin{aligned}\boldsymbol{\mathcal{S}}_2^{(1)} = \frac{8C_F\ln\delta}{\epsilon} + \int_0^1 dv\int_0^{2\pi}\frac{d\varphi}{2\pi}\,C_F\Bigg\{16\left(\frac{\ln v}{v}\right)_+ \\ + \left[8\ln\left(4\sin^2\varphi\right) + 16\ln\frac{Q\beta}{\mu} - 16\ln(1+v^2)\right]\left(\frac{1}{v}\right)_+\Bigg\}\Theta_{\text{out}}(v)\,\mathbf{1} ,\end{aligned} \tag{2.43}$$

where we keep the dependence on φ, v for the finite part. We see that there is a remaining soft singularity. Interestingly, we also see that the φ-dependence exactly cancels between the hard function $\boldsymbol{\mathcal{H}}_{3,\mathrm{I}}$ and $\boldsymbol{\mathcal{S}}_2^{(1)}$. To see this cancellation explicitly one writes $\Theta_{\mathrm{in}}(u,v) = 1 - \Theta_{\mathrm{out}}(u,v)$ in the hard piece in equation (2.33).

2.5 NLO cross section

In the previous sections, we have calculated all the relevant ingredients for the factorization theorem at NLO in α_s. By combining these ingredients, we must retrieve known fixed-order results. For the first check, we set $\Theta_{\mathrm{in}}(u,v) \equiv 1$ which means that we integrate the hard $\boldsymbol{\mathcal{H}}_2^{(1)}, \boldsymbol{\mathcal{H}}_3^{(1)}$ and soft functions $\boldsymbol{\mathcal{S}}_2^{(1)}$ over the full solid angles. In this case, the soft function vanishes since everything is considered to be a hard contribution, i.e. to be inside of the jet cones. We obtain

$$\left\langle \boldsymbol{\mathcal{H}}_2^{(1)} \otimes \mathbf{1} \right\rangle + \left\langle \boldsymbol{\mathcal{H}}_3^{(1)} \otimes \mathbf{1} \right\rangle = 3C_F \,, \tag{2.44}$$

which is precisely the well-known result for the total cross section for $e^+e^- \to 2\,\text{jets}$ at NLO, normalized to the Born contributions. The situation is more interesting once we impose a non-trivial gap size. For a jet opening angle $\alpha \leq \frac{\pi}{3}$ which corresponds to $\delta \leq \frac{1}{\sqrt{3}}$, the thrust-axis constraint is always fulfilled so that (2.32) simplifies to $\Theta(\delta - v)$. In this case, the hard and soft contributions evaluate to

$$\begin{aligned}\left\langle \boldsymbol{\mathcal{H}}_2^{(1)} \otimes \mathbf{1} \right\rangle + \left\langle \boldsymbol{\mathcal{H}}_3^{(1)} \otimes \mathbf{1} \right\rangle = C_F \Bigg[&- \frac{8\ln\delta}{\epsilon} - 2 + \frac{2\pi^2}{3} + 12\left(1-\delta^4\right)\ln 2 + 8\ln^2\delta - 12\ln\delta \\ &- 12\,\delta^2 + 9\,\delta^4 + 8\,\mathrm{Li}_2(\delta^2) - 16\ln\delta\ln\frac{\mu}{Q}\Bigg] \,, \end{aligned} \tag{2.45}$$

$$\left\langle \boldsymbol{\mathcal{H}}_2^{(0)} \otimes \boldsymbol{\mathcal{S}}_2^{(1)} \right\rangle = C_F \left[\frac{8\ln\delta}{\epsilon} - 8\,\mathrm{Li}_2(-\delta^2) - 8\ln^2\delta - \frac{2\pi^2}{3} - 16\ln\delta\ln\frac{\beta Q}{\mu} \right] , \tag{2.46}$$

where $\mathrm{Li}_2(x) = -\int_0^x dz\, \frac{\ln(1-z)}{z}$ represents the dilogarithm. We explicitly see that the remaining singularity in each of the pieces cancels once we add hard and soft contributions to obtain the one-loop coefficient

$$\sigma_{\mathrm{NLO}} = C_F \left[-16\ln\delta\ln\beta - 2 + 12\ln 2 - 12\ln\delta - 12\delta^2 + (9 - 12\ln 2)\,\delta^4 + 8\,\mathrm{Li}_2(\delta^2) - 8\,\mathrm{Li}_2(-\delta^2) \right] . \tag{2.47}$$

We remind the reader that only the combination of hard and soft functions is physical and can thus be compared with the literature. For $\delta > \frac{1}{\sqrt{3}}$, we need to also take into account the thrust-axis constraint. Performing the integrals analytically and adding hard and soft contributions, we get

$$\begin{aligned}\sigma_{\mathrm{NLO}} = C_F \Bigg[&3 - 16\ln\delta\ln\beta \\ &+ 3\left(8\delta^2 - 5 - 3\delta^4\right) - 12\ln 2 + 4\ln^2 2 + 12\,\delta^4 \ln\left(\frac{2\delta^2}{1+\delta^2}\right) + 12\ln\left(1+\delta^2\right) \\ &- 8\ln 2\ln\left(1+\delta^2\right) + 4\ln^2\left(1+\delta^2\right) + 8\mathrm{Li}_2\left(\frac{1-\delta^2}{2}\right) + 8\mathrm{Li}_2\left(\frac{1-\delta^2}{1+\delta^2}\right) \\ &- 18\ln\delta^2 - 2\ln^2\delta^2 + 8\ln\delta^2\ln\left(1-\delta^2\right) - 8\ln\delta^2\ln\left(1+\delta^2\right)\Bigg] . \end{aligned} \tag{2.48}$$

We point out that in the limit $\delta \to 1$, we retrieve the inclusive result (2.44) since all the terms starting from the second line add up to zero. We compared the analytical expressions for σ_{NLO}

with [147] for both cases and found agreement. These coefficients can also be calculated numerically within the full theory in order to verify the factorization theorem. This has been carried out for $\delta < \frac{1}{\sqrt{3}}$ in [95] and full agreement has been found for small values of β due to the fact that the factorization theorem (2.11) does not involve power corrections in β. In other words, (2.47) and (2.48) hold, in principle, for any value of δ up to terms suppressed by power(s) in β. Therefore, we can expand (2.47) in the region where δ is small

$$\sigma_{\rm NLO} = -16 \ln\delta \ln\beta - 12 \ln\delta + c_0 \,, \tag{2.49}$$

with $c_0 = -2 + 12\ln 2$, which is precisely the same structure as (2.1). The constant term differs because of the different definitions of the jet axis in this work and [149]. More formally, it has been shown in [94] that the cross section (2.11) refactorizes in the narrow-angle limit. In Laplace space we get

$$\widetilde{\sigma}(\tau,\delta) = \sigma_0\, H(Q)\, \widetilde{S}(Q\tau) \left[\sum_{m=1}^{\infty} \left\langle \boldsymbol{\mathcal{J}}_m(Q\delta) \otimes \widetilde{\boldsymbol{\mathcal{U}}}_m(Q\delta\tau) \right\rangle \right]^2 , \tag{2.50}$$

and involves hard $H(Q)$, soft $\widetilde{S}(Q\tau)$, jet $\boldsymbol{\mathcal{J}}_m(Q\delta)$ and coft $\widetilde{\boldsymbol{\mathcal{U}}}_m(Q\delta\tau)$ functions. The construction of the effective theory is more complicated in the narrow-cone case. However, the individual ingredients are more complicated to evaluate for wide cones since their dependence on the cone opening is δ is non-trivial. For instance, corrections to the hard function $H(Q)$ are not able to resolve particles inside the jet, while this is the case for $\boldsymbol{\mathcal{H}}_m$ in the wide-cone scenario. In [95] the relations between the different ingredients in the wide and narrow-cone cases has been worked out as δ becomes small.

The validity of the factorization theorem (2.11) has also been established at two loops. In [95], the next-to-next-to-leading-order corrections (NNLO) to the cross section $\sigma_{\rm NNLO}$ have been calculated to show that the logarithmic structure from the full theory is correctly reproduced by using the factorization theorem. In particular, the leading non-global logarithm, which starts at two loops, is correctly reproduced in the effective field theory. The leading non-global contribution arises from secondary emissions off hard partons inside the jet cones. This means that its contribution is given by the combination of $\boldsymbol{\mathcal{H}}_3^{(1)}$ with $\boldsymbol{\mathcal{S}}_3^{(1)}$

$$\left\langle \boldsymbol{\mathcal{H}}_3^{(1)} \otimes \boldsymbol{\mathcal{S}}_3^{(1)} \right\rangle = C_\epsilon \left(\frac{\mu}{Q}\right)^{2\epsilon} \left(\frac{\mu}{\beta Q}\right)^{2\epsilon} \delta^{-2\epsilon} \left[C_F^2 M_F(\delta,\epsilon) + C_F C_A M_A(\delta,\epsilon) \right] , \tag{2.51}$$

with the coefficients $M_F(\delta,\epsilon)$, $M_A(\delta,\epsilon)$ and a constant term $C_\epsilon = 4^\epsilon \frac{e^{\gamma_{\rm E}}}{\Gamma(1-\epsilon)}$. The non-global contribution is given by the double-pole contribution of

$$M_A(\delta,\epsilon) = \frac{1}{\epsilon^2} \left[-8{\rm Li}_2\left(\delta^4\right) + \frac{4\pi^2}{3} \right] + \cdots , \tag{2.52}$$

and is precisely the same as in [83]. The full result for $M_A(\delta,\epsilon)$ and $M_F(\delta,\epsilon)$ can be found in [95]. We point out that the separation between global and non-global is artificial and, in fact, not unique at subleading accuracy.

2.6 Renormalization-group evolution and resummation

The logarithms $\ln\beta$ arising in the cross sections (2.47), (2.48) for wide-angle cones will become large for disparate scales $Q_0 \ll Q$ and need to be resummed to guarantee reliable theory predictions. This is done by solving RG equations for the hard functions $\boldsymbol{\mathcal{H}}_m$, evolving them from their characteristic scale $\mu_h \sim Q$ down to the soft scale $\mu_s \sim Q_0$. The associated RG equations are a crucial ingredient to carry out the resummation of logarithmically enhanced contributions to all orders in perturbation theory. At the soft scale μ_s, the soft functions are free of large logarithms and can be evaluated perturbatively in $\alpha_s(\mu_s)$. Similarly, at the hard scale μ_h, the hard functions do not involve large logarithms and can be evaluated perturbatively in $\alpha_s(\mu_h)$. At the level of the factorized cross section, we denote the evolution through

$$\sigma(Q,Q_0) = \sum_{m=m_0}^{\infty} \left\langle \boldsymbol{\mathcal{H}}_m(\{\underline{n}'\},Q,\mu_h) \otimes \sum_{l\geq m}^{\infty} \boldsymbol{U}_{ml}(\{\underline{n}\},\mu_s,\mu_h)\,\hat{\otimes}\,\boldsymbol{\mathcal{S}}_l(\{\underline{n}\},Q_0,\mu_s)\right\rangle, \tag{2.53}$$

where m_0 is the number of Born-level hard particles, e.g. $m_0 = 2$ in dijet production in e^+e^- collisions. The evolution factor $\boldsymbol{U}_{ml}$ maps a configuration with m partons along the directions $\{\underline{n}'\} = \{n_1,\dots,n_m\}$ to a final-state configuration with l partons along $\{\underline{n}\} = \{n_1,\dots,n_l\}$, thereby generating additional emissions. The symbol $\hat{\otimes}$ denotes the integration over the directions of the additional emissions that are generated during the evolution, while $\otimes$ stands for the integration over the directions of the original m hard partons. The evolution factor is defined as a path-ordered exponential of the anomalous dimension $\boldsymbol{\Gamma}$

$$\boldsymbol{U}_{ml}(\{\underline{n}\},\mu_s,\mu_h) = \mathbf{P}\exp\left[\int_{\mu_s}^{\mu_h}\frac{d\mu}{\mu}\boldsymbol{\Gamma}(\{\underline{v}\},\{\underline{n}\},\mu)\right]_{ml}. \tag{2.54}$$

The ultraviolet divergences of the soft matrix elements are captured by the anomalous dimension matrix $\boldsymbol{\Gamma}$, which are in one-to-one correspondence with the infrared singularities of the hard matrix elements. These divergences can be removed by renormalization. Since we impose that the cross section (2.53) must be independent of the associated renormalization scales μ_h, μ_s, we obtain RG equations for the hard functions,

$$\mu\frac{\mathrm{d}}{\mathrm{d}\mu}\,\boldsymbol{\mathcal{H}}_m(\{\underline{n}\},Q,\mu) = -\sum_{l=m_0}^{m}\boldsymbol{\mathcal{H}}_l(\{\underline{n}\},Q,\mu)\,\boldsymbol{\Gamma}_{lm}(\{\underline{n}\},Q,\mu)\,. \tag{2.55}$$

It is also possible to formulate an evolution equation for the soft functions which is governed by the same anomalous dimension as in (2.55). This relationship between ultraviolet and infrared singularities has been used extensively to predict the infrared pattern of QCD amplitudes [166–182], in particular also involving massive legs [183–189]. We would like to emphasize that the situation we consider here is more complicated since the hard functions $\boldsymbol{\mathcal{H}}_m$ depend on the directions of the m partons and the geometry of the veto region.

In general, two types of infrared singularities arise in $\boldsymbol{\mathcal{H}}_m$. First, one or several of the partonic energies E_i become soft, or secondly, infrared divergences associated with loop corrections to the hard matrix element. We associate the former with real emissions and the latter with virtual corrections. Regardless of their origin, both singularities must be captured by the anomalous dimension matrix $\boldsymbol{\Gamma}$. We expand the anomalous dimension as a perturbative series in α_s

$$\boldsymbol{\Gamma} = \frac{\alpha_s}{4\pi}\boldsymbol{\Gamma}^{(1)} + \left(\frac{\alpha_s}{4\pi}\right)^2\boldsymbol{\Gamma}^{(2)} + \dots, \tag{2.56}$$

with the one- and two-loop contributions denoted by $\boldsymbol{\Gamma}^{(1)}$, $\boldsymbol{\Gamma}^{(2)}$. Since the hard functions $\boldsymbol{\mathcal{H}}_m$ are, in principle, QCD matrix elements integrated over the energy, we can anticipate the general

structure of the anomalous dimension. It is clear that the anomalous dimension matrix cannot be diagonal because we need lower-multiplicity virtual diagrams to cancel singularities from real-emission diagrams. This means that the one- and two-loop matrices take the form

$$\boldsymbol{\Gamma}^{(1)} = \begin{pmatrix} \boldsymbol{V}_2 & \boldsymbol{R}_2 & 0 & 0 & \dots \\ 0 & \boldsymbol{V}_3 & \boldsymbol{R}_3 & 0 & \dots \\ 0 & 0 & \boldsymbol{V}_4 & \boldsymbol{R}_4 & \dots \\ 0 & 0 & 0 & \boldsymbol{V}_5 & \dots \\ \vdots & \vdots & \vdots & \vdots & \ddots \end{pmatrix}, \qquad \boldsymbol{\Gamma}^{(2)} = \begin{pmatrix} \boldsymbol{v}_2 & \boldsymbol{r}_2 & \boldsymbol{d}_2 & 0 & \dots \\ 0 & \boldsymbol{v}_3 & \boldsymbol{r}_3 & \boldsymbol{d}_3 & \dots \\ 0 & 0 & \boldsymbol{v}_4 & \boldsymbol{r}_4 & \dots \\ 0 & 0 & 0 & \boldsymbol{v}_5 & \dots \\ \vdots & \vdots & \vdots & \vdots & \ddots \end{pmatrix}, \tag{2.57}$$

which represents the dijet case. At the $\mathcal{O}(\alpha_s)$ level, the divergences may arise either from a one-loop virtual correction denoted as $\boldsymbol{V}_m$ or from a single real emission denoted as $\boldsymbol{R}_m$. The latter generates an additional particle, which increases the number of partons from an m to an $m+1$ configuration. As a result, it occupies the row directly above the diagonal in the matrix $\boldsymbol{\Gamma}$. Moving to two loops, there are more possibilities. We need to consider double real emissions $\boldsymbol{d}_m$, real-virtual corrections $\boldsymbol{r}_m$, or two-loop virtual terms $\boldsymbol{v}_m$. This pattern illustrates that each subsequent order adds another row above the diagonal in the matrix $\boldsymbol{\Gamma}$, with no entries appearing below the diagonal. In the usual manner, the anomalous dimension is intricately linked with the $\boldsymbol{Z}$-matrix, which serves to absorb the divergences arising from both the hard and soft functions. At the two-loop level, the $\boldsymbol{Z}$-matrix takes the following form

$$\boldsymbol{Z}_{lm} = \mathbf{1} - \frac{\alpha_s}{4\pi}\frac{1}{2\epsilon}\boldsymbol{\Gamma}^{(1)}_{lm} + \left(\frac{\alpha_s}{4\pi}\right)^2 \left[\frac{1}{8\epsilon^2}\sum_{k=l}^{m}\boldsymbol{\Gamma}^{(1)}_{lk}\hat{\otimes}\boldsymbol{\Gamma}^{(1)}_{km} + \frac{\beta_0}{4\epsilon^2}\boldsymbol{\Gamma}^{(1)}_{lm} - \frac{1}{4\epsilon}\boldsymbol{\Gamma}^{(2)}_{lm}\right], \tag{2.58}$$

neglecting collinear singularities which cancel among hard functions $\boldsymbol{\mathcal{H}}_i$. In short, we extract the anomalous dimensions by looking at soft limits of the hard functions. Consistency demands that the application of this matrix to either the bare hard or bare soft functions must absorb all singularities in order to make them finite

$$\boldsymbol{\mathcal{H}}_m(\{\underline{n}\}, Q, \mu_h) = \sum_{l=m_0}^{m} \boldsymbol{\mathcal{H}}_l^{\text{bare}}(\{\underline{n}\}, Q, \epsilon)\left(\boldsymbol{Z}^{-1}\right)_{lm}(\{\underline{n}\}, Q, \epsilon, \mu_h), \tag{2.59}$$

$$\boldsymbol{\mathcal{S}}_l(\{\underline{n}\}, Q_0, \mu_s) = \sum_{m=l}^{\infty} \boldsymbol{Z}_{lm}(\{\underline{n}\}, Q, \epsilon, \mu_s)\,\hat{\otimes}\,\boldsymbol{\mathcal{S}}_m^{\text{bare}}(\{\underline{n}\}, Q_0, \epsilon). \tag{2.60}$$

The structure of the $\boldsymbol{Z}$-matrix may appear unexpected, as Wilson-line matrix elements typically undergo multiplicative renormalization. However, in this case, additional UV divergences arise in the real-emission diagrams due to the unconstrained nature of soft radiation inside the jet cones. It is precisely these divergences that give rise to NGLs. Its structure is also reflected in the anomalous dimension matrix $\boldsymbol{\Gamma}$ which is, in principle, an infinite dimensional object because, as already mentioned, soft functions of higher multiplicities are necessary to cancel the divergences present in matrix elements with fewer Wilson lines.

In the next section, we will extract the one-loop anomalous dimension which governs the LL evolution. From (2.58), we directly see that the one-loop anomalous dimension is in one-to-one correspondence with the soft divergences of one-loop corrections to the hard functions.

2.6.1 One-loop anomalous dimension

The one-loop anomalous dimension $\boldsymbol{\Gamma}^{(1)}$ contains two kinds of contributions: the real $\boldsymbol{R}_m$ and virtual $\boldsymbol{V}_m$ ones. In this section, we derive both contributions following [123]. Before we start the explicit calculation, we recall how soft gluons factorize in general. Whenever a soft gluon q is emitted from a hard amplitude involving m legs with momenta $\{\underline{p}\} = \{p_1, \dots, p_m\}$, to leading power, we can write the amplitude as a sum of eikonal factors

$$|\mathcal{M}_{m+1}(\{\underline{p}, q\})\rangle = \varepsilon^{*\mu} \boldsymbol{J}_{\mu,a}(q) |\mathcal{M}_m(\{\underline{p}\})\rangle = g_s \sum_{i=1}^{m} \boldsymbol{T}_i^a \frac{\varepsilon^* \cdot n_i}{n_i \cdot q} |\mathcal{M}_m(\{\underline{p}\})\rangle \,, \tag{2.61}$$

with ε_μ^* the polarization vector of the outgoing gluon and $\boldsymbol{T}_i^a$ denotes color generators associated with leg i in the color-space formalism [164]. The soft current $\boldsymbol{J}_{\mu,a}(q)$ is expressed at leading order in the coupling constant. One and two-loop results for this quantity are also available [190–192]. To obtain the leading-order real emission $\boldsymbol{R}_m$ contributions in the anomalous dimension, we consider the hard function for $m+1$ partons

$$\begin{aligned}\boldsymbol{\mathcal{H}}_{m+1}(\{\underline{n}, n_q\}, Q, \epsilon) = \frac{1}{2Q^2} \sum_{\text{spins}} \prod_{i=1}^{m+1} \int \frac{dE_i \, E_i^{d-3}}{\tilde{c}^\epsilon \, (2\pi)^2} |\mathcal{M}_{m+1}(\{\underline{p}, q\})\rangle\langle\mathcal{M}_{m+1}(\{\underline{p}, q\})| \\ \times (2\pi)^d \, \delta\Big(Q - \sum_{i=1}^{m+1} E_i\Big) \, \delta^{(d-1)}(\vec{p}_{\,\text{tot}} + \vec{q}) \, \Theta_{\text{in}}\big(\{\underline{p}, q\}\big) \,,\end{aligned} \tag{2.62}$$

with $\underline{n} = \{n_1, \dots, n_m\}$ the directions of the momenta, and take the limit when the emission q becomes soft according to (2.61). In addition, we apply a cutoff on E_q to isolate the soft divergence arising in the energy integral. Since we consider the emission q to be soft, it can be expanded out of the phase space constraints so that we get

$$\boldsymbol{\mathcal{H}}_{m+1}(\{\underline{n}, n_q\}, Q, \epsilon) = -g_s^2 \int_0^\Lambda \frac{dE_q \, E_q^{d-5}}{\tilde{c}^\epsilon \, (2\pi)^2} \, \theta_{\text{in}}(q) \sum_{(ij)} \frac{n_i \cdot n_j}{n_i \cdot n_q \, n_j \cdot n_q} \boldsymbol{T}_i^a \, \boldsymbol{\mathcal{H}}_m(\{\underline{n}\}, Q, \epsilon) \, \boldsymbol{T}_j^{\tilde{a}}, \tag{2.63}$$

where (ij) refers to unordered pairs of indices and a is the color index of the amplitude while $\tilde{a}$ is the one from the conjugate amplitude. In order to perform the color trace as indicated by $\langle \cdots \rangle$ in (2.11), the hard function is contracted with the leading-order soft function $\boldsymbol{\mathcal{S}}_m$ so that we can set $a = \tilde{a}$. However, we keep these indices explicit in order to separate the contributions from the amplitude versus its conjugate. Moreover, the right-hand side of (2.63) is part of the color space with m particles, whereas $\boldsymbol{\mathcal{H}}_{m+1}$ on the left-hand side lives in the color space of $m+1$ partons so that we need to make the additional color index explicit. Performing the energy integral as well as expressing the bare coupling g_s in terms of the $\overline{\text{MS}}$ one, we obtain

$$\boldsymbol{\mathcal{H}}_{m+1}(\{\underline{n}, n_q\}, Q, \epsilon) = \frac{2}{\epsilon} \frac{\alpha_s}{4\pi} \left(\frac{\mu}{2\Lambda}\right)^{2\epsilon} \theta_{\text{in}}(n_q) \sum_{(ij)} W_{ij}^q \, \boldsymbol{T}_i^a \, \boldsymbol{\mathcal{H}}_m(\{\underline{n}\}, Q, \epsilon) \, \boldsymbol{T}_j^{\tilde{a}} \,, \tag{2.64}$$

where we introduced the dipole radiator $W_{ij}^q = \frac{n_i \cdot n_j}{n_i \cdot n_q \, n_j \cdot n_q}$ which is the product of two eikonal factors. As already pointed, the color generator multiplying the amplitude is on the left and the the one multiplying the conjugate amplitude is on the right of the hard function $\boldsymbol{\mathcal{H}}_m$. To indicate from which side the color generator acts on the hard function, we write $\boldsymbol{T}_{i,L}^a$ and $\boldsymbol{T}_{i,R}^{\tilde{a}}$. Using this notation, we can read off the contribution to the anomalous dimension

$$\boldsymbol{R}_m = -4 \sum_{(ij)} \boldsymbol{T}_{i,L}^a \boldsymbol{T}_{j,R}^{\tilde{a}} \, W_{ij}^q \, \theta_{\text{in}}(n_q) \tag{2.65}$$

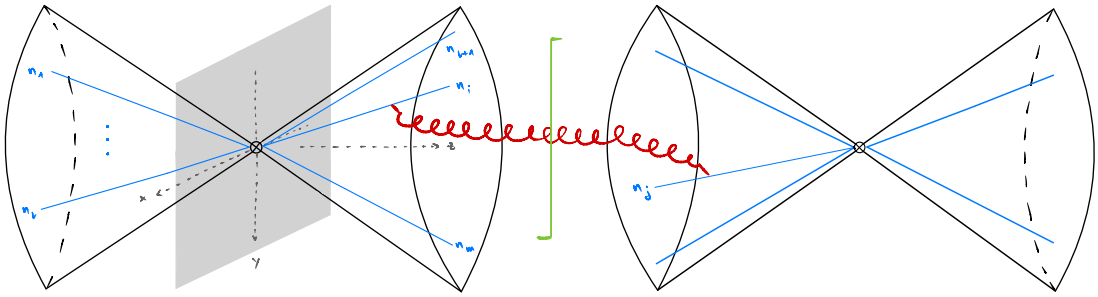

Figure 2.6: Real contribution to the one-loop anomalous dimension $\boldsymbol{\Gamma}^{(1)}$. The red gluon indicates the exchange of a (real) soft gluon between the legs i and j, which we identify as the dipole (ij).

because according to (2.58) we obtain the anomalous dimension by multiplying the coefficient of the divergence with -2. The anomalous dimension $\boldsymbol{R}_m$ transforms a hard function involving m partons into a hard function involving $m+1$ partons. We emphasize that integrals over the anomalous dimension (2.65) are a priori not well defined since $\boldsymbol{R}_m$ becomes singular in the limit where q becomes collinear to either i or j. As a consequence, (2.65) is not well defined on its own. When the anomalous dimension is applied to soft functions, these collinear divergences will cancel out the collinear divergences in the virtual corrections. We can introduce a cutoff to regulate these collinear singularities both in real and virtual contributions such that they can be calculated separately in $d = 4$ and subsequently combined. Such a cutoff is usually applied in parton showers. One can also isolate the divergences in dimensional regularization, see for instance [123].

To obtain the virtual corrections, we apply soft factorization (2.61) to the one-loop corrections, which are depicted in Figure 2.7. Since each of the m legs in the hard function is dressed with a Wilson line, we immediately obtain the one-loop correction to the amplitude as

$$\boldsymbol{\mathcal{H}}_m(\{\underline{n}\}, Q, \epsilon) = \frac{g_s^2}{2} \sum_{(ij)} \int \frac{d^d q}{(2\pi)^d} \frac{-i}{[q^2 + i0]} \frac{n_i \cdot n_j}{[n_i \cdot q + i0]\,[-n_j \cdot q + i0]} \times \boldsymbol{T}_i \cdot \boldsymbol{T}_j\, \boldsymbol{\mathcal{H}}_m(\{\underline{n}\}, Q, \epsilon) + \text{h.c.}\,, \quad (2.66)$$

with $\boldsymbol{T}_i \cdot \boldsymbol{T}_j = \sum_a \boldsymbol{T}_i^a \boldsymbol{T}_j^a$ and we add a factor of $\frac{1}{2}$ because the sum over the dipoles (ij) is unordered, i.e. each contribution appears twice hence we need to remove double counting. Strictly speaking, the hard functions $\boldsymbol{\mathcal{H}}_m(\underline{n}, Q, \epsilon)$ on the left and right sides of (2.66) are not identical, as the soft virtual correction on the right has been expanded. Consequently, the hard function on the right is one order lower in α_s. Therefore, with a slight abuse of notation, we write $\boldsymbol{\mathcal{H}}_m(\underline{n}, Q, \epsilon)$ on both sides. In (2.66), the $i0$ prescription assumes outgoing Wilson lines. The corresponding result for incoming Wilson lines is obtained through the substitution $n_k \mapsto -n_k$ for $k = i$ or $k = j$ so that the $i0$ prescription switches. Similarly to the real contribution, we need to perform the integral over q^0 and a subsequent integration over $|\vec{q}|$ where we extract the soft divergence. To do so, we first need to isolate where the divergences lie in the complex plane before applying the residue

theorem. The three propagators in (2.66) have singularities at

$$q^2 + i0 \quad \Rightarrow \quad q^0 = \pm E_q \mp i0, \tag{2.67}$$

$$n_i \cdot q + i0 \quad \Rightarrow \quad n_i^0 q^0 = \vec{n}_i \cdot \vec{q} - i0, \tag{2.68}$$

$$-n_j \cdot q + i0 \quad \Rightarrow \quad n_j^0 q^0 = \vec{n}_j \cdot \vec{q} + i0. \tag{2.69}$$

An illustration of the structure of singularities can be found in Figure 2.8. We will use the following identity to simplify the discussion

$$\frac{1}{n_i \cdot q + i0} = \frac{-1}{-n_i \cdot q + i0} - 2\pi i \delta(n_i \cdot q). \tag{2.70}$$

Inserting (2.70) in (2.66) we obtain

$$\boldsymbol{\mathcal{H}}_m(\{\underline{n}\}, Q, \epsilon) = \frac{g_s^2}{2} \sum_{(ij)} \int \frac{d^d q}{(2\pi)^d} \frac{-i}{[q^2 + i0]} \frac{n_i \cdot n_j}{[-n_j \cdot q + i0]} \left[\frac{-1}{[-n_i \cdot q + i0]} - 2\pi i \delta(n_i \cdot q) \right]$$
$$\times \boldsymbol{T}_i \cdot \boldsymbol{T}_j \, \boldsymbol{\mathcal{H}}_m(\{\underline{n}\}, Q, \epsilon) + \text{h.c.}\,, \tag{2.71}$$

so that we have shifted the singularity of the light-cone propagator $n_i \cdot n_q + i0$ to the upper half plane, where the pole from the other light-cone propagator $n_j \cdot n_q + i0$ lies as well, see Figure 2.8. The part in (2.71) without the δ-function, which we denote with a superscript $\boldsymbol{\mathcal{H}}_m^{(a)}$, contains three poles with positive imaginary parts and one with negative imaginary part. Therefore, it makes sense to close the contour in the lower half-plane in order to avoid the poles from the light-cone propagators and only pick up the pole situated at $q^0 = E_q - i0$. The next step is to impose a cutoff Λ on the energy integration such that we isolate the soft singularity

$$\boldsymbol{\mathcal{H}}_m^{(a)}(\{\underline{n}\}, Q, \epsilon) = \frac{\alpha_s}{4\pi} \sum_{(ij)} \boldsymbol{T}_i \cdot \boldsymbol{T}_j \left(\int_0^\Lambda dE_q \, E_q^{d-5} \right) \int [d\Omega_q] \, \frac{n_i \cdot n_j}{n_i \cdot n_q \, n_j \cdot n_q} \, \boldsymbol{\mathcal{H}}_m(\{\underline{n}\}, Q, \epsilon) + \text{h.c.}$$
$$= -\frac{\alpha_s}{4\pi} \frac{1}{\epsilon} \left(\frac{\mu}{2\Lambda} \right)^{2\epsilon} \sum_{(ij)} \boldsymbol{T}_i \cdot \boldsymbol{T}_j \int [d\Omega_q] \, W_{ij}^q \, \boldsymbol{\mathcal{H}}_m(\{\underline{n}\}, Q, \epsilon) + \text{h.c.}\,. \tag{2.72}$$

From (2.72) we directly get the anomalous dimension through (2.58)

$$\boldsymbol{V}_m^{(a)} = 2 \sum_{(ij)} (\boldsymbol{T}_{i,L} \cdot \boldsymbol{T}_{j,L} + \boldsymbol{T}_{i,R} \cdot \boldsymbol{T}_{j,R}) \int [d\Omega_q] \; W_{ij}^q \,, \tag{2.73}$$

where we added the contribution due to the conjugate amplitude which is proportional to $\boldsymbol{T}_{i,R} \cdot \boldsymbol{T}_{j,R}$. We see that (2.73) contains the same collinear divergence as (2.65).

The divergent part of the contribution proportional to the δ-function, which we denote with the superscript $\boldsymbol{\mathcal{H}}_m^{(b)}$, can be obtained by boosting into an appropriate frame in which we treat the perpendicular component of q as purely spatial. We get a purely imaginary part

$$\boldsymbol{\mathcal{H}}_m^{(b)}(\{\underline{n}\}, Q, \epsilon) = \frac{\alpha_s}{4\pi} \frac{i\pi}{\epsilon} \sum_{(ij)} \boldsymbol{T}_i \cdot \boldsymbol{T}_j \boldsymbol{\mathcal{H}}_m(\{\underline{n}\}, Q, \epsilon) \,, \tag{2.74}$$

from which we immediately extract its contribution to the anomalous dimension

$$\boldsymbol{V}_m^{(b)} = -2 \sum_{(ij)} [\boldsymbol{T}_{i,L} \cdot \boldsymbol{T}_{j,L} - \boldsymbol{T}_{i,R} \cdot \boldsymbol{T}_{j,R}] \times i\pi \, \Pi_{ij} \,. \tag{2.75}$$

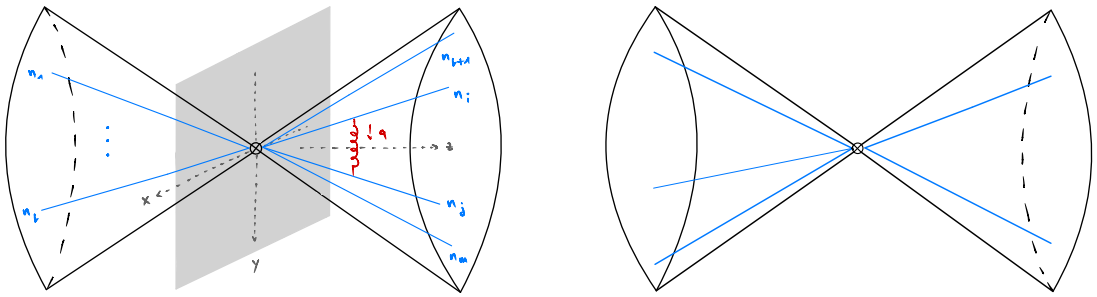

Figure 2.7: Virtual contribution to the one-loop anomalous dimension $\mathbf{\Gamma}^{(1)}$. The red gluon indicates the exchange of a (virtual) soft gluon between the legs i and j which we identify as the dipole (ij).

Since the conjugate amplitude has the opposite imaginary part, its sign is flipped compared to the amplitude. This imaginary part arises from the cut through the two eikonal lines, commonly referred to as the Glauber or Coulomb phases. This component is absent when one line is incoming and the other is outgoing. This is indicated by the factor

$$\Pi_{ij} = \begin{cases} 1, & i,j \text{ both incoming or outgoing}\,, \\ 0, & \text{otherwise}\,. \end{cases} \tag{2.76}$$

While these Glauber phases are absent both in the large-N_c limit and for processes initiated by e^+e^- annihilation, they lead to super-leading logarithms [90, 110] for processes at the LHC. Even though the leading contribution starts at four loops, their effects could become phenomenologically relevant since it is a double logarithmic effect, in particular for gluon-initiated processes [193].

To see that the collinear singularities indeed cancel between the real and virtual contribution, we apply both $\boldsymbol{R}_m$ and $\boldsymbol{V}_m$ to the trivial leading-order soft function $\boldsymbol{\mathcal{S}}_m = \mathbf{1}$. Adding the contributions, we find

$$\langle \boldsymbol{\mathcal{H}}_m \otimes \left(\boldsymbol{V}_m\,\mathbf{1} + \boldsymbol{R}_m \hat{\otimes} \mathbf{1}\right)\rangle = 4 \sum_{(ij)} \int [d\Omega_q]\; W_{ij}^q\, \theta_{\text{out}}(n_q) \langle \boldsymbol{\mathcal{H}}_m \otimes \boldsymbol{T}_i \cdot \boldsymbol{T}_j \rangle\,, \tag{2.77}$$

where we defined $\theta_{\text{out}}(n_q) = 1 - \theta_{\text{in}}(n_q)$ and moved the color generators acting on the left to the right by using the cyclicity of the color trace $\langle \dots \rangle$. From (2.77), it is evident that the angular integration is finite since the soft emission must be outside of the veto region so that it can never become collinear to the hard partons along directions i or j. It is also possible to show more generally that the collinear singularities do cancel, see [123].

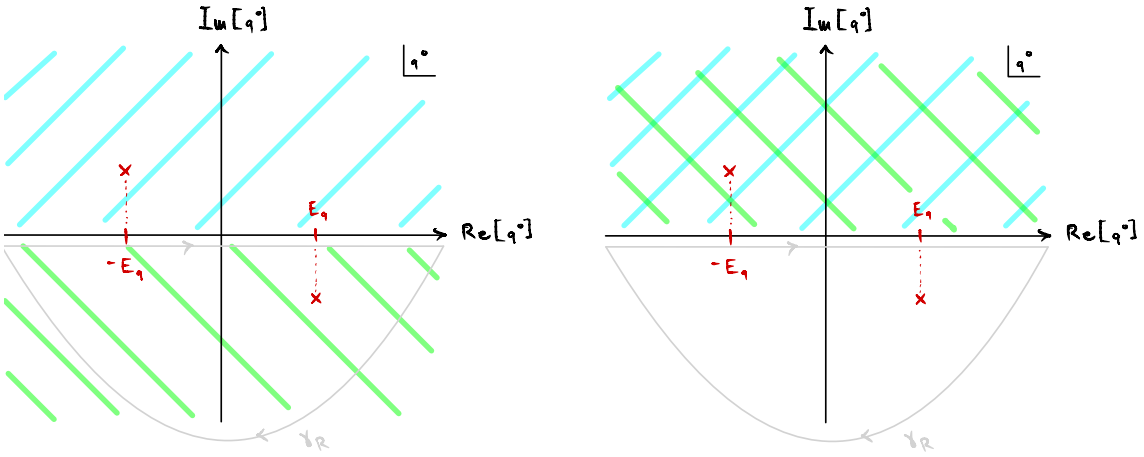

Figure 2.8: Complex plane indicating the locations of singularities. On the left, the divergences of the propagators from (2.66) are shown. In blue we indicate that the divergence from $-n_j \cdot q + i0$ is situated in the upper half plane. The divergence from $n_i \cdot q + i0$ lies in the lower half-plane as indicated in green. A red cross denotes a divergence associated with $q^2 + i0$. On the right, we show where the singularities lie after using (2.70).

2.6.2 Two-loop anomalous dimension

In this section, we will present the result for the two-loop anomalous dimension $\mathbf{\Gamma}^{(2)}$, obtained in [123]. The subleading contribution to the anomalous dimension has been derived by taking (double-) soft limits of amplitudes and isolating the infrared singularities associated with this limit.

As indicated in (2.58), it is necessary to remove contributions due to the iterations of the one-loop anomalous dimension such that we isolate the single pole contributions. There are three different entries which contribute at two loops. The double-real entries d_m capture singularities emerging from unordered double emissions off the original hard partons, extending the configuration from m to $m+2$ hard partons. The r_m entries correspond to soft singularities within real-virtual corrections and map m-parton hard functions to $m+1$-parton configurations. Lastly, the v_m entries relate to soft singularities in two-loop virtual corrections, keeping the number of hard partons fixed.

The part of the anomalous dimension associated with two emissions along the n_q and n_r directions is extracted by analyzing the soft current for emitting two particles, isolating the corresponding soft divergences, and removing the strongly ordered contribution, i.e. the iterated one-loop result. The explicit result for double-real contribution to the anomalous dimension is

$$\begin{aligned}\boldsymbol{d}_m = &\sum_{i,j,k} if^{abc}\left(\boldsymbol{T}^a_{i,L}\boldsymbol{T}^b_{j,L}\boldsymbol{T}^c_{k,R} - \boldsymbol{T}^a_{i,R}\boldsymbol{T}^b_{j,R}\boldsymbol{T}^c_{k,L}\right) K_{ijk;qr}\theta_{\rm in}(n_q)\theta_{\rm in}(n_r)\\ &- 2\sum_{(ij)} \boldsymbol{T}^c_{i,L}\boldsymbol{T}^c_{j,R} K_{ij;qr}\theta_{\rm in}(n_q)\theta_{\rm in}(n_r)\,.\end{aligned} \tag{2.78}$$

The first term present in $\boldsymbol{d}_m$ involves three color generators and is proportional to the angular function [97, 123]

$$K_{ijk;qr} = 8\left(W^q_{ik}W^r_{jk} - W^q_{ik}W^r_{jq} - W^q_{ir}W^r_{jk} + W^q_{ij}W^r_{jq}\right)\ln\left(\frac{n_{kq}}{n_{kr}}\right), \tag{2.79}$$

where we use the notation $n_{ab} = n_a \cdot n_b$. We point out that $K_{ijk;qr}$ vanishes in all collinear limits. Since the sum over k in (2.78) is unconstrained and therefore also includes $k = i$ and $k = j$, we also obtain two-particle contributions from $K_{ijk;qr}$. In the large-N_c limit, it turns out that only these contributions need to be considered. The terms $K_{iji;qr} = K_{ijj;qr} = 0$ vanish, but K_{iij} or K_{jji} yield a contribution. The second term present in $\boldsymbol{d}_m$ involves two color generators and multiplies the angular function $K_{ij;qr}$. This two-particle term is split up as [97, 123]

$$K_{ij;qr} = C_A K^{(a)}_{ij;qr} + \left[n_F T_F - 2C_A\right] K^{(b)}_{ij;qr} + \left[C_A - 2n_F T_F\right] K^{(c)}_{ij;qr}\,. \tag{2.80}$$

The individual functions are specified by

$$\begin{aligned}K^{(a)}_{ij;qr} &= \frac{4n_{ij}}{n_{iq}n_{qr}n_{jr}}\left[1 + \frac{n_{ij}n_{qr}}{n_{iq}n_{jr} - n_{ir}n_{jq}}\right]\ln\frac{n_{iq}n_{jr}}{n_{ir}n_{jq}}\,,\\ K^{(b)}_{ij;qr} &= \frac{8n_{ij}}{n_{qr}(n_{iq}n_{jr} - n_{ir}n_{jq})}\ln\frac{n_{iq}n_{jr}}{n_{ir}n_{jq}}\,,\\ K^{(c)}_{ij;qr} &= \frac{4}{n^2_{qr}}\left(\frac{n_{iq}n_{jr} + n_{ir}n_{jq}}{n_{iq}n_{jr} - n_{ir}n_{jq}}\ln\frac{n_{iq}n_{jr}}{n_{ir}n_{jq}} - 2\right).\end{aligned} \tag{2.81}$$

These functions are finite when n_q or n_r become collinear to the legs n_i and n_j. However, collinear divergences arise when n_q becomes collinear to n_r.

The real-virtual part of the anomalous dimension is calculated by taking the soft limit of amplitudes with a virtual gluon in the direction of n_r and a real emission pointing towards n_q. Similarly

to the calculation of the virtual one-loop contributions $\boldsymbol{V}_m$, we use the residue theorem to perform the energy integrals over the internal loop momenta. By doing so, one obtains

$$\begin{aligned}\boldsymbol{r}_m = & -2\sum_i\sum_{(jk)} if^{abc}(\boldsymbol{T}^a_{i,L}\boldsymbol{T}^b_{j,R}\boldsymbol{T}^c_{k,R} - \boldsymbol{T}^a_{i,R}\boldsymbol{T}^b_{j,L}\boldsymbol{T}^c_{k,L}) \int [d\Omega_r]\, K_{ijk;qr}\theta_{\text{in}}(n_q) \\ & - \sum_{(ij)} \boldsymbol{T}^a_{i,L}\boldsymbol{T}^a_{j,R} \left\{ W^q_{ij}\left[4\beta_0 \ln(2W^q_{ij}) + \gamma_1^{\text{cusp}}\right] - 2\int [d\Omega_r]\, K_{ij;qr} \right\} \theta_{\text{in}}(n_q) \\ & + 8i\pi \sum_i\sum_{(jk)} if^{abc}\left(\boldsymbol{T}^a_{i,L}\boldsymbol{T}^b_{j,R}\boldsymbol{T}^c_{k,R} + \boldsymbol{T}^a_{i,R}\boldsymbol{T}^b_{j,L}\boldsymbol{T}^c_{k,L}\right) W^q_{ij} \ln W^q_{jk}\, \theta_{\text{in}}(n_q)\,, \end{aligned} \tag{2.82}$$

with the two-loop cusp anomalous dimension

$$\gamma_1^{\text{cusp}} = 4\left(\left(\frac{67}{9} - \frac{\pi^2}{3}\right) C_A - \frac{20}{9} n_F T_F\right) \tag{2.83}$$

where n_F is the number of fermions included in the theory and T_F is the trace of the associated generator. In addition, we also use the one-loop coefficient of the β-function $\beta_0 = \frac{11}{3} C_A - \frac{4}{3} n_F T_F$. We expressed the real emission part as an angular integral to make the cancellation of singularities when n_q becomes collinear to n_r explicit between real-virtual and double-real anomalous dimensions.

To calculate the purely virtual part $\boldsymbol{v}$ of the anomalous dimension we need to consider two-loop corrections to amplitudes either involving two or three eikonal lines. The loop momenta point along n_q and n_r. We perform the energy integrals by using the residue theorem and isolate singularities by imposing a cutoff in close analogy to the previous discussion. We obtain for the double-virtual contribution

$$\begin{aligned}\boldsymbol{v}_m = & \sum_{(ijk)} if^{abc}\left(\boldsymbol{T}^a_{i,L}\boldsymbol{T}^b_{j,L}\boldsymbol{T}^c_{k,L} - \boldsymbol{T}^a_{i,R}\boldsymbol{T}^b_{j,R}\boldsymbol{T}^c_{k,R}\right) \int [d\Omega_q] \int [d\Omega_r]\, K_{ijk;qr} \\ & + \sum_{(ij)} \frac{1}{2}\left(\boldsymbol{T}^a_{i,L}\boldsymbol{T}^a_{j,L} + \boldsymbol{T}^a_{i,R}\boldsymbol{T}^a_{j,R}\right) \int [d\Omega_q]\, W^q_{ij}\left[4\beta_0 \ln(2W^q_{ij}) + \gamma_1^{\text{cusp}}\right] \\ & - i\pi \sum_{(ij)} \frac{1}{2}\left(\boldsymbol{T}^a_{i,L}\boldsymbol{T}^a_{j,L} - \boldsymbol{T}^a_{i,R}\boldsymbol{T}^a_{j,R}\right) \Pi_{ij}\, \gamma_1^{\text{cusp}}\,. \end{aligned} \tag{2.84}$$

The different parts of the anomalous dimension contain collinear divergences. For instance, terms involving W^q_{ij} in $\boldsymbol{r}_m$ and $\boldsymbol{v}_m$ become singular when the additional emission is collinear to the hard partons i or j. In addition, the two-particle contributions $K_{ij;qr}$ present in $\boldsymbol{r}_m$ and $\boldsymbol{d}_m$ diverge when the two additional emissions along n_q and n_r become collinear to each other. The results in equations (2.78), (2.82) and (2.84) have been rewritten in such a way that the cancellation between real and virtual contribution is manifest, once a physical quantity is computed. This means that we can introduce an intermediate cutoff, in close analogy to the one-loop case, to regulate these singularities. With a cutoff in place, the angular integrals can be evaluated in $d = 4$. Of course, this introduces an additional dependence on the cutoff. To ensure that the final result is cutoff-independent, it is necessary to lower the cutoff gradually until the result no longer depends on the precise value. In practice, this procedure is very delicate due to large cancellations.

2.6.3 Change to the $\overline{\text{MS}}$ scheme

In the previous section, we have presented results for the two-loop anomalous dimension in (2.78), (2.82) and (2.84), keeping the angular integrals in d-dimensions. Since keeping these d-dimensional integrals would be unconventional, we also showed that these collinear singularities manifestly cancel for physical quantities. As a result, we transition to $d = 4$, therefore allowing us to carry out subtractions in the usual $\overline{\text{MS}}$ scheme. Using the $\overline{\text{MS}}$ scheme introduces additional terms in the anomalous dimension. To see this, we show that the renormalization condition (2.58), which can be written explicitly as

$$\boldsymbol{\mathcal{S}}^{\text{ren}(1)} = \boldsymbol{\mathcal{S}}^{(1)} - \frac{1}{2\epsilon}\boldsymbol{\Gamma}^{(1)}\hat{\otimes}\mathbf{1}\,, \tag{2.85}$$

$$\begin{aligned}\boldsymbol{\mathcal{S}}^{\text{ren}(2)} = \boldsymbol{\mathcal{S}}^{(2)} &- \frac{1}{8\epsilon^2}\left[\boldsymbol{\Gamma}^{(1)}\hat{\otimes}\boldsymbol{\Gamma}^{(1)}\hat{\otimes}\mathbf{1} + 2\beta_0\boldsymbol{\Gamma}^{(1)}\hat{\otimes}\mathbf{1}\right] \\ &- \frac{1}{4\epsilon}\left[\boldsymbol{\Gamma}^{(2)}\hat{\otimes}\mathbf{1} + 2\boldsymbol{\Gamma}^{(1)}\hat{\otimes}\boldsymbol{\mathcal{S}}^{\text{ren}(1)} + 4\beta_0\boldsymbol{\mathcal{S}}^{\text{ren}(1)}\right]\,,\end{aligned} \tag{2.86}$$

differs from standard minimal subtraction. We will demonstrate this explicitly for the one-loop case, i.e. by calculating (2.85) for two-jet cross sections. The result for the bare soft function can be found in (2.46). The most compact way of writing the result is to use harmonic polylogarithms (HPLs) $H_{a_1,\ldots,a_n}(r)$ introduced in [194], a MATHEMATICA implementation can be found in [195, 196]. The bare one-loop soft function can be expressed in terms of these HPLs

$$\boldsymbol{\mathcal{S}}_2^{(1)} = 4\,C_F\left(\frac{\mu}{\beta Q}\right)^{2\epsilon}\left[\frac{H_0(r)}{\epsilon} + 2H_{-2}(r) - H_{0,0}(r) - \frac{\pi^2}{6} + \mathcal{O}(\epsilon)\right]\,, \tag{2.87}$$

with $r = \delta^2$. To obtain (2.87) we used the energy constraint $\theta(Q\beta - 2E_k)$. In the $\overline{\text{MS}}$ scheme we would simply drop the pole. However, this is not the same as (2.85) dictates since we also obtain higher-order terms in ϵ in the counter-term

$$\begin{aligned}-\frac{1}{2\epsilon}\boldsymbol{\Gamma}^{(1)}\hat{\otimes}\mathbf{1} &= -\frac{2}{\epsilon}\sum_{(ij)}\boldsymbol{T}_i\cdot\boldsymbol{T}_j\int[d\Omega_q]\;W_{ij}^q\,\theta_{\text{out}}(n_q) \\ &= -4C_F\left[\frac{H_0(r)}{\epsilon} + 2H_{-2}(r) - H_{0,0}(r) - \frac{\pi^2}{6} + \mathcal{O}(\epsilon)\right]\,.\end{aligned} \tag{2.88}$$

This subtraction removes finite terms as well and is, therefore, not a minimal subtraction. The renormalized soft function in this unconventional scheme is

$$\boldsymbol{\mathcal{S}}_2^{\text{ren}(1)} = 8C_F\,H_0(r)\,\ln\frac{\mu}{\beta Q}\,. \tag{2.89}$$

To transition to the standard $\overline{\text{MS}}$ subtraction scheme, we need to carry out subtractions in (2.85) using angular integrals in $d = 4$. To achieve this, we divide the angular integrations into two parts: an integral in $d = 4$ plus a remainder. Following the notation introduced in [123], we write

$$\boldsymbol{\Gamma}^{(1)}\hat{\otimes}\mathbf{1} = \boldsymbol{\Gamma}^{(1)}\hat{\otimes}_2\mathbf{1} + 2\epsilon\,\boldsymbol{\Gamma}^{(1)}\hat{\otimes}_\epsilon\mathbf{1}\,, \tag{2.90}$$

where the symbol $\otimes_2$ denotes the two-dimensional angular integral in pure $d = 4$, whereas $\otimes_\epsilon$ stands for the remainder. A factor 2ϵ has been factored out in the remainder term for convenience. The adapted one-loop renormalization in (2.85) reads now

$$\bar{\boldsymbol{\mathcal{S}}}^{\text{ren}(1)} = \boldsymbol{\mathcal{S}}^{(1)} - \frac{1}{2\epsilon}\boldsymbol{\Gamma}^{(1)}\otimes_2\mathbf{1}\,, \tag{2.91}$$

where $\bar{\boldsymbol{\mathcal{S}}}^{\mathrm{ren}(1)}$ is the one-loop soft function renormalized in the $\overline{\mathrm{MS}}$ scheme. In comparison to the previous result in (2.88), the counter-term is now precisely $-\frac{4}{\epsilon}C_F\,H_0(r)$ for the two-jet soft function so that it exactly removes the pole. In comparison to the prescription used in (2.85), this corresponds to a finite shift

$$\boldsymbol{\mathcal{S}}^{\mathrm{ren}(1)} = \bar{\boldsymbol{\mathcal{S}}}^{\mathrm{ren}(1)} - \boldsymbol{\Gamma}^{(1)} \otimes_\epsilon \mathbf{1}\,. \tag{2.92}$$

At two loops, changing to the $\overline{\mathrm{MS}}$ scheme not only shifts the renormalized function by a finite term, but also modifies the expression for the two-loop anomalous dimension.

$$\begin{aligned}\bar{\boldsymbol{\mathcal{S}}}^{\mathrm{ren}(2)} = \boldsymbol{\mathcal{S}}^{(2)} &- \frac{1}{8\epsilon^2}\left[\boldsymbol{\Gamma}^{(1)} \otimes_2 \boldsymbol{\Gamma}^{(1)} \otimes_2 \mathbf{1} + 2\beta_0 \boldsymbol{\Gamma}^{(1)} \otimes_2 \mathbf{1}\right] \\ &- \frac{1}{4\epsilon}\left[\bar{\boldsymbol{\Gamma}}^{(2)} \otimes_2 \mathbf{1} + 2\boldsymbol{\Gamma}^{(1)} \otimes_2 \bar{\boldsymbol{\mathcal{S}}}^{\mathrm{ren}(1)} + 4\beta_0 \bar{\boldsymbol{\mathcal{S}}}^{\mathrm{ren}(1)}\right],\end{aligned} \tag{2.93}$$

where the two-loop anomalous dimension in the $\overline{\mathrm{MS}}$ is given by [123]

$$\bar{\boldsymbol{\Gamma}}^{(2)} \otimes_2 \mathbf{1} = \boldsymbol{\Gamma}^{(2)} \otimes_2 \mathbf{1} - 2\beta_0\, \boldsymbol{\Gamma}^{(1)} \otimes_\epsilon \mathbf{1} - \left(\boldsymbol{\Gamma}^{(1)} \otimes_2 \boldsymbol{\Gamma}^{(1)} \otimes_\epsilon \mathbf{1} - \boldsymbol{\Gamma}^{(1)} \otimes_\epsilon \boldsymbol{\Gamma}^{(1)} \otimes_2 \mathbf{1}\right). \tag{2.94}$$

To obtain the additional terms in the anomalous dimension, it is necessary to rewrite the d-dimensional integrals in (2.86) in terms of 4-dimensional ones and to replace $\boldsymbol{\mathcal{S}}^{\mathrm{ren}(1)}$ according to (2.92). It is noteworthy that the second term in (2.94) has the form of a commutator involving angular integrations related with the two emissions. While this piece vanishes for uncorrelated emissions due to their symmetry, the non-global two-loop part contributes since it involves one gluon outside and one inside the jet-cone regions. In the latter case, the contributions arising at $\mathcal{O}(\epsilon)$ in the angular integrals are different such that a non-vanishing contribution survives.

The final result of the two-loop anomalous dimension, as shown in (2.94), in combination with its components $\boldsymbol{\Gamma}_m^{(2)} = \boldsymbol{d}_m + \boldsymbol{r}_m + \boldsymbol{v}_m$, as provided in equations (2.78), (2.82), and (2.84), and calculated using angular integrals in $d = 4$, is the final expression for the anomalous dimension in the $\overline{\mathrm{MS}}$ scheme. Furthermore, because we can evaluate anomalous dimensions in four dimensions, this form is also suitable for numerical implementation. In the following we will drop the bar and write $\boldsymbol{\Gamma}^{(2)}$.

Since the extraction of the two-loop anomalous dimension is very delicate and involves a lot of subtleties, a strong consistency check is necessary to validate the final result (2.94). In [95], the bare two-loop soft function $\boldsymbol{\mathcal{S}}^{(2)}$ has been calculated for the pure dijet case so that it has been explicitly verified that the anomalous dimension indeed renormalizes the divergences according to equation (2.93).

2.6.4 RG evolution at LL and NLL accuracy

Starting from the factorization theorem (2.11), stating that the cross section for jet production including a veto on radiation factorizes into hard $\boldsymbol{\mathcal{H}}_m$ and soft $\boldsymbol{\mathcal{S}}_m$ functions, we obtained RG equations for the hard functions in (2.55)

$$\mu\frac{\mathrm{d}}{\mathrm{d}\mu}\,\boldsymbol{\mathcal{H}}_m(\mu_h) = -\sum_{l=m_0}^{m} \boldsymbol{\mathcal{H}}_l(\mu_h)\,\boldsymbol{\Gamma}_{lm}(\mu_h)\,, \tag{2.95}$$

where the dependence of the hard functions $\boldsymbol{\mathcal{H}}_m$ on the direction $\{\underline{n}\}$ and the center-of-mass energy Q is implicit. These coupled differential equations are governed by an anomalous dimension $\boldsymbol{\Gamma}_{lm}$ which has been extracted up to two loops and presented in the previous sections. In this section, we will outline how to solve the RG equations perturbatively to resum the large logarithms.

Despite the fact that solving the RG equations is challenging because the anomalous dimension matrix involves an arbitrary amount of Wilson lines, one advantage of our effective field approach is that there is a clear prescription of the necessary ingredients to reach a given logarithmic accuracy. For instance, at LL accuracy, we need the leading-order contribution to the hard function with m_0 legs as well as the one-loop anomalous dimension, the leading-order soft function $\boldsymbol{\mathcal{S}}_m^{(0)} = \mathbf{1}$ is trivial. In order to capture terms beyond LL accuracy, matching corrections and subleading contributions due to the running are also necessary, the latter are driven by $\boldsymbol{\Gamma}^{(2)}$.

To perform the resummation, it is necessary to solve the RG equations iteratively to evolve the hard functions from $\mu_h \sim Q$ to the scale $\mu_s \sim Q_0$ associated with soft emissions. The formal solution to the RG equations is given by a path-ordered exponential of the anomalous dimension

$$\boldsymbol{\mathcal{H}}_2(\mu_h)\, \boldsymbol{U}_{2m}(\mu_h, \mu_s) = \boldsymbol{\mathcal{H}}_2(\mu_h)\, \mathbf{P} \exp\left[\int_{\mu_s}^{\mu_h} \frac{d\mu}{\mu}\, \boldsymbol{\Gamma}\right]_{2m} . \tag{2.96}$$

We insert the expansion of the anomalous dimension $\boldsymbol{\Gamma}$ in the exponent so that we get

$$\int_{\mu_s}^{\mu_h} \frac{d\mu}{\mu}\, \boldsymbol{\Gamma} = \int_{t_0}^{t} dt \left(\boldsymbol{\Gamma}^{(1)} + \frac{\alpha_s(\mu_h)}{4\pi} e^{2\beta_0 t} \left(\boldsymbol{\Gamma}^{(2)} - \frac{\beta_1}{\beta_0}\boldsymbol{\Gamma}^{(1)}\right) + \cdots\right) , \tag{2.97}$$

where we introduced the evolution time $t \equiv t(\mu_h, \mu_s) = \frac{1}{2\beta_0} \ln\left(\frac{\alpha_s(\mu_s)}{\alpha_s(\mu_h)}\right)$. We point out that once μ_h has been fixed, for instance $\mu_h = M_Z$, the mapping $\mu_s \mapsto t$ is unambiguous. The two-loop coefficient of the β-function $\beta_1 = \frac{34}{3}C_A^2 - \frac{20}{3}C_A T_F n_F - 4 C_F T_F n_F$ is a remnant of the running of the coupling. The first term in (2.97) does not depend on t so that we can directly perform the integration and obtain the LL evolution factor

$$\boldsymbol{U}_{kl}(t_0, t) = \mathbf{P} \exp\left[(t - t_0)\boldsymbol{\Gamma}^{(1)}\right]_{kl} , \tag{2.98}$$

which is the leading term in (2.96). The integrand in (2.97) is of the form $\boldsymbol{\Gamma}^{(1)} + \Delta\boldsymbol{\Gamma}$ where the second term $\Delta\boldsymbol{\Gamma}$ is suppressed by α_s. Therefore, most of the evolution will be driven by $\boldsymbol{\Gamma}^{(1)}$ so that it seems natural to use the interaction picture $\boldsymbol{\mathcal{H}}_b^I(t) = \boldsymbol{\mathcal{H}}_a(t)\boldsymbol{U}_{ab}(t, t_0)$. The corresponding differential equations for the hard functions are

$$\frac{\mathrm{d}}{\mathrm{d}t}\boldsymbol{\mathcal{H}}_m^I = -\sum_{l=m_0}^{m} \boldsymbol{\mathcal{H}}_l^I \left(\boldsymbol{U}_{ll'}(t_0, t)\, \Delta\boldsymbol{\Gamma}(t)_{l'k'}\, \boldsymbol{U}_{k'm}(t, t_0)\right) , \tag{2.99}$$

where the superscript specifies the interaction picture. We can immediately solve this equation to first order in $\Delta\boldsymbol{\Gamma}_{l'k'}(t')$

$$\boldsymbol{\mathcal{H}}_m^I(t) = \boldsymbol{\mathcal{H}}_2(t_0) \left[\mathbf{1} + \int_{t_0}^{t} dt'\, \boldsymbol{U}_{2l'}(t_0, t')\, \Delta\boldsymbol{\Gamma}_{l'k'}(t')\, \boldsymbol{U}_{k'm}(t', t_0)\right] , \tag{2.100}$$

where we have set $m_0 = 2$. The hard functions at the initial time t_0, which corresponds to the hard scale μ_h, are the same in the Schrödinger or interaction picture, i.e. $\boldsymbol{\mathcal{H}}_2(t_0) = \boldsymbol{\mathcal{H}}_2^I(t_0)$. By using $\boldsymbol{\mathcal{H}}_b^I(t) = \boldsymbol{\mathcal{H}}_a(t)\boldsymbol{U}_{ab}(t, t_0)$ we can also obtain the solution in the Schrödinger picture

$$\boldsymbol{\mathcal{H}}_m(t) = \boldsymbol{\mathcal{H}}_2(t_0)\, \boldsymbol{U}_{2m}(t_0, t) + \boldsymbol{\mathcal{H}}_2(t_0)\, \Delta\boldsymbol{U}_{2m}(t_0, t) + \cdots , \tag{2.101}$$

where the NLL correction is denoted by $\Delta\boldsymbol{U}_{kl}(t_0, t)$. To reach NLL accuracy, we augment the LL evolution with exactly one insertion of the two-loop anomalous dimension $\boldsymbol{\Gamma}^{(2)}$. This is sufficient to capture the effects of RG running at two loops. We denote this insertion by

$$\Delta\boldsymbol{U}_{kl}(t_0, t) = \int_{t_0}^{t} dt'\, \boldsymbol{U}_{kk'}(t_0, t') \cdot \frac{\alpha_s(t')}{4\pi} \left(\boldsymbol{\Gamma}^{(2)}_{k'l'} - \frac{\beta_1}{\beta_0}\boldsymbol{\Gamma}^{(1)}_{k'l'}\right) \cdot \boldsymbol{U}_{l'l}, (t', t). \tag{2.102}$$

where $\alpha(t') = \alpha_s(\mu_h)e^{2\beta_0 t}$. In short, this means that we start a LL evolution $\boldsymbol{U}_{kl}(t_0, t')$ which runs from t_0 until t', where we evaluate all contributions in $\boldsymbol{\Gamma}^{(2)}$, together with a β_1-correction to the running of the coupling, and then restart a LL evolution. We emphasize that we need to make an insertion at every possible intermediate time between t_0 and t. To obtain results at full NLL accuracy, it is necessary to include matching terms as well. More precisely, we need one-loop corrections to $\boldsymbol{\mathcal{H}}_2$, the tree-level result for $\boldsymbol{\mathcal{H}}_3$ and the one-loop soft functions $\boldsymbol{\mathcal{S}}_m$. These $\mathcal{O}(\alpha_s)$ corrections have been calculated perturbatively in the previous sections.

2.7 Summary

In this chapter, we have investigated jet cross sections. More specifically, we derived a factorization formula for the annihilation of an e^+e^--pair into two jets which carry most of the radiation in the process. As a consequence of radiation being restricted in certain regions of the phase space, a very intricate pattern of logarithms arises – the so-called non-global logarithms or NGLs in short – which are ubiquitous in jet cross sections. The factorization theorem states that the cross section for wide-angle jet cones factorizes into hard and soft functions

$$\sigma(Q, Q_0) = \sum_{m=2}^{\infty} \left\langle \boldsymbol{\mathcal{H}}_m(\{\underline{n}\}, Q, \mu) \otimes \boldsymbol{\mathcal{S}}_m(\{\underline{n}\}, Q_0, \mu) \right\rangle . \tag{2.103}$$

To establish the validity of this factorization formula, we calculated the full set of NLO corrections to the hard and soft functions to explicitly show that we indeed reproduced the cross section obtained by Sterman and Weinberg. The inclusive cross section depends on logarithms $\ln \frac{Q}{Q_0}$ and these become large for disparate scales and might overpower the suppression by the coupling, i.e. $\alpha_s \cdot L \sim 1$. To obtain reliable prediction, it is necessary to resum these logarithms in RG-improved perturbation theory. Starting from the factorization theorem we can derive a set of RG equations

$$\mu \frac{\mathrm{d}}{\mathrm{d}\mu} \boldsymbol{\mathcal{H}}_m(Q, \mu) = - \sum_{l=m_0}^{m} \boldsymbol{\mathcal{H}}_l(Q, \mu)\, \boldsymbol{\Gamma}_{lm}(Q, \mu) , \tag{2.104}$$

which are coupled differential equations. The natural way to perform the resummation in our effective field theory approach is to solve the RG equations and thus resum all the logarithmic contributions to all orders. The anomalous dimension matrix $\boldsymbol{\Gamma}_{lm}$ is a matrix in the space of particle multiplicities and has been extracted perturbatively up to and including two loops. The extraction is done by considering soft limits of hard amplitudes. At one loop, there are both virtual and real contributions to the anomalous dimension

$$\begin{aligned} \boldsymbol{R}_m =& -4 \sum_{(ij)} \boldsymbol{T}^a_{i,L} \boldsymbol{T}^{\tilde{a}}_{j,R}\, W^q_{ij}\, \theta_{\mathrm{in}}(n_q) , \\ \boldsymbol{V}_m =& \; 2 \sum_{(ij)} (\boldsymbol{T}_{i,L} \cdot \boldsymbol{T}_{j,L} + \boldsymbol{T}_{i,R} \cdot \boldsymbol{T}_{j,R}) \int \left[d^2\Omega_q\right] \, W^q_{ij} \\ & - i\pi \sum_{(ij)} 2 \left[\boldsymbol{T}_{i,L} \cdot \boldsymbol{T}_{j,L} - \boldsymbol{T}_{i,R} \cdot \boldsymbol{T}_{j,R}\right] \Pi_{ij} . \end{aligned} \tag{2.105}$$

The real corrections generate an additional hard particle, promoting the particle configuration from m to the $m+1$ particle configuration. As a consequence, the anomalous dimension is an infinite dimensional matrix in the space of particle multiplicities. This structure is significantly more complicated than the evolution equations for event shapes such as thrust. For global event shapes, the amount of Wilson line operators generating soft emissions is constant, e.g. for dijet

event shapes there are exactly two Wilson line operators along the jet directions. In the present case, we need to dress every additional hard particle inside the jet cones with a separate Wilson line. This multi-Wilson line configuration becomes quite intuitive in the context of wide-angle jets. In such cases, the angular separation between energetic particles inside the jet cones is sizable and similar to the typical angle of soft emissions. As a result, soft emissions resolve individual energetic partons within the jet, which means that it is impossible to collapse all these Wilson lines onto a single one. The two-loop anomalous dimension is decomposed into three different types of entries, which we refer to as double real $\boldsymbol{d}_m$, real-virtual $\boldsymbol{r}_m$ and double-virtual $\boldsymbol{v}_m$

$$\begin{aligned}\boldsymbol{d}_m = & \sum_{i,j,k} if^{abc}\left(\boldsymbol{T}^a_{i,L}\boldsymbol{T}^b_{j,L}\boldsymbol{T}^c_{k,R} - \boldsymbol{T}^a_{i,R}\boldsymbol{T}^b_{j,R}\boldsymbol{T}^c_{k,L}\right) K_{ijk;qr}\theta_{\text{in}}(n_q)\theta_{\text{in}}(n_r) \\ & - 2\sum_{(ij)} \boldsymbol{T}^c_{i,L}\boldsymbol{T}^c_{j,R} K_{ij;qr}\theta_{\text{in}}(n_q)\theta_{\text{in}}(n_r)\,, \end{aligned} \tag{2.106}$$

$$\begin{aligned}\boldsymbol{r}_m = & -2\sum_i\sum_{(jk)} if^{abc}(\boldsymbol{T}^a_{i,L}\boldsymbol{T}^b_{j,R}\boldsymbol{T}^c_{k,R} - \boldsymbol{T}^a_{i,R}\boldsymbol{T}^b_{j,L}\boldsymbol{T}^c_{k,L}) \int \left[d^2\Omega_r\right] K_{ijk;qr}\theta_{\text{in}}(n_q) \\ & - \sum_{(ij)} \boldsymbol{T}^a_{i,L}\boldsymbol{T}^a_{j,R}\left\{ W^q_{ij}\left[4\beta_0\ln(2W^q_{ij}) + \gamma_1^{\text{cusp}}\right] - 2\int\left[d^2\Omega_r\right] K_{ij;qr}\right\}\theta_{\text{in}}(n_q) \\ & + 8i\pi\sum_i\sum_{(jk)} if^{abc}\left(\boldsymbol{T}^a_{i,L}\boldsymbol{T}^b_{j,R}\boldsymbol{T}^c_{k,R} + \boldsymbol{T}^a_{i,R}\boldsymbol{T}^b_{j,L}\boldsymbol{T}^c_{k,L}\right) W^q_{ij}\ln W^q_{jk}\,\theta_{\text{in}}(n_q)\,, \end{aligned} \tag{2.107}$$

$$\begin{aligned}\boldsymbol{v}_m = & \sum_{(ijk)} if^{abc}\left(\boldsymbol{T}^a_{i,L}\boldsymbol{T}^b_{j,L}\boldsymbol{T}^c_{k,L} - \boldsymbol{T}^a_{i,R}\boldsymbol{T}^b_{j,R}\boldsymbol{T}^c_{k,R}\right)\int\left[d^2\Omega_q\right]\int\left[d^2\Omega_r\right] K_{ijk;qr} \\ & + \sum_{(ij)}\frac{1}{2}\left(\boldsymbol{T}^a_{i,L}\boldsymbol{T}^a_{j,L} + \boldsymbol{T}^a_{i,R}\boldsymbol{T}^a_{j,R}\right)\int\left[d^2\Omega_q\right] W^q_{ij}\left[4\beta_0\ln(2W^q_{ij}) + \gamma_1^{\text{cusp}}\right] \\ & - i\pi\sum_{(ij)}\frac{1}{2}\left(\boldsymbol{T}^a_{i,L}\boldsymbol{T}^a_{j,L} - \boldsymbol{T}^a_{i,R}\boldsymbol{T}^a_{j,R}\right)\Pi_{ij}\,\gamma_1^{\text{cusp}}\,. \end{aligned} \tag{2.108}$$

Similar to the one-loop result, each time a real emission is involved, the particle configuration changes. The two-loop anomalous dimension represents the key element to achieve full NLL accuracy. We have written the different parts of the two-loop anomalous dimension in such a way that the collinear singularities manifestly cancel so that we can evaluate the angular integrals in $d = 4$. By expressing the anomalous dimension in the conventional $\overline{\text{MS}}$-scheme we also need to take into account additional contributions due to ϵ-terms in the angular integrals of the iterated one-loop corrections. Finally, the anomalous dimension in the $\overline{\text{MS}}$ scheme is given by

$$\bar{\boldsymbol{\Gamma}}^{(2)} \otimes_2 \mathbf{1} = \boldsymbol{\Gamma}^{(2)} \otimes_2 \mathbf{1} - 2\beta_0\,\boldsymbol{\Gamma}^{(1)} \otimes_\epsilon \mathbf{1} - \left(\boldsymbol{\Gamma}^{(1)} \otimes_2 \boldsymbol{\Gamma}^{(1)} \otimes_\epsilon \mathbf{1} - \boldsymbol{\Gamma}^{(1)} \otimes_\epsilon \boldsymbol{\Gamma}^{(1)} \otimes_2 \mathbf{1}\right)\,. \tag{2.109}$$

In general, the solution of the RG equations is very complicated. This is not surprising since one can show that in the large-N_c approximation, the RG equations at LL are in one-to-one correspondence with the non-linear BMS equation [84]. It is quite remarkable that linear RG equations can capture this very intricate pattern, in particular, even at subleading accuracy. We have written the solution of (2.104) as an expansion

$$\boldsymbol{\mathcal{H}}_m(t) = \boldsymbol{\mathcal{H}}_2(t_0)\,\boldsymbol{U}_{2m}(t_0,t) + \boldsymbol{\mathcal{H}}_2(t_0)\,\Delta\boldsymbol{U}_{2m}(t_0,t) + \cdots\,, \tag{2.110}$$

where the first term $\boldsymbol{U}_{2m}$ represents the LL evolution and the second $\Delta\boldsymbol{U}_{2m}$ captures corrections to the running. Combining one insertion of the two-loop anomalous dimension with matching corrections guarantees NLL accuracy. MC methods are a natural way to implement (2.110) and obtain a

resummed prediction since, analytically, it is not possible to solve (2.110). In the next chapter, we will present our parton shower framework specifically designed to solve the RG equations (2.104) according to (2.110).

Chapter 3

Implementation in MARZILI

In the previous chapter, we have shown how jet cross sections factorize in e^+e^- collisions involving a veto on radiation outside of the jet cones. Following (2.11), the hard radiation, which is constrained inside the jet cones, and the soft radiation, which is essentially unconstrained as indicated in Figure 2.3, are separated and can be calculated independently. We also argued that an intricate pattern of NGLs arises in such cases. These logarithms cannot be resummed by analytical methods, but Dasgupta and Salam showed in their original paper that the leading NGLs can be captured by using an angular dipole shower [82]. Parton showers are typically constructed using a Markovian algorithm, which probabilistically transforms an n-parton state into an $n+1$-parton state. By iterating this procedure from an initial configuration, one obtains events with multiple partons. This is how the shower reproduces emissions across disparate scales and eventually resums large logarithms. Traditionally, this approach is based on factorization properties of QCD amplitudes. On the other hand, in our effective field theory approach, we need to solve RG equations for the hard functions

$$\mu \frac{\mathrm{d}}{\mathrm{d}\mu} \boldsymbol{\mathcal{H}}_m(Q,\mu) = -\sum_{l=m_0}^{m} \boldsymbol{\mathcal{H}}_l(Q,\mu)\, \boldsymbol{\Gamma}_{lm}(Q,\mu)\,, \tag{3.1}$$

where m_0 is the number of partons present in the Born process. By solving (3.1), we evolve the hard functions from an initial hard scale μ_h, where they are free of large logarithms, down to the soft scale μ_s which corresponds to the natural scale of the soft functions, i.e. the scale where the soft functions are free from large logarithmic contributions. Since the anomalous dimension $\boldsymbol{\Gamma}$ is a matrix in the infinite space of particle multiplicities, hard functions $\boldsymbol{\mathcal{H}}_l$ mix under renormalization. As a result, solving (3.1) is complicated, but in the previous chapter we have written the NLL solution (2.110) to the RG equations in a way that is suitable for numerical implementation. In this chapter, we will show that (3.1) can be transformed into recursive equations, which can be solved iteratively by applying parton-shower MC methods. At LL accuracy in the large-N_c limit, our approach is equivalent to the one of Dasgupta and Salam. Since our approach is based on effective field theory techniques, one of the main advantages is that the ingredients needed to systematically improve the logarithmic accuracy are clear. While matching corrections have been implemented in [107], in order to resum the full set of NLL corrections, one insertion of $\boldsymbol{\Gamma}^{(2)}$ is necessary. In this chapter, we introduce MARZILI (Monte-cArlo for the RenormaliZation group Improved calculation of non-global LogarIthms), which is a parton shower framework extending `ngl-resum` [108] beyond LL accuracy.

This chapter is organized as follows, in Section 3.1 we present a pedagogical example of a toy-model RG equation to illustrate the numerical methods. In 3.2, we will explicitly show the

relationship between RG evolution and parton shower MC and then present the LL implementation within MARZILI in Section 3.2.2. Section 3.3 is dedicated to the contributions arising at NLL accuracy. In particular, Section 3.3.3 is concerned with the implementation of $\mathbf{\Gamma}^{(2)}$ in MARZILI. To validate the results obtained using our parton shower framework, we compare our results to GNOLE and PanScales in Section 3.4.

3.1 Toy-model RG equation

To explain the numerical methods we use to solve the RG equations in (3.1), we first study a toy model as a pedagogical introduction. We will consider the following first-order ordinary differential equation for a function $H(t)$

$$\frac{d}{dt}H(t) = -\left(\Gamma^{(1)}_{\text{toy}} + \Delta\Gamma^{(2)}_{\text{toy}}(t)\right) H(t)\,, \tag{3.2}$$

where the constant $\Gamma^{(1)}_{\text{toy}}$ is the leading contribution to a fictitious anomalous dimension and $\Delta\Gamma^{(2)}_{\text{toy}}(t) = \alpha t$ is the subleading contribution, respectively. We will assume that α is a small parameter to expand our solution perturbatively in α. By separating the variables, we can directly integrate (3.2) and obtain the analytical solution

$$H(t) = H(0)e^{-t\Gamma^{(1)}_{\text{toy}}-\frac{1}{2}\alpha t^2} = H(0)\, e^{-t\Gamma^{(1)}_{\text{toy}}}\left[1-\tfrac{1}{2}\alpha t^2 + \mathcal{O}(\alpha^2)\right], \tag{3.3}$$

where we used the specific form of $\Delta\Gamma^{(2)}_{\text{toy}}$ and expanded the solution in α. We will now solve (3.2) order-by-order numerically. While it is easily possible to solve (3.2) numerically using methods such as Runge-Kutta [197, 198], we will adopt a MC approach that can be generalized to solve (3.1). The leading contribution to the solution in (3.3) is given by

$$\widehat{H}_{\text{LL}}(t) \equiv \Gamma^{(1)}_{\text{toy}} \cdot H_{\text{LL}}(t) = H(0)\,\Gamma^{(1)}_{\text{toy}}\, e^{-t\Gamma^{(1)}_{\text{toy}}}\,, \tag{3.4}$$

where we multiplied by $\Gamma^{(1)}_{\text{toy}}$ for convenience. We interpret $\int_0^t dt'\,\Gamma^{(1)}_{\text{toy}}\, e^{-t'\Gamma^{(1)}_{\text{toy}}} = e^{-t\Gamma^{(1)}_{\text{toy}}}$ as a probability. In other words, we can obtain the numerical solution for $\widehat{H}_{\text{LL}}(t)$ by repeatedly drawing random numbers $z \in [0,1]$ and inserting the corresponding weight $w = 1$ into a t-histogram

$$e^{-t\Gamma^{(1)}_{\text{toy}}} = z \quad \Leftrightarrow \quad t = -\tfrac{1}{\Gamma^{(1)}_{\text{toy}}}\ln(z)\,. \tag{3.5}$$

A pseudo-code is provided in Listing 3.1. We show numerical results in Figure 3.1. We can see that the numerical and analytical results are in good agreement. To include corrections due to $\Delta\Gamma^{(2)}_{\text{toy}}$, we use a simplification from (2.102). Since we assume that α is small, the subleading correction can be obtained by exactly inserting $\Delta\Gamma^{(2)}_{\text{toy}}$ once

$$\widehat{H}_{\text{NLL}}(t) \equiv \Gamma^{(1)}_{\text{toy}} \cdot H_{\text{NLL}}(t) = H(0)\int_0^t dt'\,\left[\Gamma^{(1)}_{\text{toy}}\, e^{-t'\Gamma^{(1)}_{\text{toy}}}\right]\cdot\frac{\Delta\Gamma^{(2)}_{\text{toy}}(t')}{\Gamma^{(1)}_{\text{toy}}}\cdot\left[\Gamma^{(1)}_{\text{toy}}\, e^{-(t-t')\Gamma^{(1)}_{\text{toy}}}\right]. \tag{3.6}$$

The interpretation of (3.6) is straightforward. We first carry out a LL evolution, as indicated by the first term inside the brackets, then we evaluate the correction before we restart a LL evolution according to the second bracket. We provide pseudo-code in Listing 3.2. The results for the subleading correction are shown in Figure 3.2. We see a good agreement between the numerical and analytical results.

It is also possible to recover numerically the full result of (3.2) by inserting $\Delta\Gamma^{(2)}_{\text{toy}}$ multiple times. In practice, we repeat the combination of a LL step with a subsequent evaluation of $\frac{\Delta\Gamma^{(2)}_{\text{toy}}(t_{\text{tot}})}{\Gamma^{(1)}_{\text{toy}}}$ until

the total time t_{tot} reaches t. In this way, we recover the full result. The result for the exponentiated result is given in Figure 3.3.

Even though this toy model is much simpler than an actual shower, it offers valuable insights and illustrates the insertion of the subleading correction between two LL evolutions. While the LL evolution is trivial for the toy model, notable complications arise in the next section because we need to take into account additional particles that are generated during the shower evolution, which may act as emitters. As a result, the shower not only needs to integrate over t, but also over the directions of every additional emission. In addition, the angular functions present in the two-loop anomalous dimension are very delicate to sample because of their singular behavior around collinear limits. Therefore, the insertion is particularly challenging.

```
//start evolution from a certain time t0
t_tot = t0;

//generate time step according to probability distribution
delta_t = time(rand(1));

//update time
t_tot += delta_t;

//insert weight into a histogram at t_tot
w = 1.0;
hist.insrt(t_tot,w);
```

Listing 3.1: Pseudo code for the leading-order solution to the toy-model. By iterating many times and averaging over the histograms, we obtain the numerical solution.

```
//set up the shower
t_tot = t0;
w = 1.0;

//make first LL step; thereby generating first time step Δt₁
ll(t_tot,w);

//evaluate the insertion weight at t_ins = t_tot + Δt₁
weight_nll = deltagamma2(t_ins) / gamma1

//make second LL step; here we insert the nll weight
ll(t_ins,weight_nll);
```

Listing 3.2: Pseudo code for the pure NLO correction to the toy-model. By iterating many times and averaging over the histograms, we obtain numerical solutions. More precisely, the histogram filled by `ll(t_tot,w)` yields $\widehat{H}_{\text{LL}}$ while the histogram obtained from `ll(t_ins,weight_nll)` is the NLO contribution $\widehat{H}_{\text{NLL}}$.

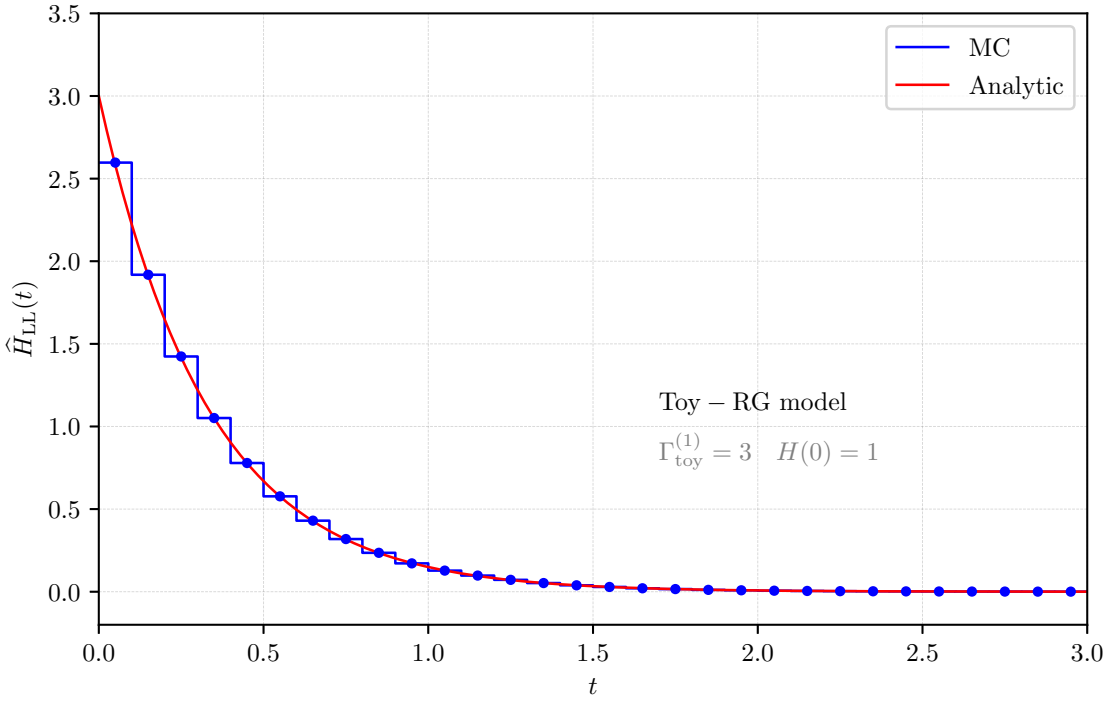

Figure 3.1: Numerical result for $\widehat{H}_{\text{LL}}(t)$.

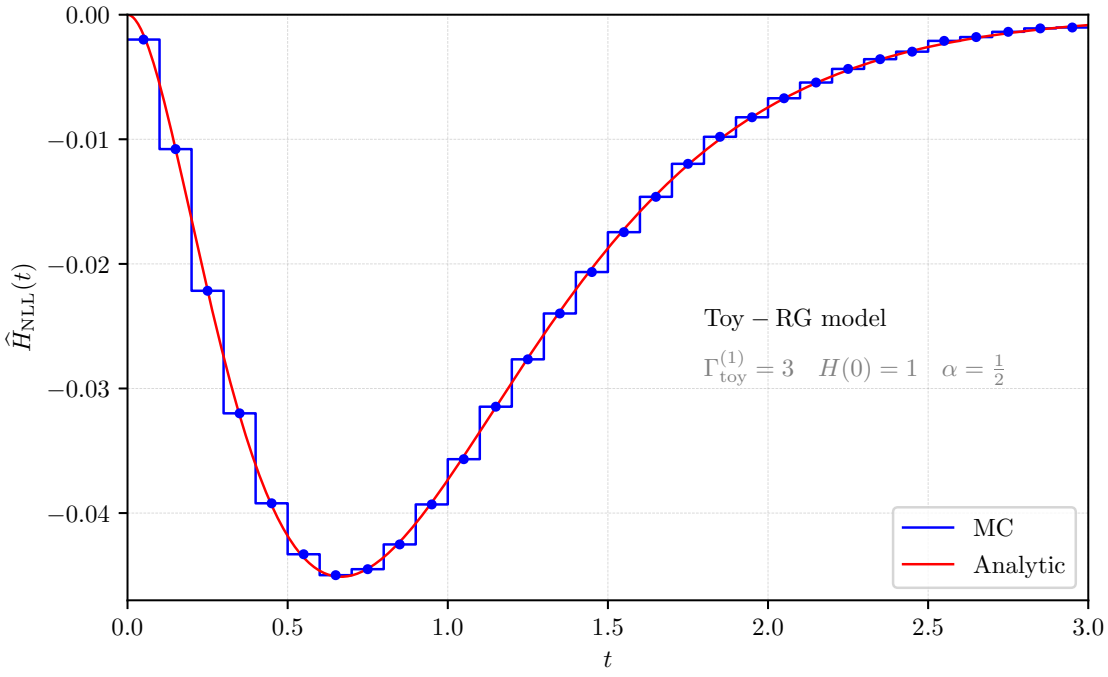

Figure 3.2: Numerical result for $\widehat{H}_{\text{NLL}}(t)$.

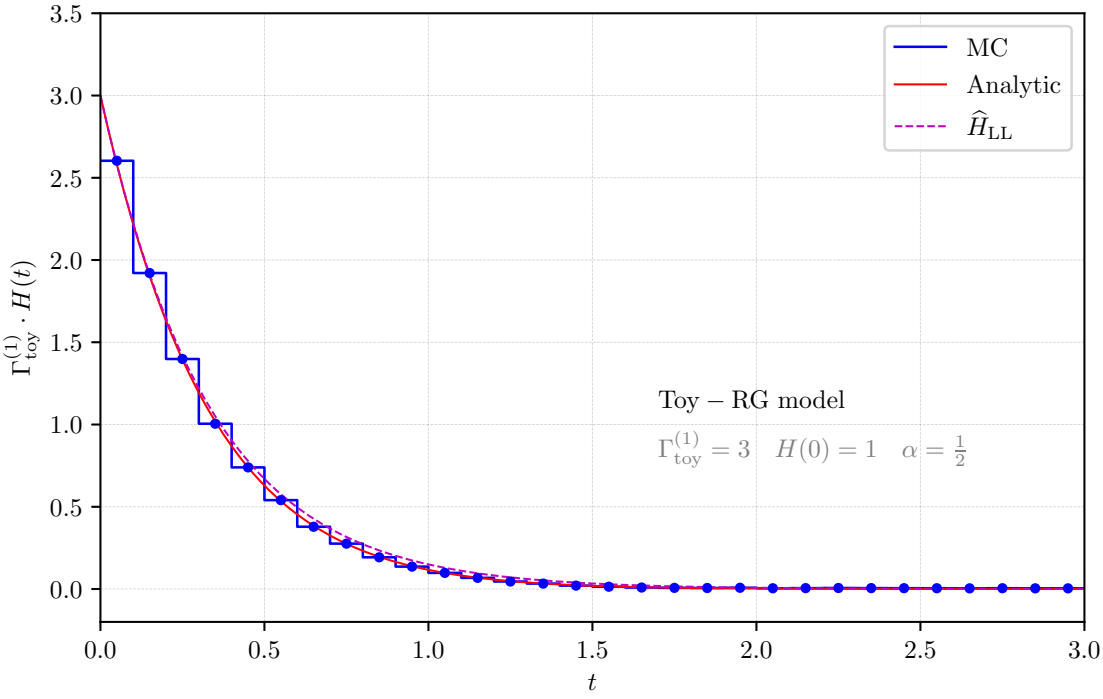

Figure 3.3: Numerical result for $\Gamma^{(1)}_{\mathrm{toy}} \cdot H(t)$. We find for this particular example that the subleading corrections are, in general, small in comparison to the leading contribution, see purple dashed line. As a result, the exponentiated result is almost indistinguishable from $\widehat{H}_{\mathrm{LL}} + \widehat{H}_{\mathrm{NLL}}$.

3.2 Reformulation of RG evolution as a parton shower

In this section, we will investigate the relationship between the RG equations for the hard functions $\boldsymbol{\mathcal{H}}_m$ and parton shower algorithms. Eventually, we will see that these a priori totally different concepts are very much intertwined since the solution to the RG equation can be formulated as a parton shower algorithm [106].

We will first focus on the RG equations at LL accuracy since we explained in Section 2.6 that subleading corrections to the running, which are driven by $\boldsymbol{\Gamma}^{(2)}$, can be taken into account as a perturbation. The virtual entries $\boldsymbol{V}_m$ sit on the diagonal of $\boldsymbol{\Gamma}^{(1)}$, while the real contributions $\boldsymbol{R}_m$ are located just above the diagonal elements, as shown in (2.57). Taking into account this specific form, the RG equations (3.1) simplify to

$$\frac{d}{dt}\,\boldsymbol{\mathcal{H}}_m(t) = \boldsymbol{\mathcal{H}}_m(t)\,\boldsymbol{V}_m + \boldsymbol{\mathcal{H}}_{m-1}(t)\,\boldsymbol{R}_{m-1}\,, \tag{3.7}$$

where we changed variables from μ into t-space, see below (2.97). The homogeneous part of this differential equation is given by an exponential. The full solution is obtained using variation of the constants as

$$\boldsymbol{\mathcal{H}}_m(t) = \boldsymbol{\mathcal{H}}_m(t_0)\,e^{(t-t_0)\boldsymbol{V}_m} + \int_{t_0}^{t} dt'\,\boldsymbol{\mathcal{H}}_{m-1}(t')\,\boldsymbol{R}_{m-1}\,e^{(t-t')\boldsymbol{V}_m}\,. \tag{3.8}$$

The interpretation of this result is straightforward. We evolve from a starting time t_0 to a (later) time t either without any emission, which corresponds to the first term in (3.8), or by starting from an $m-1$ particle configuration and applying $\boldsymbol{R}_m$ at time t' which generates an additional emission. This is typically how parton shower algorithms are presented. We point out that the factor $e^{(t-t')\boldsymbol{V}_m}$ is usually referred to as the Sudakov factor in parton shower jargon. However, in our case the term is not fully appropriate since our problem is single logarithmic. The connection to parton showers becomes even more apparent when writing the solution to the RG equations iteratively. Starting at the high scale μ_h which corresponds to $t = t_0$, only the hard function $\boldsymbol{\mathcal{H}}_{m_0}$ is present, since all hard functions $\boldsymbol{\mathcal{H}}_l$ with $l > m_0$ are supressed by $\alpha_s^{l-m_0}$. The hard function $\boldsymbol{\mathcal{H}}_{m_0}(t_0)$ is free of large logarithms for this scale choice. By using (3.8) iteratively, we generate an entire tower of hard functions at higher multiplicities, here for $t_0 = 0$

$$\begin{aligned}
\boldsymbol{\mathcal{H}}_k(t) &= \boldsymbol{\mathcal{H}}_k(0)\,e^{t\boldsymbol{V}_k}\,,\\
\boldsymbol{\mathcal{H}}_{k+1}(t) &= \int_0^t dt'\,\boldsymbol{\mathcal{H}}_k(t')\,\boldsymbol{R}_k\,e^{(t-t')\boldsymbol{V}_{k+1}}\,,\\
\boldsymbol{\mathcal{H}}_{k+2}(t) &= \int_0^t dt'\,\boldsymbol{\mathcal{H}}_{k+1}(t')\,\boldsymbol{R}_{k+1}\,e^{(t-t')\boldsymbol{V}_{k+2}}\,,\\
\boldsymbol{\mathcal{H}}_{k+3}(t) &= \dots\,.
\end{aligned} \tag{3.9}$$

This shower of successive emissions transforms the entire system from k particles at the hard scale μ_h to a multi-parton state m at the low scale μ_s. This is precisely how the LL evolution $\boldsymbol{U}_{km}$ takes place. To get the resummed cross section, we evolve to the appropriate value of t. In practice, this is determined by the shower time associated with the scales μ_h and μ_s. The LL result for the cross section is

$$\begin{aligned}
\sigma_{\mathrm{LL}}(Q, Q_0) &= \sum_{m=k}^{\infty} \big\langle \boldsymbol{\mathcal{H}}_m(t) \,\hat{\otimes}\, \mathbf{1} \big\rangle \\
&= \Big\langle \boldsymbol{\mathcal{H}}_k(t) + \int \frac{d\Omega_1}{4\pi} \boldsymbol{\mathcal{H}}_{k+1}(t) + \int \frac{d\Omega_1}{4\pi} \int \frac{d\Omega_2}{4\pi} \boldsymbol{\mathcal{H}}_{k+2}(t) + \dots \Big\rangle\,,
\end{aligned} \tag{3.10}$$

where we have taken into account that the leading-order soft function is trivial $\boldsymbol{\mathcal{S}}_m = \mathbf{1}$. The angular integrals over the directions of the additional emissions, which are generated while showering, have been written out explicitly in (3.10). To obtain a resummed cross section, we need to integrate both over the angles of the emissions as well as over all possible times. Since it is challenging to perform the angular integrations for an increasing number of emissions, we resort to numerical MC methods. There is a second challenge in that directly implementing equations (3.9) is currently out of reach because the hard functions and the anomalous dimension are matrices in the color space of the involved partons. This space grows very rapidly with an increasing number of emissions, therefore performing the color trace is complicated. While there is progress to include subleading color effects in parton showers [88, 113, 199–207], numerical methods are numerically very demanding. In this work, we will use the large-N_c limit. At large N_c, the amplitude corresponds to a set of color dipoles. Effectively, in this construction the emissions only arise between neighboring legs and we use the simple rule

$$\boldsymbol{T}_i \cdot \boldsymbol{T}_j \to -\frac{N_c}{2}\delta_{i,j\pm1}\,\mathbf{1}\,, \tag{3.11}$$

to replace the scalar product of color generators. Inserting (3.11) into the one-loop anomalous dimension, we obtain

$$\boldsymbol{R}_m = +\,4N_c\,\frac{n_{ij}}{n_{iq}n_{jq}}\,\theta_{\text{in}}(n_q) \equiv 4N_c W_{ij}^q\,\theta_{\text{in}}(n_q)\,, \tag{3.12}$$

$$\boldsymbol{V}_m = -\,4N_c\int\frac{\mathrm{d}\Omega_q}{4\pi}\,W_{ij}^q \;\equiv\; -4N_c\int[\mathrm{d}^2\Omega_q]\,W_{ij}^q\,, \tag{3.13}$$

in the large-N_c limit. For each loop or additional real emission we add a factor of N_c. When the real emission operator $\boldsymbol{R}_m$ acts on the amplitude, e.g. by acting on the legs i and j, and increases the number of legs, the corresponding dipole (ij) is split into two new ones. It is evident that individually both $\boldsymbol{R}_m$ and $\boldsymbol{V}_m$ suffer from collinear divergences. Even though these singularities cancel in physical observables, they need to be regularized separately in our shower since according to (3.8) we exponentiate the virtual corrections. Perhaps the most natural way to regularize the collinear singularity is by imposing a cutoff in the laboratory (LAB) frame through

$$W_{ij}^q \to W_{ij}^q\,\theta(n_q\cdot n_i-\lambda^2)\,\theta(n_q\cdot n_j-\lambda^2)\,, \tag{3.14}$$

both in $\boldsymbol{V}_m$ and $\boldsymbol{R}_m$. However, as we will see in the next section, it turns out to be numerically more advantageous to impose a cutoff on the rapidity $\hat{y}$ in the center-of-mass (COM) frame of the dipole (ij).

In this section, we have shown that the solution of the RG equations (3.1) is a parton shower algorithm, which is quite fascinating given the fact that we started our analysis from a completely different perspective. Even though this is not a general-purpose shower, we are guaranteed to obtain the correct pattern of (non-global) logarithms for a specific class of observables since we numerically solve RG equations which has been obtained from a factorization theorem. We would like to emphasize that our non-global shower (3.9) differs in some important aspects from standard Monte-Carlo showers. For instance, unlike general-purpose showers, we do not conserve momentum because we assume the radiation to be soft so that we systematically expand away small momenta. In addition, since the evolution naturally generates logarithms of the energy, it is only necessary to generate new directions for real emissions. In the next section, we will carefully outline the LL implementation of our MC procedure in MARZILI. We will follow closely [106, 108].

3.2.1 Details of the LL implementation in MARZILI

Starting from the iterative solution (3.9) of the RG equations, we will carefully derive a MC algorithm in this section. However, before doing so, we need to specify the collinear cutoff we are using to regulate $\boldsymbol{V}_m$ and $\boldsymbol{R}_m$. The angular integrals $I(\lambda, n_i, n_j)$ involving a cutoff take the form

$$I(\lambda, n_i, n_j) = \int \left[d^2\Omega_q\right] \frac{n_i \cdot n_j}{n_i \cdot n_q \, n_q \cdot n_j} \, \Theta_{\text{cutoff}}(n_i, n_j, n_q, \lambda) \,, \tag{3.15}$$

where we specify the collinear cutoff $\lambda^2 = 1 - \tanh(\eta_c)$ in terms of a rapidity η_c. The function $\Theta_{\text{cutoff}}(n_i, n_j, n_q, \lambda)$ dictates the form of the cutoff, e.g. to put small cones around the particles i, j in the LAB frame we would use $\Theta_{\text{cutoff}}(n_i, n_j, n_q, \lambda) = \theta(n_q \cdot n_i - \lambda^2)\,\theta(n_q \cdot n_j - \lambda^2)$. To compute (3.15) it makes sense to transform into the COM of the (ij)-dipole since the integrand becomes constant

$$I(\lambda, M) = \int_0^{2\pi} \frac{d\hat{\phi}_q}{2\pi} \int_{-\infty}^{\infty} d\hat{y}_q \; \Theta_{\text{cutoff}}(\hat{y}_q, \lambda) \,, \tag{3.16}$$

where $M^2 = 2n_i \cdot n_j$ is the invariant mass of the dipole system (ij), $\beta = \sqrt{1 - M^2/4}$ and the cutoff in the COM frame $\Theta_{\text{cutoff}}(\hat{y}_q, \lambda)$. The new integration variables are the azimuthal angle $\hat{\phi}_q$ and the rapidity $\hat{y}_q$ of the emission n_q in the COM frame. We impose a cutoff only on the rapidity $\hat{y}_q$ so that the angular integral becomes

$$\begin{aligned} I(\lambda, M) &= \int_0^{2\pi} \frac{d\hat{\phi}_q}{2\pi} \int_{-\infty}^{\infty} d\hat{y}_q \; \theta\left[\frac{M^2(1 - \tanh \hat{y}_q)}{4(1 - \beta \operatorname{sech} \hat{y}_q)} - \lambda^2\right] \\ &= \int_0^{2\pi} \frac{d\hat{\phi}_q}{2\pi} \int_{-y_{\max}}^{y_{\max}} d\hat{y}_q = 2 y_{\max} \,, \end{aligned} \tag{3.17}$$

where $y_{\max} = \ln\left(\beta + \sqrt{\alpha + \beta^2}\right)$ with $\alpha = (M^2 - 2\lambda^2)/(2\lambda^2)$. For a back-to-back configuration $M^2 = 4$ and the maximum simplifies to $y_{\max} = \eta_c$. We point out that the choice of the collinear cutoff is not unique. The cutoff introduced in (3.17) is the one used by Dasgupta and Salam in [82] and turns out to be numerically efficient.

A fundamental ingredient of our shower is a list of m vectors $\{\underline{n}\} = \{n_1, n_{i_1}, \ldots, n_{i_{m-2}}, n_2\}$ describing an event E at time t with weight w. This list of vectors defines color dipoles with which we associate a virtual correction

$$V_E = V_{1 i_1} + V_{i_1 i_2} + \cdots + V_{i_{m-2} 2} \,, \tag{3.18}$$

where we use

$$V_{ij} = \int \left[d^2\Omega_l\right] R^l_{ij} = 4N_c \int \left[d^2\Omega_l\right] W^l_{ij} \, \Theta_{\text{cutoff}}(\hat{y}_l, \lambda) \,, \tag{3.19}$$

with (3.17) to evaluate V_{ij}. We note in passing that while $\boldsymbol{V}_m$ is negative, the quantity V_{ij} is strictly positive. The time steps in our LL shower are computed according to the distribution

$$\mathcal{P}_E(\Delta t) = V_E \, e^{-V_E \Delta t} \,, \tag{3.20}$$

after which an additional parton is generated and added to the event. We will use a shorthand notation $\mathcal{P}_n$ to denote a probability distribution corresponding to an event E with n partons.

To present the MC algorithm, we will work with the concrete example process of the interjet energy flow in e^+e^-. In this case, the leading-order hard function $\boldsymbol{\mathcal{H}}_2(t_0)$ involves two back-to-back

partons along the directions $n_1 = (1,0,0,1)$ and $n_2 = (1,0,0,-1)$. Therefore, we set $k = 2$ in (3.9) so that the resummed cross section takes the form

$$\widehat{\sigma}_{\mathrm{LL}}(t_0,t) = \widehat{\mathcal{H}}_2(t) + \int \left[d^2\Omega_3\right] \widehat{\mathcal{H}}_3(t,n_3) + \int \left[d^2\Omega_3\right] \int \left[d^2\Omega_4\right] \widehat{\mathcal{H}}_4(t,n_3,n_4) + \cdots , \tag{3.21}$$

where we have changed the normalization for the cross section $\widehat{\sigma}_{\mathrm{LL}}(t_0,t) = \frac{V_{12}}{\sigma_0}\sigma_{\mathrm{LL}}(Q,Q_0)$ and analogously for the hard functions $\mathcal{H}_m$, as indicated with the hat. The first term $\widehat{\mathcal{H}}_m$ is a purely virtual contribution since no additional particle is created during the evolution from $t_0 = 0$ to t. By changing the normalization, i.e. multiplying with V_{12}, we re-interpret the hard function in terms of a probability density

$$\widehat{\mathcal{H}}_2(t) = \mathcal{P}_2(t) = V_{12}\, e^{-t\, V_{12}} , \tag{3.22}$$

because the integral $\int_0^\infty dt\, \widehat{\mathcal{H}}_2(t) = 1$. According to (3.22), $\widehat{\mathcal{H}}_2(t)$ is the probability that no emission is produced during the evolution. The second term $\widehat{\mathcal{H}}_3(t)$ in (3.21) involves exactly one emission. More precisely, $\widehat{\mathcal{H}}_3(t)$ corresponds to the situation where the initial two-particle configuration evolves until t', at which time a new particle is created along the direction n_3. After this emission, the three-particle system evolves further to t, without any additional emissions. Concretely, we obtain

$$\begin{aligned}\widehat{\mathcal{H}}_3(t) &= \int_0^t dt'\, \widehat{\mathcal{H}}_2(t')\, R_{12}^3\, e^{-(t-t')V_3} , \\ &= \int_0^t dt'\, \mathcal{P}_2(\Delta t)\, \frac{R_{12}^3}{V_2}\, \frac{V_2}{V_3}\, \mathcal{P}_3(\Delta t') , \end{aligned} \tag{3.23}$$

where the virtual part involving the new emission is $V_3 = V_{13} + V_{32}$ according to (3.18), $\Delta t = t'$ and $\Delta t' = t - t'$. To get from the first line to (3.23) we introduced some factors to retrieve an emission probability $\mathcal{P}_3$. We call the factor $\frac{R_{12}^3}{V_2}\frac{V_2}{V_3}$ the weight of the emission. In practice, we insert this weight into a t-histogram and continue the evolution according to $\mathcal{P}_3$. The next term in the evolution is $\widehat{\mathcal{H}}_4(t)$. Previously, there was only one dipole capable of emitting a new particle. However, with three particles present, there are now two dipoles that can emit, resulting in the hard function $\widehat{\mathcal{H}}_4(t)$ having two components

$$\widehat{\mathcal{H}}_4(t) = \widehat{\mathcal{H}}_4^{(1)}(t) + \widehat{\mathcal{H}}_4^{(2)}(t) . \tag{3.24}$$

The first term $\widehat{\mathcal{H}}_4^{(1)}(t)$ in (3.24) arises due to an emission from the dipole formed by n_1 and n_3, while $\widehat{\mathcal{H}}_4^{(2)}(t)$ corresponds to inserting a new parton between n_3 and n_2. In fact, starting from $\widehat{\mathcal{H}}_4(t)$, every hard function is a sum consisting of all the possible dipoles that could generate an emission. To rearrange (3.24) in a similar way as (3.23), we insert some factors and rearrange them accordingly

$$\widehat{\mathcal{H}}_4(t) = \int_0^t dt''\, \widehat{\mathcal{H}}_3(t'') \left[\frac{R_{13}^4}{V_{13}}\frac{V_{13}}{V_3}\frac{V_3}{V_4^{(1)}}\mathcal{P}_4^{(1)}(\Delta t'') + \frac{R_{32}^4}{V_{32}}\frac{V_{32}}{V_3}\frac{V_3}{V_4^{(2)}}\mathcal{P}_4^{(2)}(\Delta t'') \right] , \tag{3.25}$$

where $V_4^{(1)} = V_{14} + V_{43} + V_{32}$, $V_4^{(2)} = V_{13} + V_{34} + V_{42}$ and $\Delta t'' = t - t''$. In comparison to (3.23) additional factors $\frac{V_{13}}{V_3}$ and $\frac{V_{32}}{V_3}$ emerge. A smart way of implementing (3.25) is to use the probabilistic nature of the factors present in the integrand. To be specific, we consider the first term

$$\widehat{\mathcal{H}}_4^{(1)}(t) = \int_0^t dt''\, \widehat{\mathcal{H}}_3(t'')\, \frac{V_{13}}{V_3}\frac{R_{13}^4}{V_{13}}\frac{V_3}{V_4^{(1)}}\, \mathcal{P}_4^{(1)}(\Delta t'') . \tag{3.26}$$

Note that both $\frac{V_{13}}{V_3} < 1$ and $\frac{V_3}{V_4^{(1)}} < 1$ using the collinear cutoff in the COM frame. This means that in order to evaluate this integral we can interpret $\frac{V_{13}}{V_3}$ as the probability of choosing the dipole formed by n_1 and n_3. Once we have chosen the dipole, we generate an additional emission along the direction n_4 to which we associate the weight $w = \frac{R_{13}^4}{V_{13}}$. To implement the factor $\frac{V_3}{V_4^{(1)}}$ we throw a random number z and throw the event away with if $z > \frac{V_3}{V_4^{(1)}}$. As we argued at the beginning of this section, it makes sense to generate the new emission in the back-to-back frame of the dipole. Since the shower will be integrating over all possible directions of the emission, this means that we will integrate R_{13}^4

$$\int \left[d^2\Omega_4\right] R_{13}^4 \, \Theta_{\text{cutoff}}(\hat{y}_4, \lambda) \tag{3.27}$$

with the collinear cutoff which is exactly the same as for the virtual term V_{13}. Changing variables according to (3.17), the weight w becomes constant and we obtain unweighted events, which is a great advantage from a numerical point of view. Moving to higher multiplicities, i.e. $\widehat{\mathcal{H}}_5(t)$, $\widehat{\mathcal{H}}_6(t)$ etc., no further complications arise and the algorithm outlined above can be used. A pictorial representation of our shower can be found in Figure 3.4. Once the shower terminates, which is indicated by the final soft emission entering the veto region, we restart another shower with the same initial partons described by leading-order hard function $\boldsymbol{\mathcal{H}}_2(t_0)$. By repeating this procedure numerous times and averaging over the outcome, we obtain a numerical result for the resummed cross section (3.21).

As explained at the beginning of this section, once a dipole (ij) has been chosen according to a certain probability, it is very convenient to evaluate (3.15) in the COM frame of the dipole. To construct the boost for the massless particles, we rely on the Lorentz transformation [208]

$$\Lambda^\mu_\nu(n, \tilde{n}) = \delta^\mu_\nu - \frac{2}{\Delta^2}\Delta^\mu \Delta_\nu, \tag{3.28}$$

with $\Delta_\mu = n_\mu - \tilde{n}_\mu$ being the difference of two light-like vectors n_μ and $\tilde{n}_\mu$. The Lorentz transformation (3.28) is a rotation[2] together with an inversion $\vec{n} \to -\vec{n}$. One easily verifies that $\Lambda^\mu_\nu(n, \tilde{n})\, n^\nu = \tilde{n}^\mu$, so the transformation maps $n_\mu \to \tilde{n}_\mu$. Furthermore, we point out that $\Lambda^\mu_\rho \Lambda^\rho_\nu = \delta^\mu_\nu$ and $\det(\Lambda) = -1$. In order to construct the boost of two arbitrary light-like vectors along n_i and n_j into a frame in which these momenta are back-to-back along the z-axis, we will apply Λ^μ_ν three times. Starting from n_i and n_j in the lab frame (see Figure 3.5, top), we first rotate the dipole such that its total three momentum $n_i + n_j$ points solely along the y-direction (Figure 3.5 bottom). Then, we rotate the dipole around y so that it aligns back-to-back with the z-axis (Figure 3.6, top), and finally, we boost along into the center-of-mass frame (Figure 3.6, bottom). We will outline the construction in more detail in the following. The first and second steps are both carried out using a rotation according to (3.28). To get to

$$n_i' = \left(1, 0, \beta, \tfrac{M}{2}\right) , \tag{3.29}$$

$$n_j' = \left(1, 0, \beta, -\tfrac{M}{2}\right) , \tag{3.30}$$

with $M = 2n_i \cdot n_j$ and $\beta = \sqrt{1 - M^2/4}$, we first rotate the sum of the directions of the dipole $n_i + n_j$ onto the y-axis using

$$r_1 = \Lambda\left(n_i + n_j, n_i' + n_j'\right). \tag{3.31}$$

[2]Only if $n^0 = \tilde{n}^0$

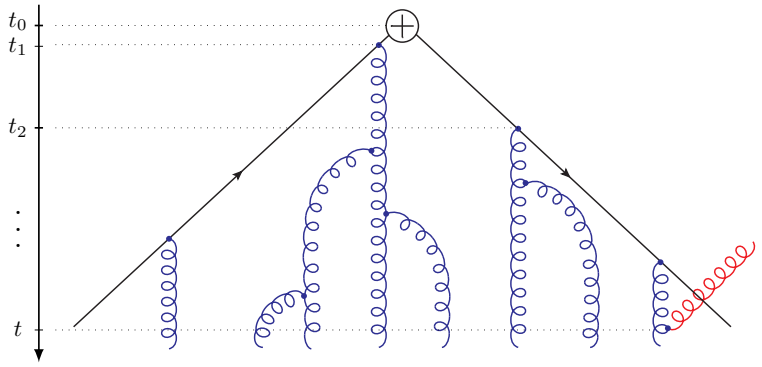

Figure 3.4: Pictorial representation of the LL shower. Black lines represent the initial hard partons in $\boldsymbol{\mathcal{H}}_2(t_0)$. Blue lines denote hard emissions inside the jets generated by the shower evolution. The red line depicts a soft emission into the veto region, which terminates the shower.

The next step is to apply a rotation around the y-axis such that the x-component vanishes and we obtain alignment with the z-axis. This is achieved using

$$r_2 = \Lambda\left(r_1 \cdot n_i, n_i'\right) . \tag{3.32}$$

Applying succesively the rotation matrices r_1 and r_2 we obtain $n_i' = r_2 \cdot r_1 \cdot n_i$, respectively $n_j' = r_2 \cdot r_1 \cdot n_j$. Finally, we apply a boost along the y-axis to transform n_i', n_j' into the center-of-mass frame,

$$\hat{n}_i = \tfrac{M}{2}\,(1,0,0,1) = b \cdot n_i' \,, \tag{3.33}$$

$$\hat{n}_j = \tfrac{M}{2}\,(1,0,0,-1) = b \cdot n_j' \,, \tag{3.34}$$

again using (3.28) to construct the specific boost $b = \Lambda(n_i' + n_j', \hat{n}_i + \hat{n}_j)$. In conclusion, we can write the transformation L from the lab frame into a frame where $\hat{n}_i$ and $\hat{n}_j$ are back-to-back and aligned along the z-axis as the product

$$L = b \cdot r_2 \cdot r_1 \,, \tag{3.35}$$

for massless particles. In practice, we directly generate the new emission $\hat{n}_q$ in the back-to-back frame of the emitting dipole and then transform the emission back into the lab frame, i.e. $n_q = L^{-1} \cdot \hat{n}_q$ with $L^{-1} = r_1 \cdot r_2 \cdot b$.

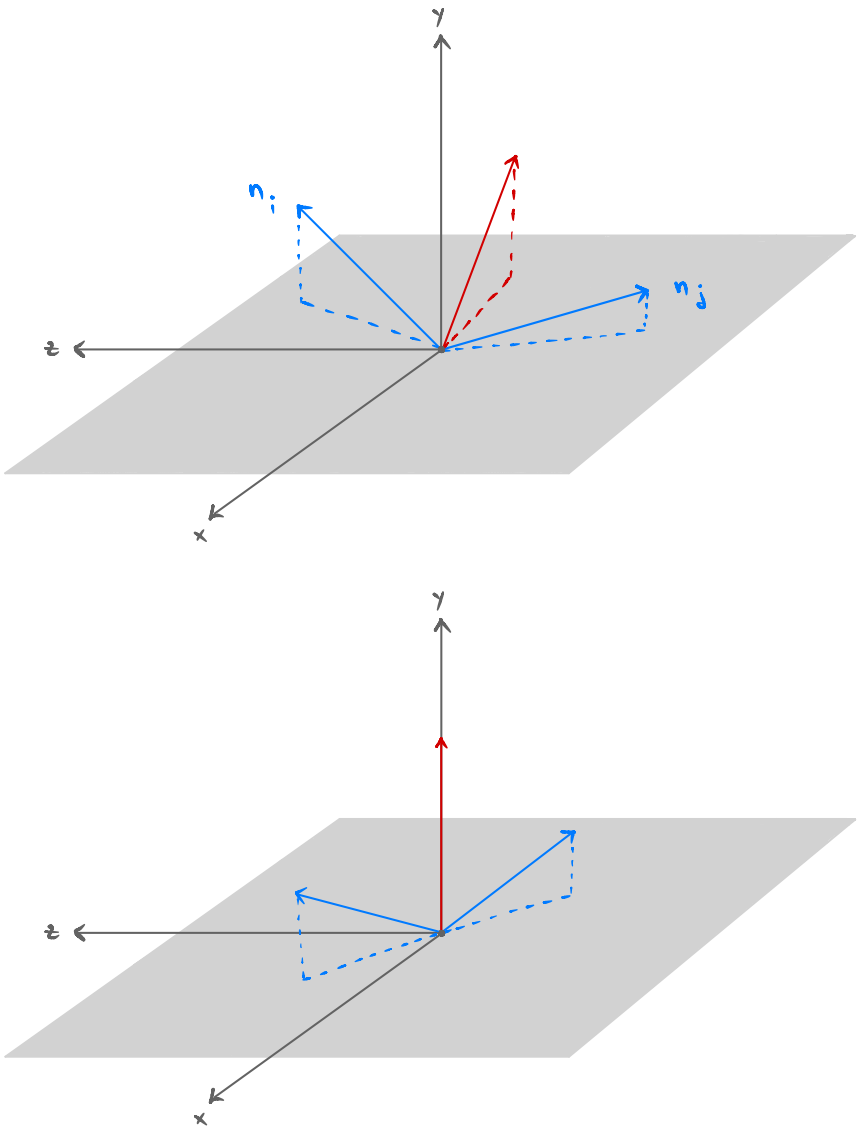

Figure 3.5: Upper figure: Dipole in the lab frame. In blue we denote the directions along n_i and n_j while in red we show the direction of $n_i + n_j$. Lower figure: Applying the first rotation r_1, the red arrow is aligned with the y-axis.

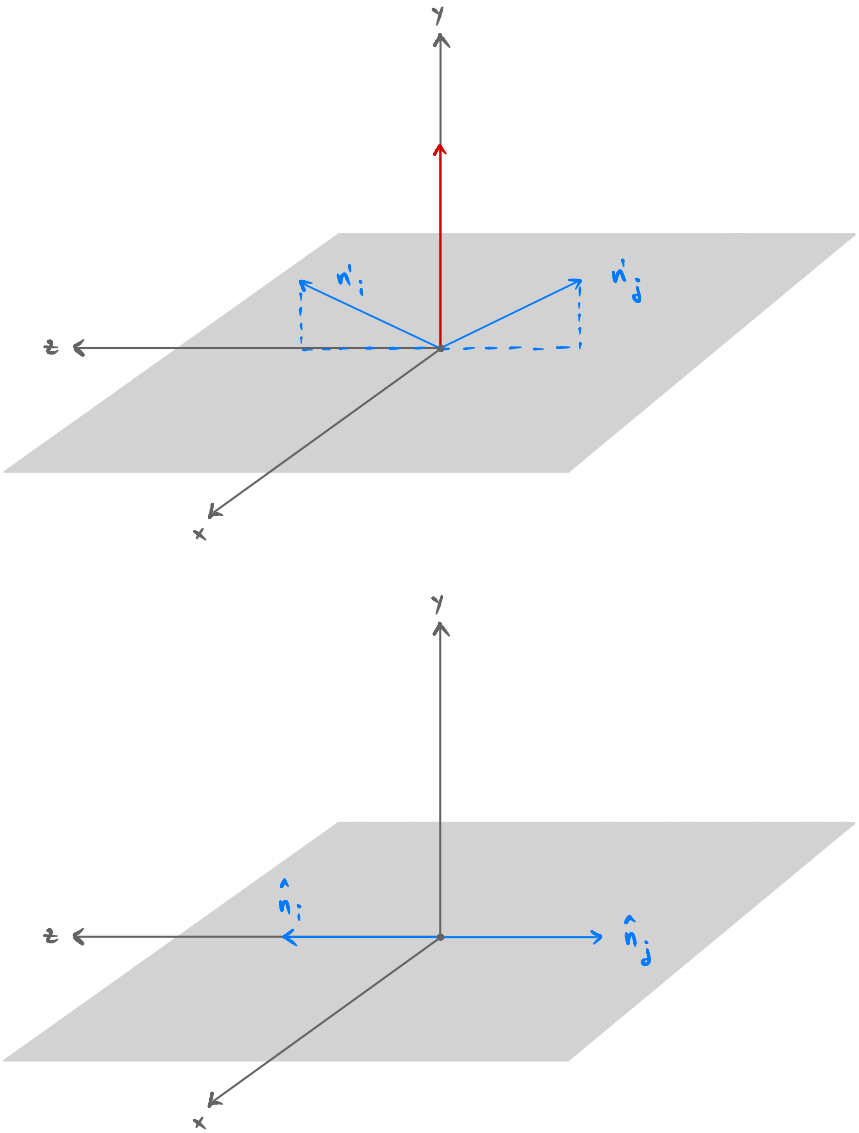

Figure 3.6: Upper figure: After rotation r_2 the dipole is aligned with the z-axis. Lower figure: Back-to-back configuration of the dipole after applying the boost b.

3.2.2 Qualitative discussion of NGLs

In this section, we analyze the numerical impact of NGLs at LL accuracy. To do so, we use the LL implementation in MARZILI, which is largely based on [106,108]. The observable we will investigate is the canonical example where NGLs arise, namely the interjet energy flow in e^+e^- annihilation into two jets.

To understand the phenomenological implications of secondary emissions into the veto region that give rise to the NGLs, it is interesting to compare the results with the full non-global structure versus primary emissions. In this context, primary emissions are soft gluons arising entirely from the two initial Wilson lines which we associate with the two original hard particles. An illustration of these primary emissions is given in Figure 2.2. We show results for this comparison in Figure 3.7. We immediately notice two things. First, taking $t = 0.05$ as a reference value, neglecting non-global effects overestimates the cross section $\sigma(t)$ by roughly 30%. At higher t-values this becomes even more dramatic. Second, while the green histogram is a straight line (on a logarithmic scale), the blue clearly is not. As a consequence, we conclude that NGLs do not exponentiate.

The contribution from primary emissions as shown in green in Figure 3.7 can be calculated analytically. At first order in α_s, the global contribution is due to an incomplete cancellation between real and virtual corrections

$$\sigma_{\text{GL}}^{(1)} = -8C_F \frac{\alpha_s}{4\pi} \int_{Q_0}^{Q} \frac{d\mu}{\mu} \int_{-\frac{\Delta Y}{2}}^{\frac{\Delta Y}{2}} dy \int \frac{d\phi}{2\pi} = -8C_F \Delta Y\, t\,, \tag{3.36}$$

where $t = \frac{\alpha_s}{4\pi} \ln \frac{Q}{Q_0} + \mathcal{O}\big(\alpha^2\big)$ includes running coupling effects. To promote (3.36) to all orders is straightforward since we only need to exponentiate $\sigma_{\text{GL}}^{(1)}$

$$\frac{\sigma_{\text{GL}}^{\text{LL}}}{\sigma_0} = \exp\big(-8C_F \Delta Y\, t\big)\,. \tag{3.37}$$

From our effective field theory point of view, these global logarithms arise directly from $\boldsymbol{\mathcal{S}}_2$, while the NGLs emerge from complicated multi-Wilson line operators. To obtain the global logarithms, we prevent any additional emission from acting itself as an emitter, which means that we decouple the one-loop anomalous dimension $\boldsymbol{\Gamma}^{(1)}$ matrix and configurations with higher particle multiplicities never occur. In Figure 3.8 we show the analytical result in red. The leading global logarithm in (3.36) can be read off from the NLO cross section σ_{NLO} in (2.47) or (2.48).

We can also calculate analytically the leading non-global logarithm for the same observable. This contribution is a two-loop correction and takes the form

$$\frac{\sigma_{\text{NGL}}^{\text{LL}}}{\sigma_0} = 4\,C_F C_A \left[-\frac{2\pi^2}{3} + 4\,\text{Li}_2\left(e^{-2\Delta y}\right)\right] t^2. \tag{3.38}$$

We obtain this contribution directly from (2.51) that arises from a hard gluon emission inside one of the cone jets, which subsequently emits a soft gluon inside the gap. We have added this contribution to the global result, see cyan curve in Figure 3.8. We see that including this correction decreases the global prediction such that around $t \approx 0.02$ the cyan curve is closer to the all-order result. However, beyond $t \approx 0.02$ the fixed-order result breaks down and it is necessary to include higher-order terms. As already emphasized previously in this section, since NGLs do not exponentiate, we cannot naively exponentiate (3.38) to obtain the all-order result.

Let us briefly summarize the discussion in this section. We have implemented the one-loop anomalous dimension in MARZILI to resum the leading NGLs. To make a numerical implementation feasible, we expanded the anomalous dimension in the large-N_c limit. The results we obtain are

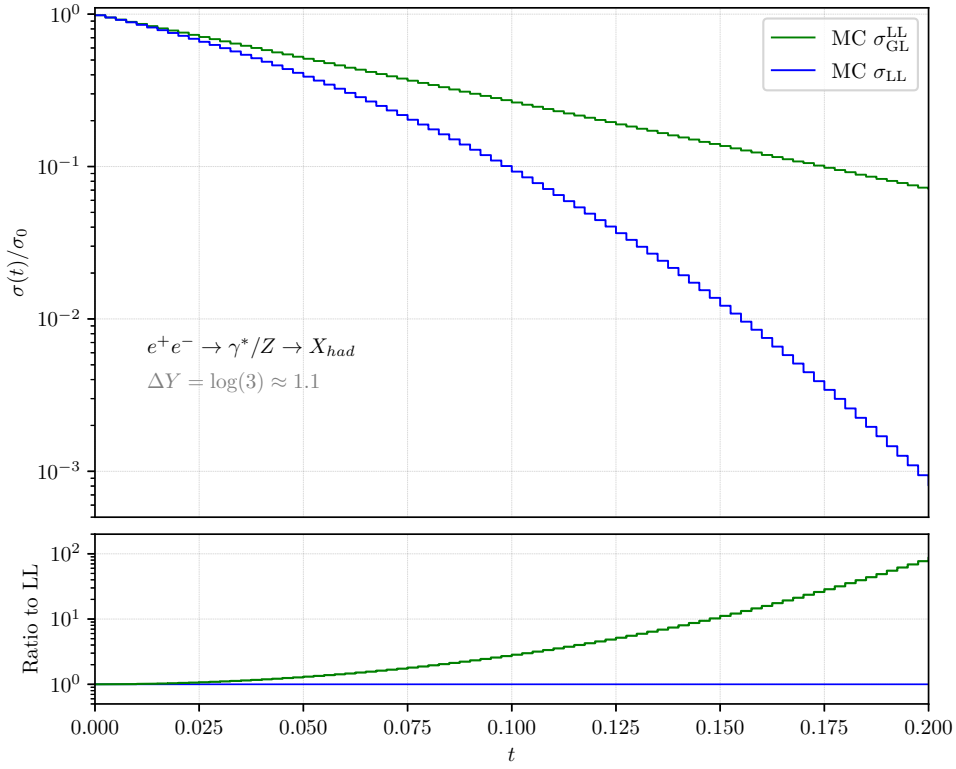

Figure 3.7: Gap fraction for two different patterns of radiation. The blue histogram represents the full result, including the NGLs in the large-N_c limit, while the green histogram only takes into account primary emissions. We also refer to these primary emissions as global, hence the notation $\sigma_{\mathrm{GL}}^{\mathrm{LL}}$. The lower panel shows the relative comparison between the full result and primary emissions.

compatible with the predictions from the dipole shower by Dasgupta and Salam [82]. Using our shower, we have carried out a qualitative analysis for the interjet energy flow to quantify the impact of NGLs. We find that neglecting NGLs overestimates the cross section significantly. When converting the from the t-space to the energy Q_0, we will see in Chapter 4 that the LL results suffer from large uncertainties from the scale variation. To improve our predictions, we need to extend our resummation to NLL accuracy. We have presented the analytical ingredients, more precisely matching correction in Sections 2.3, 2.4 and, most importantly, the two-loop anomalous dimension in Section 2.6.2. In the next sections, we will carefully explain how each ingredient is implemented in our framework and then present phenomenological results.

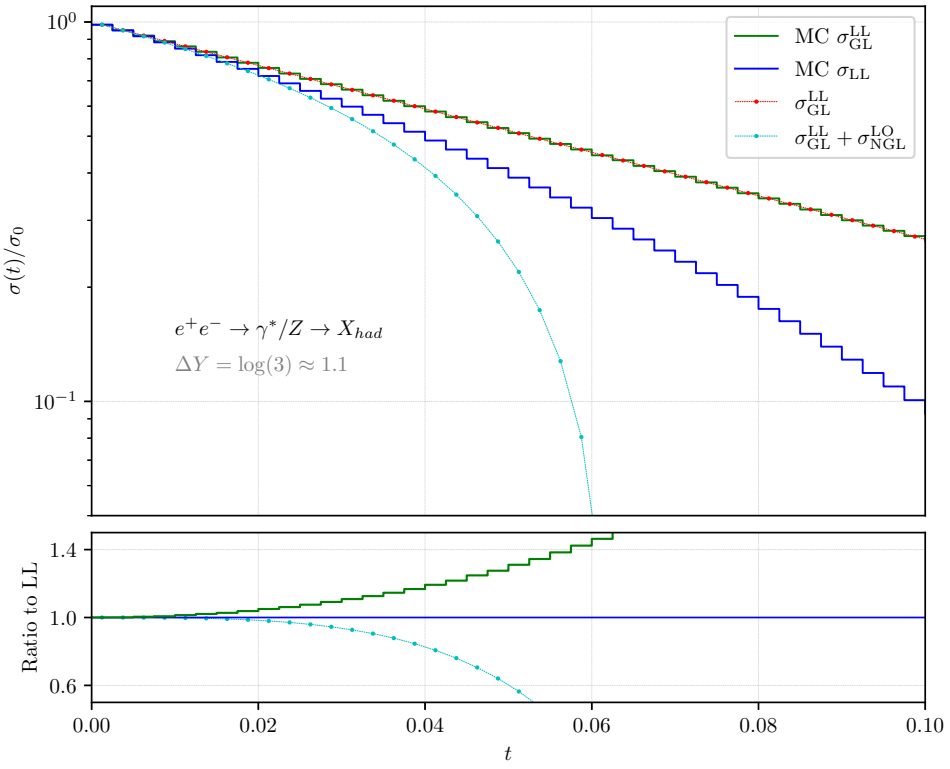

Figure 3.8: Comparison between analytical and numerical results for the gap fraction. In red we show the global contribution obtained by exponentiating the fixed-order result. In cyan we add the leading non-global contribution. The lower panel shows results relative to the full LL.

3.3 NLL contributions in MARZILI

To extend previous results to NLL, we need to implement one-loop matching corrections and include the two-loop anomalous dimension in the shower evolution. The perturbative expansion of the matching corrections was introduced in (2.13)–(2.15). Using this notation we can write the resummed cross section at NLL accuracy

$$\begin{aligned}\frac{\sigma^{\mathrm{NLL}}(Q,Q_0)}{\sigma_0} &= \sum_{m=2}^{\infty}\left\langle \boldsymbol{\mathcal{H}}_2^{(0)}(\{n_1,n_2\},Q,\mu_h)\otimes \boldsymbol{U}_{2m}(\{\underline{n}\},\mu_s,\mu_h)\,\hat{\otimes}\,\mathbf{1}\right\rangle \\ &+\frac{\alpha_s(\mu_h)}{4\pi}\sum_{m=2}^{\infty}\left\langle \boldsymbol{\mathcal{H}}_2^{(1)}(\{n_1,n_2\},Q,\mu_h)\otimes \boldsymbol{U}_{2m}(\{\underline{n}\},\mu_s,\mu_h)\,\hat{\otimes}\,\mathbf{1}\right\rangle \\ &+\frac{\alpha_s(\mu_h)}{4\pi}\sum_{m=3}^{\infty}\left\langle \boldsymbol{\mathcal{H}}_3^{(1)}(\{n_1,n_2,n_3\},Q,\mu_h)\otimes \boldsymbol{U}_{3m}(\{\underline{n}\},\mu_s,\mu_h)\,\hat{\otimes}\,\mathbf{1}\right\rangle \\ &+\frac{\alpha_s(\mu_s)}{4\pi}\sum_{m=2}^{\infty}\left\langle \boldsymbol{\mathcal{H}}_2^{(0)}(\{n_1,n_2\},Q,\mu_h)\otimes \boldsymbol{U}_{2m}(\{\underline{n}\},\mu_s,\mu_h)\,\hat{\otimes}\,\boldsymbol{\mathcal{S}}_m^{(1)}(\{\underline{n}\},Q_0,\mu_s)\right\rangle \\ &+\sum_{m=2}^{\infty}\left\langle \boldsymbol{\mathcal{H}}_2^{(0)}(\{n_1,n_2\},Q,\mu_h)\otimes \Delta\boldsymbol{U}_{2m}(\{\underline{n}\},\mu_s,\mu_h)\,\hat{\otimes}\,\mathbf{1}\right\rangle,\end{aligned} \tag{3.39}$$

where we used that the leading-order soft function is given by the unity $\mathbf{1}$ in color space. The first line in (3.39) is the LL result discussed thoroughly in Section 3.2.2. The second and third lines represent hard corrections, which are discussed in Section 3.3.1, while the fourth line denotes one-loop correction to the soft function, see Section 3.3.2. Finally, the last line represents the insertion of the two-loop anomalous dimension, which is the most difficult subleading contribution. The implementation of the single insertion is discussed in Section 3.3.3.

3.3.1 Hard corrections

In this section, we discuss the implementation of the hard functions derived in Section 2.3 into the parton shower framework MARZILI. We will start the discussion with the real emission contributions. We can rewrite the angular integral involving $\boldsymbol{\mathcal{H}}_3^{(1)}$ as

$$\left\langle \boldsymbol{\mathcal{H}}_3^{(1)}(\{\underline{n}\},Q,\mu_h)\otimes \widehat{\boldsymbol{\mathcal{S}}}_3(\{\underline{n}\},\mu_h)\right\rangle = \int_0^1 du\int_0^1 dv\int_0^{2\pi}\frac{d\varphi}{2\pi}\left\langle \boldsymbol{\mathcal{H}}_3^{(1)}(u,v,\varphi,Q,\mu_h)\,\widehat{\boldsymbol{\mathcal{S}}}_3(u,v,\varphi,\mu_h)\right\rangle, \tag{3.40}$$

with $\widehat{\boldsymbol{\mathcal{S}}}_3(u,v,\varphi,\mu_h)=\sum_{m=3}^{\infty}\boldsymbol{U}_{3m}(\{\underline{n}\},\mu_s,\mu_h)\,\hat{\otimes}\,\mathbf{1}$, which is the LL evolution of a hard event with three particles. We calculate (3.40) by using MC methods. This means that we randomly generate u,v and φ, then use these quantities to build the vectors representing the directions of the quark n_q, the anti-quark $n_{\bar{q}}$ and the gluon n_g and dress this event with a shower $\widehat{\boldsymbol{\mathcal{S}}}_3(u,v,\varphi,\mu_h)$. In other words, we run a LL shower $\widehat{\boldsymbol{\mathcal{S}}}_3(u,v,\varphi,\mu_h)$ for the given particle configuration. While this seems straightforward, at least in principle, the situation is more complicated since the hard functions $\boldsymbol{\mathcal{H}}_3^{(1)}$ are distribution valued and act on a quantity which we do not have analytically. In short, this means that we cannot simply integrate point-by-point. One way to circumvent this problem would be to evaluate $\widehat{\boldsymbol{\mathcal{S}}}_3(u,v,\varphi,\mu_h)$ on a grid, create interpolation tables and then perform the integration over u,v and φ numerically. Since $\widehat{\boldsymbol{\mathcal{S}}}_3(u,v,\varphi,\mu_h)$ is a smooth function this approach works reasonably well. We point out that in the limit $v\to 0$, the quark and gluonic Wilson line combine, reproducing the same radiation pattern as a single quark, which we write as

$$\lim_{v\to 0}\widehat{\boldsymbol{\mathcal{S}}}_3(u,v,\varphi,\mu_h)=\widehat{\boldsymbol{\mathcal{S}}}_2(\mu_h). \tag{3.41}$$

This relation is obvious from a color flow perspective. A disadvantage of using interpolation tables is that once the phase-space constraints change, e.g. modifying the cone size or more generally the veto region, the interpolation tables need to be recomputed which is not efficient. As a result, it seems much more natural to calculate the convolution (3.40) directly within the MC code. In [107], a slicing method was proposed to calculate the plus distributions numerically. We will closely follow this approach, in contrast to [148], where a counter-term is constructed using the projection-to-born subtraction method [209].

As seen in Section 2.3, the hard functions depend on δ functions and plus distributions of the angles u, v. For the sake of simplicity, we will only consider the variable v to illustrate the slicing method and disregard (for now) the dependence on both u and φ. Collecting terms proportional to distributions in v we write the convolution in (3.40) as

$$\mathcal{H}_3^{(1)} \otimes \widehat{\mathcal{S}}_3 = \int_0^1 dv \left[A\,\delta(v) + B(v) + \sum_{i=0}^{1} C_i(v) \left(\frac{\ln^i v}{v} \right)_+ \right] \widehat{\mathcal{S}}_3(v), \tag{3.42}$$

where non-bold symbols for $\mathcal{H}$ and $\mathcal{S}$ indicate scalar quantities once the color trace has been performed. These scalar quantities are the ones relevant for the numerical integration. The function $B(v)$ is regular in v, so we can directly evaluate it by randomly generating values for $v \in [0, 1]$ and then starting a shower for the given three-particle configuration. Using the relation (3.41) we can directly evaluate the term proportional to A. In practice, we multiply the LL result with the constant A. In the slicing method, a minimum cutoff value, represented as v_0, is introduced in the integrals of the plus distributions acting on $C_i(v)$ to prevent v from approaching zero. Therefore, we can calculate the integral of the subtraction term

$$\int_0^1 \frac{dv}{v} \left[\widehat{\mathcal{S}}_3(v) - \widehat{\mathcal{S}}_2 \right] = \int_{v_0}^1 \frac{dv}{v}\, \widehat{\mathcal{S}}_3(v) + \ln v_0\, \widehat{\mathcal{S}}_2 + \mathcal{O}(v_0), \tag{3.43}$$

where all the remaining terms are finite. Hence, we can use the same MC methods as for the $B(v)$ case to obtain the first term involving the collinear cutoff v_0. The second term contains a logarithm of the cutoff parameter multiplying the LL result so that we directly combine it with the constant contribution A. Up to power corrections in v_0 the cutoff dependence will cancel out in (3.43). While this slicing method proves to be very useful, there is primarily one drawback. To reduce power corrections, it is necessary to set the cutoff parameter v_0 to small values which leads to large cancellations between the two terms on the right-hand side of (3.43). Since the cancellation is delicate, this might threaten the numerical stability of the MC integration. Because of the cancellation, a slicing scheme needs to be implemented carefully. In practice, one lowers the cutoff parameter v_0 until the result no longer depends on the cutoff, but before numerical instabilities arise. To apply this slicing method to the finite parts of (2.33), (2.35), (2.38), we also need to take into account the dependence on u, but this treatment is exactly the same as shown above. When applying the slicing method to the plus distributions, we collect (counter-)terms proportional to $\delta(u)\,\delta(v)$ and directly combine them with the virtual corrections (2.40) and obtain a finite contribution $\mathcal{H}_{3,\text{finite}}^{(1)}$

$$\mathcal{H}_{3,\text{finite}}^{(1)} = -2 + \frac{2\pi^2}{3} + 12\ln 2 - 12\ln v_0 + 8\ln^2 v_0, \tag{3.44}$$

which multiplies the LL result $\widehat{\mathcal{S}}_2$. Since the third region $\mathcal{H}_{3,\text{III}}^{(1)}$ does not involve any singularities,

no slicing is required. The full expressions for $\boldsymbol{\mathcal{H}}_3$ in the slicing scheme are

$$\mathcal{H}_{3,\mathrm{I}}^{(1)}(u,v,\varphi,Q,\mu_h) = \int_0^1 du \int_0^1 dv \int_0^{2\pi} \frac{d\varphi}{2\pi}\, C_F \Bigg\{ \Bigg[8\ln u_0 - 8\ln\frac{\mu}{Q} + 8\ln v\,, \\ + 4\ln\left(4\sin^2\varphi\right) \Bigg] \delta(u)\,\frac{\theta(v-v_0)}{v} + F(u,v)\,\frac{\theta(u-u_0)\theta(v-v_0)}{uv} \Bigg\} \Theta_{\mathrm{in}}(u,v)\,, \tag{3.45}$$

$$\mathcal{H}_{3,\mathrm{II}}^{(1)}(u,v,\varphi,Q,\mu_h) = \int_0^1 du \int_0^1 dv \int_0^{2\pi} \frac{d\varphi}{2\pi}\, C_F \left\{ G(u,v)\frac{\theta(v-v_0)}{v} \right\} \Theta_{\mathrm{in}}(u,v)\,, \tag{3.46}$$

$$\mathcal{H}_{3,\mathrm{III}}^{(1)}(u,v,\varphi,Q,\mu) = \int_0^1 du \int_0^1 dv \int_0^{2\pi} \frac{d\varphi}{2\pi}\, C_F\, H(u,v)\, \Theta_{\mathrm{in}}(u,v)\,. \tag{3.47}$$

Listing 3.3 shows an example of how we implement these functions.

We would like to point out that (3.45) and (3.46) involve terms proportional to $\frac{1}{v}$ or $\frac{1}{uv}$. Since we do not use any importance sampling on the variables u, v, the integration suffers from singular contributions as $u, v \sim u_0, v_0$ which spoil the numerical integration. To guarantee reliable numerical accuracy, we need to perform a change of variables in such a way that the integrand is as flat as possible. In principle, the optimal variables would transform the integrand to be exactly one. In our case it is not possible to transform analytically the integrand to be one, but we can substitute

$$t_1 = \ln v \qquad t_2 = \ln u\,, \tag{3.48}$$

so that we eliminate the singular behavior of the denominators near the boundaries. In this way, the integrand is more suitable for numerical integration and our result is more stable. In practice, the cutoffs on u and v are given by

$$u_0 = v_0 = e^{-\eta_{\mathrm{slice}}-1}\,, \tag{3.49}$$

where we set $\eta_{\mathrm{slice}} = \eta_c$ as default. The cutoff η_c is the rapidity cut imposed in the parton shower when additional emissions are generated. We find that using $\eta_c = 5$ yields accurate results and the remaining dependence on the slicing parameter is small. However, to test the robustness of the numerical integration we also run with $\eta_c = 8$, which is much more time-consuming. We remind the reader that although the hard functions presented here involve the color factors at finite N_c, we eventually take the large-N_c limit to be consistent with the parton shower.

```
//create array to store the result
let mut res: Vec<f64>;

//fix cutoffs for the slicing
//here we choose etacut the same as in the LL
let v0 = (-1. - etacut).exp();
let u0 = (-1. - etacut).exp();

//Monte Carlo
for _i in 0..nev {

    //generate three random numbers
    let u,v,phi = rand(3);

    //build vectors
    let nq = [1, ... ];
    let nqbar = [1, ... ];
    let ngluon = [1, ... ];

    //check thrust-axis and in-constraint
    let a:  bool;    //either true or false

    //if a is satisfied, we evaluate the integrand
    if a == true {

        //evaluate the purely hard contribution
        let integrand = hard_func(u,v,phi);

        //dress the event with a LL shower
        let hardevents = [nq,ngluon,nqbar];
        hardevents.llshower();

        //assemble the result
        res += integrand * hardevents.llres() / nev;

    } else {

        //discard event
        continue

    }
}

//return result
return res;
```

Listing 3.3: Pseudo code to shower hard real emission contributions.

3.3.2 Soft corrections

The implementation of the one-loop contributions to the soft function is closely related to the LL parton shower. Once we start a LL shower, it generates emissions between neighboring dipoles (n_i, n_j) using the rapidity $\hat{y}$ and azimuthal angle $\hat{\phi}$ of the emission in the back-to-back frame of the emitting parents. The hat specifies that a given quantity is in the back-to-back frame. The shower runs, keeps emitting hard partons, until an emission enters the veto region at which point the shower terminates. This means that the natural way to calculate

$$\left\langle \boldsymbol{\mathcal{H}}_2^{(0)}(\{n_1,n_2\},Q,\mu_h) \otimes \boldsymbol{U}_{2m}(\{\underline{n}\},\mu_s,\mu_h) \hat{\otimes} \boldsymbol{\mathcal{S}}_m^{(1)}(\{\underline{n}\},Q_0,\mu_s) \right\rangle \tag{3.50}$$

is to start a shower, let it evolve as indicated by $\boldsymbol{U}_{2m}$ and once an emission is vetoed, evaluate $\boldsymbol{\mathcal{S}}_m^{(1)}$ for the given m-particle configuration. By repeating these steps, we obtain a MC result for the one-loop corrections. In practice, we evaluate the one-loop soft function as a weight and fill a histogram.

In the following we express $\boldsymbol{\mathcal{S}}_m^{(1)}$ in a suitable way to be implemented, in close analogy to [107]. Since the one-loop soft function $\boldsymbol{\mathcal{S}}_m^{(1)}$ introduced in (2.15) depends a priori on a sum of unordered pairs of dipoles (ij),

$$\frac{\alpha_s(\mu_s)}{4\pi} \boldsymbol{\mathcal{S}}_m^{(1)}(\{\underline{n}\},Q_0,\epsilon) = -\frac{g_s^2\,\tilde{\mu}^{2\epsilon}}{(2\pi)^{d-1}} \sum_{(ij)} \boldsymbol{T}_{i,L}\cdot\boldsymbol{T}_{j,R} \int \frac{d^{d-1}k}{2k^0} \frac{n_i\cdot n_j}{n_i\cdot k\, n_j\cdot k} \Theta_{\text{out}}(n_k)\theta\left(Q_0-k^0\right) , \tag{3.51}$$

with $\tilde{\mu}^{2\epsilon} = \left(\frac{e^{\gamma_E}\mu^2}{(4\pi)}\right)^{\epsilon}$, we will take the large-N_c limit which is compatible with our shower. In this limit, only neighboring legs contribute so that we replace

$$\boldsymbol{T}_{i,L}\cdot\boldsymbol{T}_{j,R} \to -\frac{N_c}{2}\,\delta_{i,j\pm1}\,. \tag{3.52}$$

We remind the reader that (3.52) is only true if the particles are already color-ordered. We restrict the energy of the radiation inside the veto region by using $\theta(Q_0-k^0)=\theta(Q_0-v\cdot k)$ with $v=(1,0,0,0)$. To write (3.51) in a way that is suitable for the numerical implementation, we evaluate the contribution from the (ij) dipole in a frame where the vectors n_i and n_j are back-to-back. The explicit vectors are taken as

$$\hat{n}_i^\mu = \frac{M}{2}(1,0,0,1)\,, \qquad \hat{n}_j^\mu = \frac{M}{2}(1,0,0,-1)\,, \tag{3.53}$$

$$\hat{v}^\mu = \frac{2}{M}(1,0,\beta,0)\,, \qquad k = \hat{k}_T(\cosh\hat{y},\sin\hat{\phi},\cos\hat{\phi},\sinh\hat{y}), \tag{3.54}$$

with $M^2 = 2\,n_i\cdot n_j$ which is the invariant mass of the dipole pair and $\beta=\sqrt{1-M^2/4}$. The integration momentum k is parameterized in cylindrical coordinates in rapidity. Expressing the integral in (3.51) in terms of these vectors and expanding the measure in $d=4-2\epsilon$ we obtain

$$\int \frac{d^{d-1}k}{2k^0}\,\theta\left(Q_0-\hat{v}\cdot k\right) = \frac{\Omega_{1-2\epsilon}}{2}\int_0^\infty d\hat{k}_T\,\hat{k}_T^{1-2\epsilon}\int_{-\infty}^{\infty}d\hat{y}\int_0^\pi d\hat{\phi}\left(\sin^2\hat{\phi}\right)^{-\epsilon}\theta\left(Q_0-\hat{v}\cdot k\right), \tag{3.55}$$

where Ω_d represents the d-dimensional surface of the unit sphere. Inserting the dipole factor $\frac{2}{k_T^2}$ and introducing the auxiliary function $f_{ij}(\hat{y},\hat{\phi})$

$$k\cdot\hat{v} = f_{ij}(\hat{y},\hat{\phi})\,\hat{k}_T = \frac{2}{M}\big(\cosh\hat{y}-\beta\cos\hat{\phi}\big)\hat{k}_T\,, \tag{3.56}$$

we can integrate over k_T and expand in ϵ. We obtain a soft divergence which we renormalize in the $\overline{\text{MS}}$ scheme. The divergence is exactly the same as we already obtained in Section 2.4. The reason we are using a different parametrization here, is because we are interested in the one-loop contributions with m final states whereas in Section 2.4 we only considered the case with $m = 2$. The finite contribution of the one-loop soft function involves integrations over $\hat{y}$ and $\hat{\phi}$, which we perform numerically with the shower since it already generates additional emissions using the variables $\hat{y}$ and $\hat{\phi}$. The explicit expression is given by

$$\mathcal{S}_m^{(1)}(\{\underline{n}\}, Q_0, \mu_s) = -4N_c \int d\hat{y} \int_0^{2\pi} \frac{d\hat{\phi}}{2\pi} \left[\ln \frac{\mu_s}{Q_0} + \ln f_{ij}(\hat{\phi}, \hat{y}) - \tfrac{1}{2} \ln \left(4 \sin^2 \hat{\phi} \right) \right] \Theta_{\text{out}}^{\text{lab}}(\hat{y}, \hat{\phi}) \,. \quad (3.57)$$

We would like to point out a subtlety concerning the $\ln \left(4 \sin^2 \hat{\phi} \right)$ term present in (3.57), which is a remainder of the d-dimensional measure. Naively, the azimuthal angle $\hat{\phi}$ is defined in the back-to-back frame of the (n_i, n_j) dipole such that as long as the veto region defined through $\Theta_{\text{out}}^{\text{lab}}(\hat{y}, \hat{\phi})$ is symmetric in $\hat{\phi}$ we can directly use the randomly generated angle to calculate the associated weight. However, once the veto region is asymmetric, it is necessary to use a consistent definition of the azimuthal angle ϕ_q in both frames. To write the azimuthal angle of the additional emission in a Lorentz invariant way, we introduce an additional light-like reference vector $n_x = (1, 1, 0, 0)$ in the LAB frame. In terms of this vector $\phi_q \equiv \phi_{qx}$ can be written as

$$\cos^2(\phi_{qx}) = \frac{(n_{ix} n_{jq} + n_{iq} n_{jx} - n_{ij} n_{qx})^2}{4 n_{iq} n_{jq} n_{ix} n_{jx}} \,, \quad (3.58)$$

where the direction of the emission n_q is taken in the LAB frame so that we attribute the correct weight to the event.

This procedure to evaluate the soft corrections is general and also applicable to other processes. Furthermore, this algorithm is efficient since we can directly obtain the soft contribution from running a LL shower. Starting from the LL parton shower, the incorporation of the one-loop soft function at the level of the cross section reads

$$\sum_{m=2}^{\infty} \left\langle \boldsymbol{\mathcal{H}}_m(\mu_s) \,\hat{\otimes}\, \boldsymbol{\mathcal{S}}_m^{(1)} \right\rangle = \left\langle \boldsymbol{\mathcal{H}}_2(\mu_s) \boldsymbol{\mathcal{S}}_2^{(1)} + \int \frac{d\Omega_1}{4\pi} \boldsymbol{\mathcal{H}}_3(\mu_s) \boldsymbol{\mathcal{S}}_3^{(1)} + \int \frac{d\Omega_1}{4\pi} \int \frac{d\Omega_2}{4\pi} \boldsymbol{\mathcal{H}}_4(\mu_s) \boldsymbol{\mathcal{S}}_4^{(1)} + \dots \right\rangle , \quad (3.59)$$

where $\boldsymbol{\mathcal{H}}_m(\mu_s)$ denotes the evolution of the hard function from the initial (hard) scale to the soft scale. During the evolution, new particles are generated, thereby changing the multiplicity. At the soft scale μ_s we evaluate $\boldsymbol{\mathcal{S}}_m^{(1)}$. In (3.57) a veto was imposed on the total energy of the emission, however, another choice would be to use the transverse energy E_T. In this case, we need to add an additional term to (3.57)

$$\frac{1}{2} \ln \left(\frac{2 n_{1q} n_{2q}}{n_{12}} \right) , \quad (3.60)$$

where n_1 and n_2 denote the initial dipole. The soft function is the only ingredient at NLL accuracy sensitive to the definition of the veto energy Q_0.

3.3.3 Two-loop running corrections

In this section, we will present the implementation of the two-loop anomalous dimension $\bar{\mathbf{\Gamma}}^{(2)}$ in the dedicated framework MARZILI. In Section 2.6.4 the result for the two-loop anomalous dimension in the $\overline{\text{MS}}$ scheme was presented in two pieces $\bar{\mathbf{\Gamma}}^{(2)} = \mathbf{\Gamma}^{(2)} + \delta\mathbf{\Gamma}^{(2)}$. The extra piece

$$\delta\mathbf{\Gamma}^{(2)} = -2\beta_0\,\mathbf{\Gamma}^{(1)} \otimes_\epsilon \mathbf{1} - \left(\mathbf{\Gamma}^{(1)} \otimes_2 \mathbf{\Gamma}^{(1)} \otimes_\epsilon \mathbf{1} - \mathbf{\Gamma}^{(1)} \otimes_\epsilon \mathbf{\Gamma}^{(1)} \otimes_2 \mathbf{1}\right), \tag{3.61}$$

involves ϵ-terms in angular integrals, in other words contributions proportional to $\mathcal{O}(\epsilon)$ in the d-dimensional integral measure, as defined in Table 3.1. Our first task will be to evaluate these terms carefully to make their form explicit and combine them with $\mathbf{\Gamma}^{(2)}$ in the large-N_c limit. We find that the combination of $\bar{\mathbf{\Gamma}}^{(2)} = \mathbf{\Gamma}^{(2)} + \delta\mathbf{\Gamma}^{(2)}$ is manifestly Lorentz invariant[3], while the individual contributions $\mathbf{\Gamma}^{(2)}$ and $\delta\mathbf{\Gamma}^{(2)}$ are not. Lorentz invariance is, in fact, crucial for implementing the anomalous dimension in the shower framework in an efficient way since it allows us to choose an arbitrary frame to generate the emissions. Secondly, we will precisely explain the insertion of $\bar{\mathbf{\Gamma}}^{(2)}$ in our parton shower according to (2.102)

$$\Delta\boldsymbol{U}_{kl}(t_0,t) = \int_{t_0}^{t} dt'\,\boldsymbol{U}_{kk'}(t_0,t')\cdot\frac{\alpha_s(t')}{4\pi}\left(\bar{\mathbf{\Gamma}}^{(2)}_{k'l'} - \frac{\beta_1}{\beta_0}\mathbf{\Gamma}^{(1)}_{k'l'}\right)\cdot\boldsymbol{U}_{l'l},(t',t)\,, \tag{3.62}$$

alongside with corrections to running of α_s, i.e. the ones proportional to β_1. Finally, we provide details about the implementation, e.g. derive the precise insertion weight and explain the different parametrizations we are using to sample the angular functions $K_{ij;qr}$ and $K_{ijk;qr}$ in $\mathbf{\Gamma}^{(2)}$ efficiently.

Calculation of ϵ-terms

Before evaluating the ϵ-terms in $\delta\mathbf{\Gamma}^{(2)}$, we will show that the one-loop anomalous dimension is indeed Lorentz invariant. The form presented in (2.105) involves pure angular integrals of the form

$$\int \left[d^2\Omega_q\right]\, W^q_{ij}\,, \tag{3.63}$$

which seems to violate Lorentz invariance because the measure is clearly frame-dependent. Naively, one would think that additional terms arise when evaluating this integral in the back-to-back frame of the (ij)-dipole.

To discuss the anomalous dimension in an arbitrary frame, it is useful to repeat the derivation of the anomalous dimension in a frame that differs from the lab frame. As in [123], we extract the anomalous dimension from the soft limit using a constraint on the energy E_{lab} of the emissions in the lab frame. To write this constraint in an arbitrary frame, we introduce a reference four-vector v_μ which is related to the energy $E_{\text{lab}} = v\cdot q$ for an emission with four-momentum q^μ. This vector encodes the frame-dependence, i.e. by including it, we can safely evaluate the anomalous dimension in any frame. We then recompute the soft integrals that arise in the derivation of the anomalous dimension in an arbitrary frame by integrating out the energies in the new frame while keeping the angular dependence. The dipole real emission soft integral at one loop now reads

$$S_{ij} = \int \frac{d^{d-1}q}{(2\pi)^{d-1}2E_q}\,\frac{n_i\cdot n_j}{n_i\cdot q\, n_j\cdot q}\,\theta(\Lambda - v\cdot q)\,\Theta_{\text{in}}(\tilde{n}_q)\,. \tag{3.64}$$

In the derivation, loop integrals also arise, which are put into the same form as the real-emission integrals using the residue theorem to carry out the energy integrals. In the lab frame $v_{\text{lab}} = (1,\vec{0})$,

[3] Up to the gap constraints.

Convolution Symbol	Associated angular integral(s)
$\otimes$	$\int [d\Omega_i] = \tilde{c}^{\epsilon}\,(v\cdot n_i)^{2\epsilon}\int \frac{d^{d-2}\Omega_i}{2(2\pi)^{d-3}}$
$\otimes_2$	$\int \left[d^2\Omega_i\right] = \int \frac{d^2\Omega_i}{4\pi}$
$\otimes_\epsilon$	$\int [d\Omega_i] = \int \left[d^2\Omega_i\right] + 2\epsilon \int [d\Omega_i]_\epsilon$
	$\otimes = \otimes_2 + 2\epsilon\,\otimes_\epsilon$

Table 3.1: Angular convolution symbols and associated angular integrals for the individual partons $i = 1 \ldots m$. In the final result, the factors $\tilde{c} = e^{\gamma_E}/\pi$ cancel against the ones in the energy integrals. The factor $v \cdot n_i = 1$ in the lab frame. Table adapted from [123].

and the integral therefore puts a constraint on the energy in the lab frame. Up to the $\Theta_{\rm in}(\tilde{n}_q)$ constraint, the integrand is a Lorentz invariant function depending on Q_0, the time-like reference vector v^μ, and the light-like reference vectors n_i, n_j. The jet constraint is formulated in terms of angles in the lab frame vector $\tilde{n}_q$, and if we evaluate the integral in an arbitrary frame, we obtain the lab frame vector as

$$\tilde{n}_q = \frac{\Lambda_\nu{}^\mu q^\nu}{v\cdot q}\,, \tag{3.65}$$

where $\Lambda_\nu{}^\mu$ is the Lorentz transformation to the lab frame. We now parameterize $q^\mu = \omega\, n_q^\mu$, with $n_q^\mu = (1, \vec{n}_q)$ so that the quantity ω is the energy in the chosen frame. Performing the energy integral now leads to

$$\begin{aligned} S_{ij} &= \int \frac{d\omega}{(2\pi)^2\,\omega^{1+2\epsilon}} \int \frac{d^{d-2}\Omega_q}{2(2\pi)^{d-3}}\, W_{ij}^q\;\theta(Q_0 - \omega\, v\cdot n_q)\,\Theta_{\rm gap}(\tilde{n}_q) \\ &= -\frac{Q_0^{-2\epsilon}}{2\epsilon}\int [d\Omega_q]\, W_{ij}^q \Theta_{\rm in}(\tilde{n}_q)\,. \end{aligned} \tag{3.66}$$

For convenience, we have absorbed a factor of $v\cdot n_q$ into the definition of the angular integrals so that

$$\int [d\Omega_q]\, W_{ij}^q = \tilde{c}^{\epsilon}\,(v\cdot n_i)^{2\epsilon}\int \frac{d^{d-2}\Omega_i}{2(2\pi)^{d-3}} W_{ij}^q \tag{3.67}$$

is frame independent in $d = 4-2\epsilon$ dimensions. One then expands the integral S_{ij} in ϵ and obtains the anomalous dimension from the coefficient of the $1/\epsilon$ divergence. Including the color structure, this yields the familiar result

$$\begin{aligned} \boldsymbol{R}_m =& -4\sum_{(ij)} \boldsymbol{T}_{i,L}^a \boldsymbol{T}_{j,R}^{\tilde{a}}\, W_{ij}^q\, \theta_{\rm in}(\tilde{n}_q)\,, \\ \boldsymbol{V}_m =& 2\sum_{(ij)} \left(\boldsymbol{T}_{i,L}\cdot\boldsymbol{T}_{j,L} + \boldsymbol{T}_{i,R}\cdot\boldsymbol{T}_{j,R}\right)\int \left[d^2\Omega_q\right]\, W_{ij}^q \\ & - i\pi\sum_{(ij)} \frac{1}{2}\left[\boldsymbol{T}_{i,L}\cdot\boldsymbol{T}_{j,L} - \boldsymbol{T}_{i,R}\cdot\boldsymbol{T}_{j,R}\right]\,\Pi_{ij}\,\gamma_0^{\rm cusp}\,, \end{aligned} \tag{3.68}$$

where the angular integrals are two-dimensional. In general, the integrals in (3.68) involve a singularity in $d = 2$ when the emission q becomes collinear to either i or j. To regularize this singularity, we impose a cutoff as explained in 3.2.1. Importantly, the result is independent of the frame in which it was extracted. The angular integrals

$$\int \left[d^2\Omega_q\right] W_{ij}^q \tag{3.69}$$

are therefore frame independent in $d = 2$. The invariance can be understood physically from the fact that the anomalous dimension follows from the part of the integral S_{ij} where the energy goes to zero, which stays invariant under a boost.

Proceeding to $\mathbf{\Gamma}^{(2)}$, we have repeated the derivation of the two-loop anomalous dimension in an arbitrary frame, using the constraint

$$\theta(\Lambda - v \cdot q - v \cdot r) \tag{3.70}$$

for the case of two real emissions q and r. The modifications of the result are very minor. First of all, the angular integrals in the extra piece $\delta\mathbf{\Gamma}^{(2)}$ in (3.61) involve a term proportional to $\ln(v \cdot n_q)$ and $\ln(v \cdot n_r)$ from expanding the angular integrals, see (3.67). Since we have included these in the definition of the measure in the angular integrals, see Table 3.1, the form of the extra terms given in (3.67) remains valid in an arbitrary frame. The other terms which involve v^μ dependence are the three-particle contributions $K_{ijk;qr}$ which become

$$K_{ijk;qr} = 8\left(W_{ik}^q W_{jk}^r - W_{ik}^q W_{jq}^r - W_{ir}^q W_{jk}^r + W_{ij}^q W_{jq}^r\right) \ln\left(\frac{n_{kq}}{n_{kr}} \frac{v \cdot n_r}{v \cdot n_q}\right), \tag{3.71}$$

and the term involving a logarithm of the dipole, which gets replaced by

$$W_{ij}^q \ln(2W_{ij}^q) \longrightarrow W_{ij}^q \ln \frac{2\, n_i \cdot n_j\, (v \cdot n_q)^2}{n_i \cdot n_q\, n_j \cdot n_q}, \tag{3.72}$$

As for the case of $K_{ijk;qr}$, the velocity terms in the logarithm are such that the argument becomes invariant under a rescaling of the light-cone vector associated with the emission. Interestingly, the two-particle function $K_{ij;qr}$ remains unchanged and has the same rescaling property. Our goal is to combine the terms in $\delta\mathbf{\Gamma}^{(2)}$ and $\mathbf{\Gamma}^{(2)}$ and show that the velocity dependence cancels among the two.

The simplest velocity-dependent contributions are terms proportional to β_0 in $\delta\mathbf{\Gamma}^{(2)}$ and $\mathbf{\Gamma}^{(2)}$. These only arise in the real-virtual $\boldsymbol{r}_m$ and double-virtual part $\boldsymbol{v}_m$. To illustrate the cancellation of velocity-dependent terms, we consider the purely virtual anomalous dimension $\bar{\boldsymbol{v}}_m$. In the $\overline{\text{MS}}$ scheme, the combination of both contributions takes the form

$$\bar{\boldsymbol{v}}_m\Big|_{\beta_0} = 4\beta_0 \sum_{(ij)} \frac{1}{2}\left(\boldsymbol{T}_{i,L}^a \boldsymbol{T}_{j,L}^a + \boldsymbol{T}_{i,R}^a \boldsymbol{T}_{j,R}^a\right) \left\{ \int \left[d^2\Omega_q\right] \ln\left(2W_{ij}^q\, (v \cdot n_q)^2\right) - 2\int \left[d\Omega_q\right]_\epsilon \right\} W_{ij}^q\,, \tag{3.73}$$

where the vertical bar indicates that we only consider terms proportional to β_0. Since $\bar{\boldsymbol{v}}_m$ is Lorentz invariant, we now choose to evaluate the contribution in the back-to-back frame and parameterize

$$n_i = (1, \vec{0}, 0, 1)\,, \qquad n_j = (1, \vec{0}, 0, -1)\,, \qquad n_q = (1, \hat{n}_q\, s_\theta s_{\phi_q}, s_{\theta_q} c_{\phi_q}, c_{\theta_q})\,, \tag{3.74}$$

where $\vec{0}$ and $\hat{n}_q$ are $(d-3)$-dimensional zero and unit vectors. The angles θ, ϕ run from 0 to π and we abbreviate their cosine and sines as $c_\theta = \cos\theta$ and $s_\theta = \sin\theta$. We can view the parameterization

of the vector n_q as a series of rotations applied to the vector n_i. In fact, to ensure we do not miss any angular contributions, we should also introduce an additional angle α_q. However, we can immediately integrate it out since the angular integral in (3.73) is only sensitive to the sign of c_{α_q}. As a result, the azimuthal angle for ϕ_q runs from 0 to 2π. With the parameterization of the angular integral at hand, we can derive the explicit form of the term (3.73). Up to terms of $\mathcal{O}(\epsilon^2)$, the ϵ-expansion of the dipole integral can be written as

$$\int [d\Omega_q]\, W_{ij}^q = \frac{1}{4\pi}\int_{-1}^{1} dc_\theta \int_0^{2\pi} d\phi_q\; W_{ij}^q \Big\{ 1 + \epsilon \ln\Big(2W_{ij}^q (v\cdot n_q)^2\Big) - \epsilon \ln\big(4\sin^2(\phi_q)\big)\Big\}\,, \tag{3.75}$$

which implies that the β_0-terms in (3.73) take the simple form

$$\bar{\boldsymbol{v}}_m\Big|_{\beta_0} = 4\beta_0 \sum_{(ij)} \frac{1}{2}\left(\boldsymbol{T}_{i,L}^a \boldsymbol{T}_{j,L}^a + \boldsymbol{T}_{i,R}^a \boldsymbol{T}_{j,R}^a\right) \int \big[d^2\Omega_q\big]\, X_{ij}^q\,, \tag{3.76}$$

with $X_{ij}^q = W_{ij}^q \ln\big(4\sin^2(\phi_q)\big)$. The angle ϕ_q is the azimuthal angle of the emission in the dipole frame of partons i and j. To write $\sin^2(\phi_q)$ in a lorentz-invariant form we use a light-like reference vector $n_x = (1,1,0,0)$ pointing along the x-direction and (3.58). Similarly, one finds

$$\bar{\boldsymbol{r}}_m\Big|_{\beta_0} = -4\beta_0 \sum_{(ij)} \boldsymbol{T}_{i,L}^a \boldsymbol{T}_{j,R}^a\, X_{ij}^q\, \theta_{\text{in}}(\tilde{n}_q)\,, \tag{3.77}$$

for real-virtual contributions. Since neither (3.76) nor (3.77) depend on the velocity term v^μ, we conclude that the contributions proportional to β_0 are manifestly frame independent, in other words, Lorentz invariant. We point out that in the dijet case, where $\Theta_{\text{jet}}(\tilde{n}_q)$ is ϕ_q-independent, the β_0-contributions to $\bar{\boldsymbol{r}}_2, \bar{\boldsymbol{v}}_2$ from the primary hard partons vanishes because

$$\int_0^{2\pi} d\phi_q \ln(4\sin^2(\phi_q)) = 0\,. \tag{3.78}$$

For $m > 2$, the contributions no longer vanish since the extra partons can be emitted along any direction with respect to the jet cones.

In the large-N_c limit only dipole structures contribute. As a consequence the three-particle terms $K_{ijk;qr}$ only contribute when two legs coincide, these are the only non-vanishing terms in the large-N_c limit. Since our parton shower framework operates within this limit, this contribution is all we need to address. In the following, we will focus on the real-virtual contribution $\boldsymbol{r}_m$, but the procedure carries over to the double-real contributions $\boldsymbol{d}_m$. We observed in Section 2.6.2 that $K_{ijk;qr}$ vanishes for $i = k$ or $j = k$. Therefore, the only two-particle contributions in the large-N_c limit arise from the combination

$$\begin{aligned}\boldsymbol{r}_m &= \sum_{(ij)} N_c^2 \int \big[d^2\Omega_r\big]\, \big(K_{iij;qr} + K_{jji;qr}\big)\, \theta_{\text{in}}(n_q) \\ &= \sum_{(ij)} 8N_c^2 \int \big[d^2\Omega_r\big]\, L_{ij;qr} \ln \frac{n_i\cdot n_q\, n_j\cdot n_q}{n_i\cdot n_r n_j\cdot n_r} \frac{(v\cdot n_r)^2}{(v\cdot n_q)^2}\, \theta_{\text{in}}(n_q)\,,\end{aligned} \tag{3.79}$$

where the velocity terms are again present to ensure Lorentz invariance. We introduced the quantity $L_{ij;qr}$

$$L_{ij;qr} = \big(W_{ij}^q W_{ij}^r - W_{ij}^{qr} - W_{ij}^{rq}\big) \tag{3.80}$$

and

$$W_{ij}^{qr} = \frac{n_{ij}}{n_{iq} n_{qr} n_{rj}} = W_{ij}^q W_{jq}^r = W_{ij}^r W_{ir}^q\,. \tag{3.81}$$

The quantity $L_{ij;qr}$ has a simple interpretation. It is the combination of dipoles that arises when considering strongly ordered emissions from a dipole (ij). The above two-particle contributions only arise for the double real and in the real-virtual contributions since double-virtual terms vanish entirely in the large-N_c limit.

Unsurprisingly, the two-particle terms in (3.79) will combine with two-particle terms from $\delta\mathbf{\Gamma}^{(2)}$ in (3.61). These arise from the part of $\delta\mathbf{\Gamma}^{(2)}$ which corresponds to strongly ordered emissions and involves two angular integrals. To extract the expansion of the angular integrals, we introduce different parameters ϵ_q and ϵ_r in the two integrations, i.e. we substitute $d = 4 - 2\epsilon_q$ in the first integral and $d = 4 - 2\epsilon_r$ in the second. The angular integral then takes the form

$$J_{ij}(\epsilon_q, \epsilon_r) = \int [d\Omega_q] \int [d\Omega_r]\, L_{ij;qr}\, \theta_{\text{in}}(\tilde{n}_q)\,, \tag{3.82}$$

where $\theta_{\text{in}}(\tilde{n}_q)$ indicates the angular constraint for the real-virtual integration. In terms of this angular integral, the commutator term in $\delta\mathbf{\Gamma}^{(2)}$ takes the form

$$\mathbf{\Gamma}^{(1)} \otimes_2 \mathbf{\Gamma}^{(1)} \otimes_\epsilon \mathbf{1} - \mathbf{\Gamma}^{(1)} \otimes_\epsilon \mathbf{\Gamma}^{(1)} \otimes_2 \mathbf{1} = \sum_{(ij)} 16\, N_c^2 \times \lim_{\epsilon\to 0} \frac{1}{2\epsilon} \Big[J_{ij}(0,\epsilon) - J_{ij}(\epsilon, 0) \Big]\,, \tag{3.83}$$

in the large-N_c limit. We now again choose the dipole rest frame to evaluate the contributions. We parameterize the vector n_q as in (3.74). However, we introduce the angles for n_r relative to n_q, by parameterizing the vector as

$$n_r = \ldots \cdot R_{34}(\alpha_{qr}) \cdot R_{23}(\phi_{qr}) \cdot R_{12}(\theta_{qr}) \cdot n_q\,, \tag{3.84}$$

where $R_{ij}(\phi)$ rotates by the angle ϕ in the plane of the i and j coordinates. The advantage of working with relative angles is that the scalar product of the two vectors takes the simple form

$$n_q \cdot n_r = 1 - \cos\theta_{qr}\,, \tag{3.85}$$

while a parameterization of n_r as in (3.74) would lead to a dependence of the scalar product on spurious angles such as α_{qr} and α_q which are not present in $d = 4$. Using this parametrization, we can carry out the commutator integral in (3.83) and divide it into two contributions

$$\mathbf{\Gamma}^{(1)} \otimes_2 \mathbf{\Gamma}^{(1)} \otimes_\epsilon \mathbf{1} - \mathbf{\Gamma}^{(1)} \otimes_\epsilon \mathbf{\Gamma}^{(1)} \otimes_2 \mathbf{1} = \sum_{(ij)} 8 N_c^2 \int \big[d^2\Omega_q\big] \int \big[d^2\Omega_r\big]\, L_{ij;qr} \left\{ \ln \frac{s^2_{\theta_q}}{s^2_{\theta_{qr}}} \frac{(v\cdot n_q)^2}{(v\cdot n_r)^2}\, \theta_{\text{in}}(n_q) - \ln \frac{s^2_{\phi_{qr}}}{s^2_{\phi_q}}\, \theta_{\text{in}}(n_q) \right\}. \tag{3.86}$$

We observe that the velocity-dependent terms will cancel exactly between (3.86) and (3.79) which means that we indeed have established Lorentz invariance for this piece as well. Due to the relation

$$s^2_{\theta_q} = 2\, \frac{n_i \cdot n_q\, n_j \cdot n_q}{n_i \cdot n_j} = 2\, W^q_{ij} \tag{3.87}$$

also the W^q_{ij} terms cancel. We stress, however, that $s^2_{\theta_{qr}} \neq 2 W^r_{ij}$, since the angle θ_{qr} was defined not with respect to the dipole axis but to n_q. Similarly, the angle ϕ_{qr} is not the azimuthal angle in the dipole frame, i.e. $\phi_r \neq \phi_{qr}$. Nevertheless, adding up the contributions from (3.86) and (3.79) we end up with the simple result

$$\bar{\boldsymbol{r}}_m = \sum_{(ij)} 8 N_c^2 \int \big[d^2\Omega_r\big]\, L_{ij;qr} \ln\left(\frac{s^2_{\phi_{qr}}}{s^2_{\phi_{qx}}} \right) \theta_{\text{in}}(n_q) \equiv \sum_{(ij)} 8 N_c^2 \int \big[d^2\Omega_r\big]\, M_{ij;qr}\, \theta_{\text{in}}(n_q)\,. \tag{3.88}$$

A Lorentz invariant expression for $s^2_{\phi_{qx}}$, where the subscript ϕ_{qx} serves as a reminder that ϕ_q is defined w.r.t the x-axis, directly in terms of the reference vectors was given in (3.58). Similarly, $s^2_{\phi_{qr}}$ is the same expression with $q \to r$ and $x \to q$ and corresponds to the azimuthal angle difference in the dipole rest frame. The derivation for the double-real contributions $\boldsymbol{d}_m$ is analogous, so we do not carry it out here. The combination of the ϵ-terms with $K_{ijk;qr}$ when all indices are different, i.e. $i \neq j \neq k$, is a more complicated task and we leave this for future work.

To summarize, we managed to combine $\mathbf{\Gamma}^{(2)}$ with its extra piece $\delta\mathbf{\Gamma}^{(2)}$ in this section. More precisely, the terms proportional to β_0 could be combined without imposing any constraints on the color structure, while the more complicated three-particle terms were obtained in the large-N_c limit, which is sufficient to implement the anomalous dimension in MARZILI. In addition, we also demonstrated that velocity-dependent terms cancel. As a consequence, the final result for the anomalous dimension, at least in the large-N_c limit, is manifestly Lorentz invariant.

Taking the large-N_c limit of the remaining two-particle contributions in $\mathbf{\Gamma}^{(2)}$, the anomalous dimension reduces to a sum over dipoles

$$\mathbf{\Gamma}^{(2)}_{mn} = \sum_{(ij)} \left[\boldsymbol{v}^{ij}_m \, \delta_{m,n} + \boldsymbol{r}^{ij}_m \, \delta_{m,n-1} + \boldsymbol{d}^{ij}_m \, \delta_{m,n-2} \right] , \tag{3.89}$$

as indicated by the superscripts ij. In the following, we write $\mathbf{\Gamma}^{(2)}$ instead of $\bar{\mathbf{\Gamma}}^{(2)}$. The three entries describe double virtual $\boldsymbol{v}^{ij}_m$, real-virtual $\boldsymbol{r}^{ij}_m$ and double-real $\boldsymbol{d}^{ij}_m$ contributions. The result for these reads

$$\begin{aligned}
\boldsymbol{d}^{ij}_m =& + N_c \big(K_{ij;qr} + K_{ji;qr}\big)\, \theta_{\text{in}}(n_q)\, \theta_{\text{in}}(n_r) \\
& - 8\, N_c^2\, M_{ij;qr}\, \theta_{\text{in}}(n_q)\, \theta_{\text{in}}(n_r) \,, \\
\boldsymbol{r}^{ij}_m =& - N_c \int \big[d^2\Omega_r\big] \big(K_{ij;qr} + K_{ji;qr}\big)\, \theta_{\text{in}}(n_q) \\
& + 8\, N_c^2 \int \big[d^2\Omega_r\big]\, M_{ij;qr}\, \theta_{\text{in}}(n_q) \\
& + N_c \big(4\beta_0\, X^q_{ij} + \gamma_1^{\text{cusp}}\, W^q_{ij}\big)\, \theta_{\text{in}}(n_q) \,, \\
\boldsymbol{v}^{ij}_m =& - N_c \int \big[d^2\Omega_q\big] \big(4\beta_0\, X^q_{ij} + \gamma_1^{\text{cusp}}\, W^q_{ij}\big) \,.
\end{aligned} \tag{3.90}$$

As described above, the resulting angular integrals are Lorentz invariant up to the gap constraints. The invariance allows us to generate the emissions in the back-to-back frame of the emitting dipole and was instrumental in finding efficient parametrizations for sampling the integrals, which is crucial for obtaining reliable MC predictions. We will get back to this point when the details of the implementation are presented. The result in (3.90) represents the final analytical ingredient to achieve NLL accuracy. The implementation of the two-loop anomalous dimension within our parton shower framework will be carefully documented in the two following sections.

Insertion of the two-loop anomalous dimension

In this section, we will outline the NLL shower algorithm, focusing on the single insertion of the two-loop anomalous dimension (3.90). We assume that the reader is familiar with the LL shower, see Section 3.2.2, and will explain the computation of

$$\Delta\boldsymbol{U}_{kl}(t_0, t) = \int_{t_0}^{t} dt' \, \boldsymbol{U}_{kk'}(t_0, t') \cdot \frac{\alpha_s(t')}{4\pi} \left(\mathbf{\Gamma}^{(2)}_{k'l'} - \frac{\beta_1}{\beta_0} \mathbf{\Gamma}^{(1)}_{k'l'} \right) \cdot \boldsymbol{U}_{l'l}(t', t) \,. \tag{3.91}$$

To compute the correction (3.91), we run two showers. At shower time $t_0 = 0$ we start a LL shower with a list of vectors $\{\underline{n}\}$ along the direction of the hard partons in the Born level process

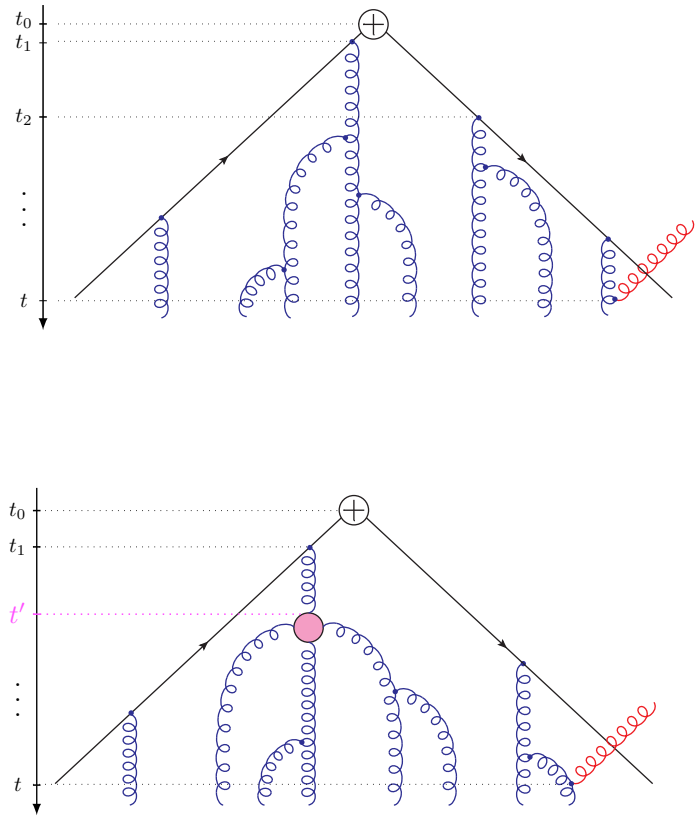

Figure 3.9: Pictorial representations of the LL shower (up) and the NLL shower (down). Blue lines denote hard emissions inside the jets generated by the shower evolution. The red lines depict a soft emission into the veto region, which terminates the shower. The pink blob is an insertion of the two-loop double-real contribution $\boldsymbol{d}_m$ at time t'.

and weight $w = 1/V_E$. The purpose of the first shower, which we refer to as master shower, is to generate event configurations with different amounts of particles at subsequent times. For instance, in the upper Figure 3.9 we have

$$\begin{aligned} t_1 &: E_1 = \{n_1, n_2\}\,, \\ t_2 &: E_2 = \{n_1, n_3, n_2\}\,, \\ t_3 &: E_3 = \{n_1, n_3, n_4, n_2\}\,, \\ &\vdots \\ t_8 &: E_8 = \{n_1, n_6, n_9, n_3, n_8, n_5, n_4, n_7, n_2\}\,. \end{aligned} \tag{3.92}$$

This represents $\boldsymbol{U}_{2k'}(t_0, t')$ in (3.91). At $t' = t_1, t_2, \ldots$, we then insert the two-loop anomalous dimension correction, which increases the number of vectors by 0, 1 or 2, depending on whether $\boldsymbol{v}_m$, $\boldsymbol{r}_m$ or $\boldsymbol{d}_m$ is computed. After this, we start a second LL shower, which corresponds to the factor $\boldsymbol{U}_{l'l}(t', t)$ in (3.91). This is depicted in the lower part of Figure 3.9 for the example of $t' = t_2$.

To be precise, the insertion time t' is not exactly t_i, but slightly shifted. To see this, recall that the LL evolution operator $\boldsymbol{U}_{kk'}(t_0, t')$ is built up iteratively according to (3.9). Starting from an event configuration with k' particles, a time step Δt_n is generated according to the corresponding probability distribution $\mathcal{P}_{k'}$ before inserting the two-loop anomalous dimension. The evolution takes the form

$$\mathcal{P}_{k'}(\Delta t_n) \cdot \frac{\alpha_s(t')}{4\pi} \left(\boldsymbol{\Gamma}^{(2)}_{k'l'} - \frac{\beta_1}{\beta_0} \boldsymbol{\Gamma}^{(1)}_{k'l'} \right) \cdot \boldsymbol{U}_{l'l}(t', t)\,, \tag{3.93}$$

where the insertion time is $t' = t_{\text{tot}} + \Delta t_n$. We point out that the first insertion is carried out with the initial particle configuration, i.e. $k' = 2$. This algorithm is depicted in Figure 3.10.

Let us now explain how the insertion is implemented in our shower code, using, as an example, a term involving a single emission, such as the X^q_{ij} term in $\boldsymbol{r}_m$, or the single angular integral terms in $\boldsymbol{v}_m$.

1. Pick a dipole in E_i with the probability V_{ij}/V_{E_i}. Then generate an additional direction n_q and evaluate its weight $\Delta\Gamma$, which is just the integrand of one of the terms in $\boldsymbol{\Gamma}^{(2)} - \beta_1/\beta_0 \boldsymbol{\Gamma}^{(1)}$ under consideration.
2. For real contributions, we need to update the list of vectors by inserting the additional emission between its parents, i.e. for a single emission $E'_i = \{n_1, \ldots, n_i, n_q, n_j, \cdots, n_2\}$, while we leave $E'_i = E_i$ for virtual contributions.
3. Compute an insertion weight
$$w_I = \Delta\Gamma \, \frac{V_{E_i}}{V_{ij}}\,, \tag{3.94}$$
where the factor V_{E_i}/V_{ij} cancels the one introduced when selecting the dipole.
4. Start a LL shower with weight $w_{\text{new}} = w_I/V_{E'_i}$ and list of vectors E'_i at t'. The insertion time t' needs to be calculated according to (3.93). The time values arising in the second shower correspond to values of t in (3.91) and the weight w_{new} is filled into a histogram at each time t.

For concreteness, we described the implementation of terms involving a single emission or a single angular integral. The contributions with two directions n_q, n_r are implemented analogously. By repeating the entire procedure N times and averaging the histograms, we get a numerical estimate for the integral in (3.91). Pseudo-code is provided in Listing 3.4 to illustrate the steps 1. – 4. from above.

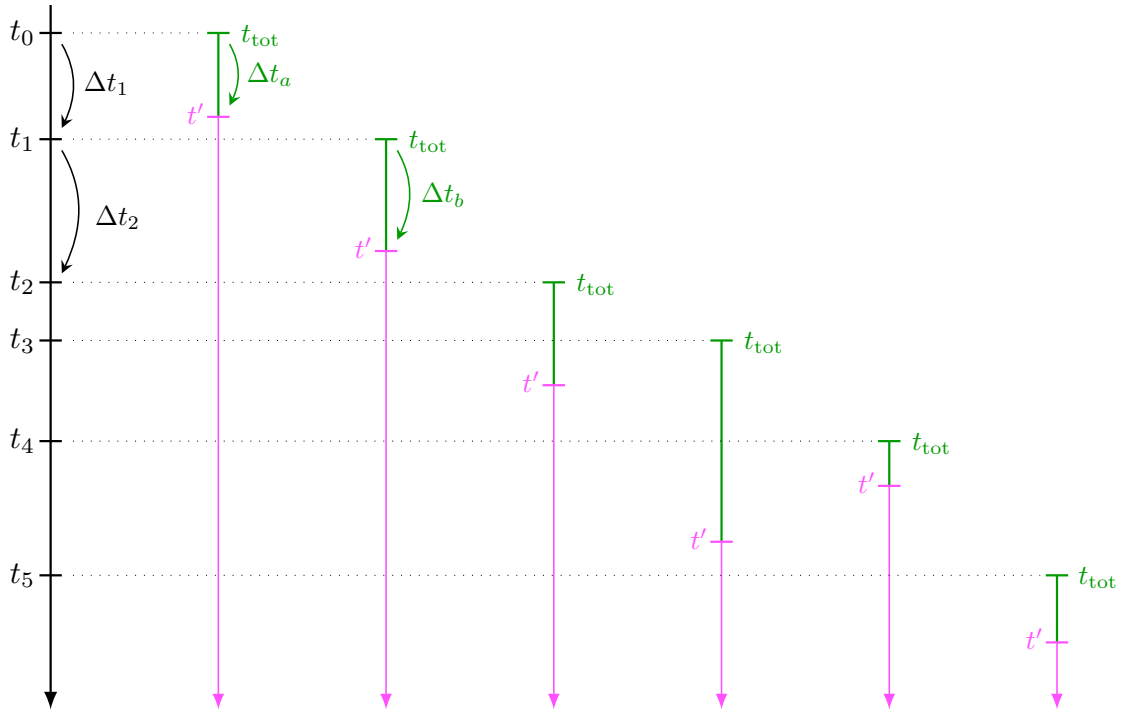

Figure 3.10: Algorithmic description of the insertion of the two-loop anomalous dimension. In black, we show the so-called master shower which we use to generate event configurations. At each intermediate time t_i, we perform an insertion and restart a LL shower at t', as indicated in pink. The time steps $\Delta t_{a,b}$ shown in green represent Δt_n in (3.93). The first insertion, denoted by $\mathcal{P}_2$ when $k' = 2$, is directly carried out with the initial particle configuration. While we keep the insertion and the master shower completely separate by generating two (random) time steps according to the corresponding probability distribution, it is also possible to directly reuse the time step from the insertion for the master shower – or the opposite, to use Δt_1 for the insertion. Once the master shower terminates, we restart a new one. In this way, we evaluate the integral over t', i.e. we insert the two-loop anomalous dimension at all possible times in the interval between t_0 and t.

```
//initial dipole
let nparton1 = [1.0, 0.0, 0.0, 1.0];
let nparton2 = [1.0, 0.0, 0.0, -1.0];

//Monte Carlo
for _i in 0..nev {

    //set up the master shower
    let ttot = 0.;
    let hardevent = [nparton1,nparton2];

    while ttot < tmax {

        //generate random time step Δt
        let delta = rand();
        let ttot_ins = ttot + delta;

        //determine which dipole radiates
        let ni,nj = hardevent.find_emitter();

        //generate weight and emissions
        let weight,nq,nr = kijb(hardevent,ni,nj);

        //REAL-VIRTUAL contribution

        //insert nq
        hardevent.insert(nq);
        //restart LL shower ↓
        hardevent.llshower(ttot_ins,weight_virt);

        //REAL-REAL contribution

        if nr.inside() {

            //insert nr
            hardevent.insert(nr);
            //restart LL shower ↓
            hardevent.llshower(ttot_ins,weight_real);

        }

        //run/continue the master shower ↓

        //generates Δt which increases ttot

        //adds an emission to hardevent before the next insertion

        //bins LL result

    }
}
```

Listing 3.4: Pseudo code for the insertion of the $K^{(b)}_{ij;qr}$ piece.

Details about the implementation

In this section, we will derive the form of the insertion weight given in (3.94) and explain some details about the implementation of the angular functions. The initial configuration for e^+e^- annihilation into two jets involves two back-to-back particles along the directions $n_1 = (1, 0, 0, 1)$ and $n_2 = (1, 0, 0, -1)$. The corresponding hard function is $\widehat{\mathcal{H}}_2(t')$, where we use the same normalization as in Section 3.2.2. We also set $t_0 = 0$.

The first insertion happens with the original configuration, as shown in Figure 3.10. For a single emission term, such as X_{ij}^q or γ_1^{cusp} we get

$$\begin{aligned}\Delta\boldsymbol{U}_{2l}(0,t) &= \int_0^t dt'\,\widehat{\mathcal{H}}_2(t')\,\Delta\Gamma^{(2)}_{2\to3}(t')\,\frac{1}{V_3}\left[V_3\boldsymbol{U}_{3l}(t',t)\right] \\ &= \int_0^t dt'\,\widehat{\mathcal{H}}_2(t')\,\frac{\Delta\Gamma^{(2)}_{2\to3}(t')}{V_{12}}\,\frac{V_2}{V_3}\left[V_3\boldsymbol{U}_{3l}(t',t)\right], \end{aligned} \tag{3.95}$$

where the insertion weight has been written out explicitly. The subscript of $\Delta\Gamma^{(2)}_{a\to b}$ indicates that we insert the generated emission n_q between its parents and restart a LL evolution $\boldsymbol{U}_{3l}(t',t)$ from an event containing three particles $\{n_1, n_q, n_2\}$. Therefore, equation (3.95) represents a single-real contribution. Its virtual counterpart is obtained by not updating the list of particles, such that we restart a LL shower $\boldsymbol{U}_{2l}(t',t)$ shower with $\{n_1, n_2\}$. The corresponding weight simplifies in this case to

$$\Delta\boldsymbol{U}_{2l}(0,t) = \int_0^t dt'\,\widehat{\mathcal{H}}_2(t')\,\frac{\Delta\Gamma^{(2)}_{2\to2}(t')}{V_{12}}\left[V_2\boldsymbol{U}_{2l}(t',t)\right]. \tag{3.96}$$

We point out that only the sum of real and virtual contributions is finite. In practice, we always calculate the corresponding real and virtual contributions once we generate an emission n_q to which we associate a certain weight. By doing so, large cancellations between real and virtual corrections are mitigated.

The master shower continues to evolve according to the LL algorithm and generates an additional particle n_3. This corresponds to the situation at[4] t_1 in Figure 3.10. Since three particles make up two dipoles, there are two possibilities for picking a dipole in the next insertion. The real contribution is given by

$$\Delta\boldsymbol{U}_{3l}(0,t) = \int_0^t dt'\,\widehat{\mathcal{H}}_3(t')\left[\frac{\Delta\Gamma^{(2)}_{3\to4}(t')}{V_{13}}\frac{V_{13}}{V_3}\frac{V_3}{V_4^{(1)}} + \frac{\Delta\Gamma^{(2)}_{3\to4}(t')}{V_{32}}\frac{V_{32}}{V_3}\frac{V_3}{V_4^{(2)}}\right]\left[V_4\boldsymbol{U}_{4l}(t',t)\right], \tag{3.97}$$

where $V_4^{(1)} = V_{14} + V_{43} + V_{32}$, $V_4^{(2)} = V_{13} + V_{34} + V_{42}$. In close analogy to the LL, we interpret the factors $\frac{V_{13}}{V_3}$, $\frac{V_{32}}{V_3}$ as the probability of choosing the corresponding dipole for the insertion. The virtual counterpart is given by

$$\Delta\boldsymbol{U}_{3l}(0,t) = \int_0^t dt'\,\widehat{\mathcal{H}}_3(t')\left[\frac{\Delta\Gamma^{(2)}_{3\to3}(t')}{V_{13}}\frac{V_{13}}{V_3} + \frac{\Delta\Gamma^{(2)}_{3\to3}(t')}{V_{32}}\frac{V_{32}}{V_3}\right]\left[V_3\boldsymbol{U}_{3l}(t',t)\right]. \tag{3.98}$$

Iterating this procedure, all possible insertions are carried out while the master shower is running. We conclude that the insertion weight is given by (3.94), where $\Delta\Gamma$ denotes the value of the integrand of the angular function which is evaluated during the shower evolution. Depending on whether we calculate a real or a virtual contribution, we either insert the generated emission or we do not. This affects the subsequent LL shower $\boldsymbol{U}_{k'l}(t',t)$.

[4] In fact, we first generate a time-step, insert the weight in a histogram and only then generate a new emission.

Once the master shower terminates, another one is started, and an insertion takes place at each intermediate time. By repeatedly generating emissions, the shower not only carries out the integral over the insertion time t', but also the angular integrals in (3.90). Since the anomalous dimension in the large-N_c limit is manifestly Lorentz invariant, we generate additional emissions in the back-to-back frame of the emitting dipole. This was instrumental in finding efficient parametrizations for sampling the weight of the integrals, which is crucial for obtaining reliable MC predictions. For instance, we note that the angular functions become singular when additional emissions along n_q and n_r are either collinear to one of the parents n_i, n_j or to each other. To regularize these singularities we impose a cut $\tan(\vartheta/2) > e^{-\eta_{\text{cut}}}$ on all angles ϑ between two directions in the lab frame. As mentioned previously, once real and virtual contributions are combined, the singular regions cancel. Nevertheless, in order to guarantee a smooth cancellation, it is important to isolate the singularity in one variable. More precisely, since the function $K_{ij;qr}$ contains an explicit $\frac{1}{n_{qr}}$ factor, it is reasonable to use the relative angle between n_q and n_r as an integration variable. To construct such a parameterization, we start with two vectors

$$n_q' = (1, 0, 0, 1)\,, \tag{3.99}$$

$$n_r' = (1,\ \sin\theta_{qr}\cos\phi_{qr},\ \sin\theta_{qr}\sin\phi_{qr},\ \cos\theta_{qr})\,, \tag{3.100}$$

which are rotated around the y- and z-axis

$$n_q = R_z(\theta_q)\cdot R_y(\phi_q)\cdot n_q'\,, \tag{3.101}$$

$$n_r = R_z(\theta_q)\cdot R_y(\phi_q)\cdot n_r'\,. \tag{3.102}$$

Using these coordinates we see immediately that $n_{qr} = 1 - \cos\theta_{qr}$. Performing the substitution $\cos\theta_{qr} = 1 - e^{\tilde{\eta}}$ we obtain for integrals involving a term n_{qr} in the denominator

$$\int_0^\pi d\theta_{qr}\sin\theta_{qr}\,\frac{1}{1-\cos\theta_{qr}} = \int_{-\infty}^{\ln(2)} d\tilde{\eta}\,. \tag{3.103}$$

The singularity has been isolated and exposed in the lower bound of the integral and can be handled by a cut. In addition, we replace the integration over θ_q with the rapidity $\eta_q = \frac{1}{2}\log\left(\frac{1+\cos\theta_q}{1-\cos\theta_q}\right)$. We note that the rapidity makes the following singularity explicit

$$\int_0^\pi d\theta_q\sin\theta_q\,\frac{1}{1-\cos^2\theta_q} = \int_{-\infty}^{\infty} d\eta_q\,, \tag{3.104}$$

which arises in angular integrals of the one-loop anomalous dimension. Even though such a singularity does not appear in $K_{ij;qr}$, we still find it useful to generate emissions using the rapidity. To quantify the impact of a suitable parameterization, we have implemented the $K^{(b)}_{ij;qr}$-piece of the anomalous dimension in two different ways. First, using the naive choice of spherical coordinates with four individual angles. Secondly, using the relative parameterization from (3.103). The result for the contribution of the $K^{(b)}_{ij;qr}$-piece to the resummed cross section $\sigma(t)$ as a function of the shower time is given in Figure 3.11. In Figure 3.11a we show the result using the naive spherical parameterization. We see that the result fluctuates significantly. As a consequence, it is necessary to increase the amount of statistics significantly to obtain a reliable prediction. The situation is different for the result we obtain using the relative parameterization in Figure 3.11b. While the results for the spherical parameterization fluctuate, the result from the relative parameterization is much more stable, i.e. oscillates very little around its average. We emphasize that both results were obtained using the same amount of statistics. For the remaining angular functions in (3.90) we extensively use the relative parameterization.

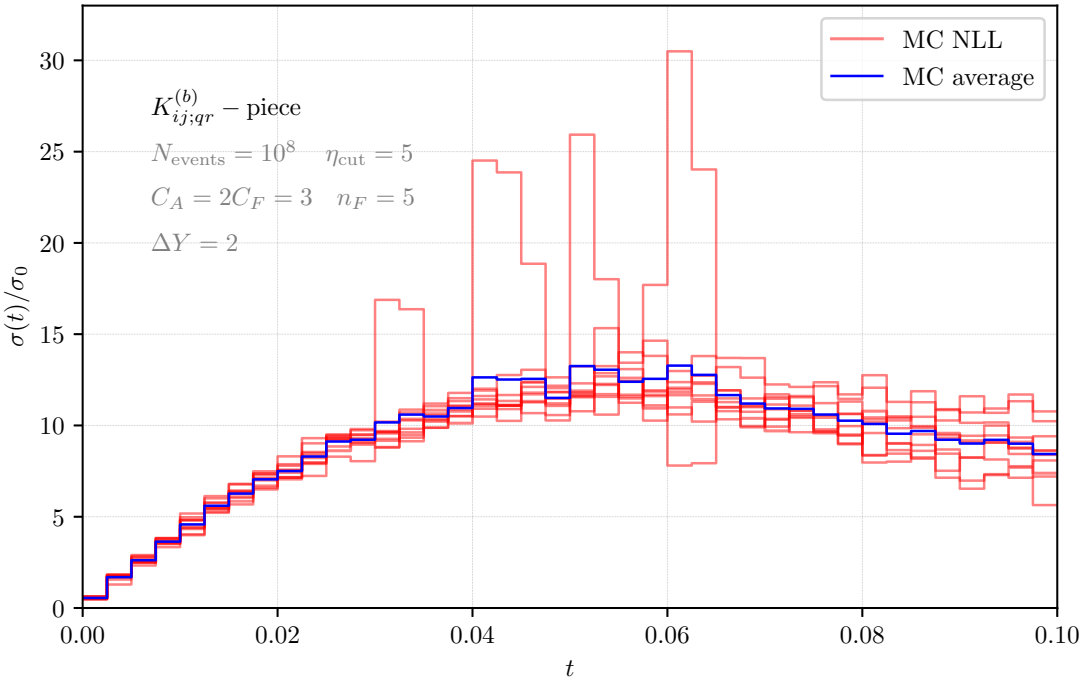

(a) Spherical parameterization.

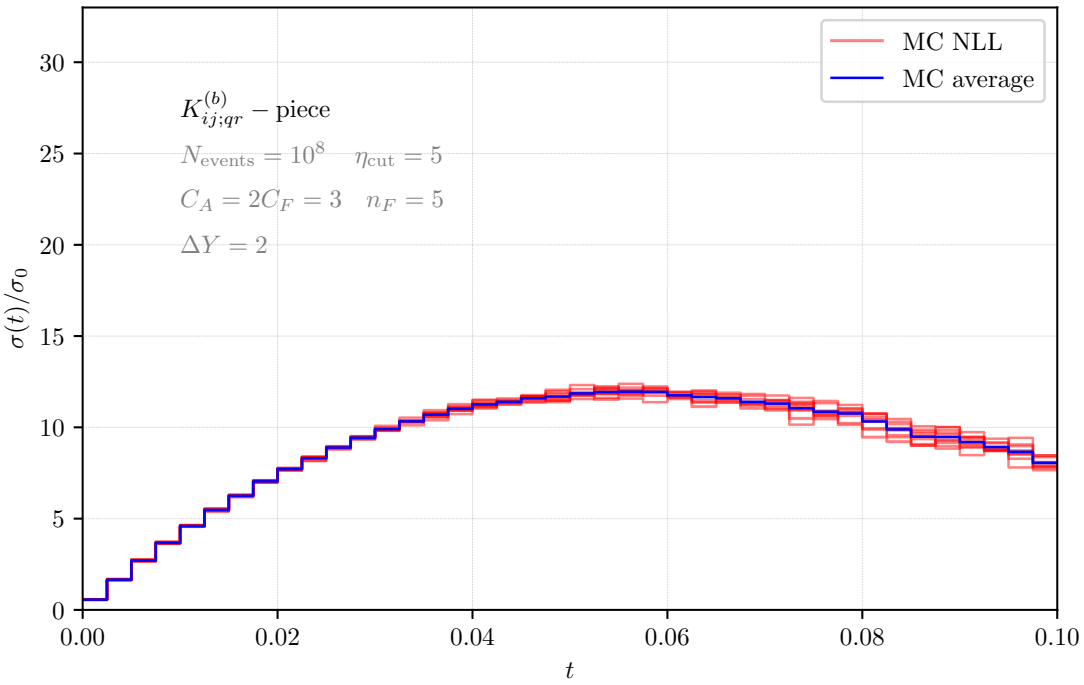

(b) Relative parameterization.

Figure 3.11: Shower result for the $K^{(b)}_{ij;qr}$-piece from the anomalous dimension. Different parameterizations were used to evaluate the angular integral. Each red histogram represents one numerical evaluation of $K^{(b)}_{ij;qr}$ with 10^8 events. The blue line represents the average over the ten evaluations.

Using relative parameterization, contributions from singular regions are exposed clearly and large contributions are mitigated, as shown in Figure 3.11. However, since we introduced a (small) cutoff parameter η_{cut}, it is necessary to verify whether remaining cutoff effects are negligible because the physical result must not depend on the particular value of η_{cut}. We set $\eta_{\text{cut}} = \eta_c$ as default in our MC. In practice, numerical cutoffs are decreased until the dependence on them becomes negligible. This is a non-trivial task since reducing the cutoff increases the cancellation between real and virtual contributions, making it numerically more expensive to obtain a certain precision.

To investigate cutoff dependence in MARZILI, we calculate separately the double-real and real-virtual contribution of $K^{(b)}_{ij;qr}$ using two different values for η_{cut}. Results for $\eta_{\text{cut}} = 5$ are shown in Figure 3.12. In the upper Figure 3.12a we provide separate results for the double-real and real-virtual contributions. Combining double-real and real-virtual contributions, we obtain the full result for $K^{(b)}_{ij;qr}$, which is shown in Figure 3.12b. We clearly see a cancellation of one order of magnitude when we compare the upper and lower Figure of 3.12. We point out that the numerical fluctuations decrease in Figure 3.12b compared to 3.11b, where the same cutoff was used. This is due to an increase in the number of events that were evaluated. Since the error from the numerical simulation scales as $\frac{1}{\sqrt{N}}$, this is a good indication that our MC implementation is reliable.

The cutoff was decreased to $\eta_{\text{cut}} = 8$ in Figure 3.13. Unsurprisingly, the cancellations between real-virtual and double-real corrections increase by an order of magnitude. This is due to the fact that by reducing the cutoff, we allow emissions to become more collinear than before. As a result, problematic numerators, such as $\frac{1}{n_{qr}}$ or $\frac{1}{n_{iq}}$, become even larger. To obtain reliable results nonetheless, we need to increase the statistics to deal with singular numerators. Unfortunately, this comes at the cost of computing time.

Decreasing the cutoff itself increases the computing time. This is due to the fact that the t-steps become much shorter, which means that the amount of additional particles generated while showering heavily increases. Therefore, the LL evolution before and after the insertion takes more computer time. In Figure 3.13 we increased the amount of statistics by a factor of ten compared to the results in Figure 3.12. As a consequence, the combined effect of both increasing the statistics as well as decreasing the cutoff η_{cut}, increases the computing time roughly by a factor of ~ 100 – and not only ten.

Even though numerical fluctuations are larger in Figure 3.13b in comparison to 3.12b, the numerical average for the cutoff $\eta_{\text{cut}} = 8$ is reliable. Comparing Figure 3.13b with Figure 3.14, we see that numerical noise can be significantly reduced if real-virtual and double-virtual contributions are showered together. In this way, large cancellations are mitigated since they directly cancel.

In practice, we observe that to completely eliminate any dependence on the cutoff η_{cut} for the entire NLL contribution, we need to decrease it to $\eta_{\text{cut}} = 8$.

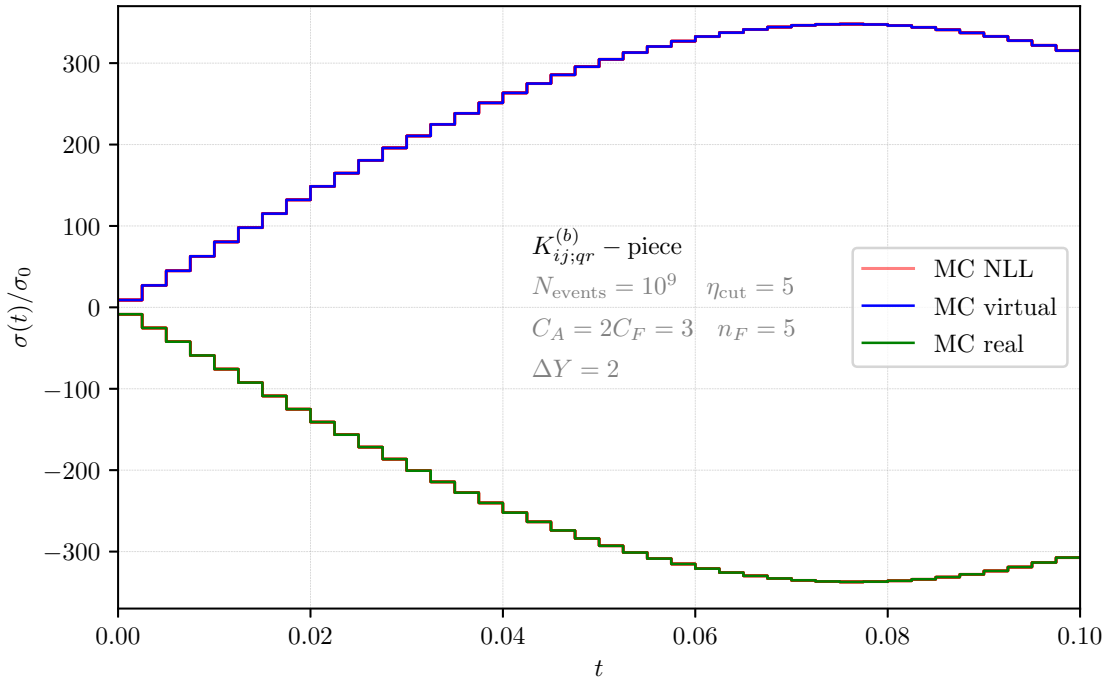

(a) Separated double-real and real-virtual contributions for $K^{(b)}_{ij;qr}$.

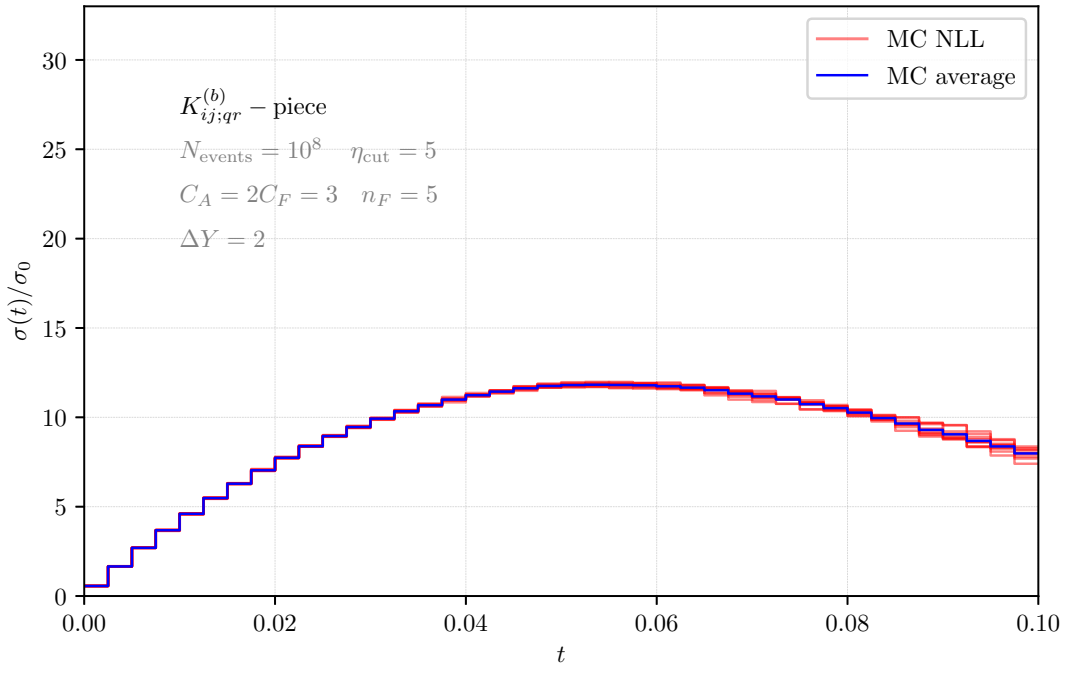

(b) Sum of double-real and real-virtual contributions for $K^{(b)}_{ij;qr}$.

Figure 3.12: Separate shower result for double-real (green) and real-virtual (blue) corrections of the $K^{(b)}_{ij;qr}$-piece. A cut of $\eta_{\text{cut}} = 5$ was used. Red histograms represent one numerical evaluation with 10^9 events. In total, ten separate evaluations of double-real and real-virtual corrections were carried out. The lower figure represents the sum of double-real and real-virtual contributions.

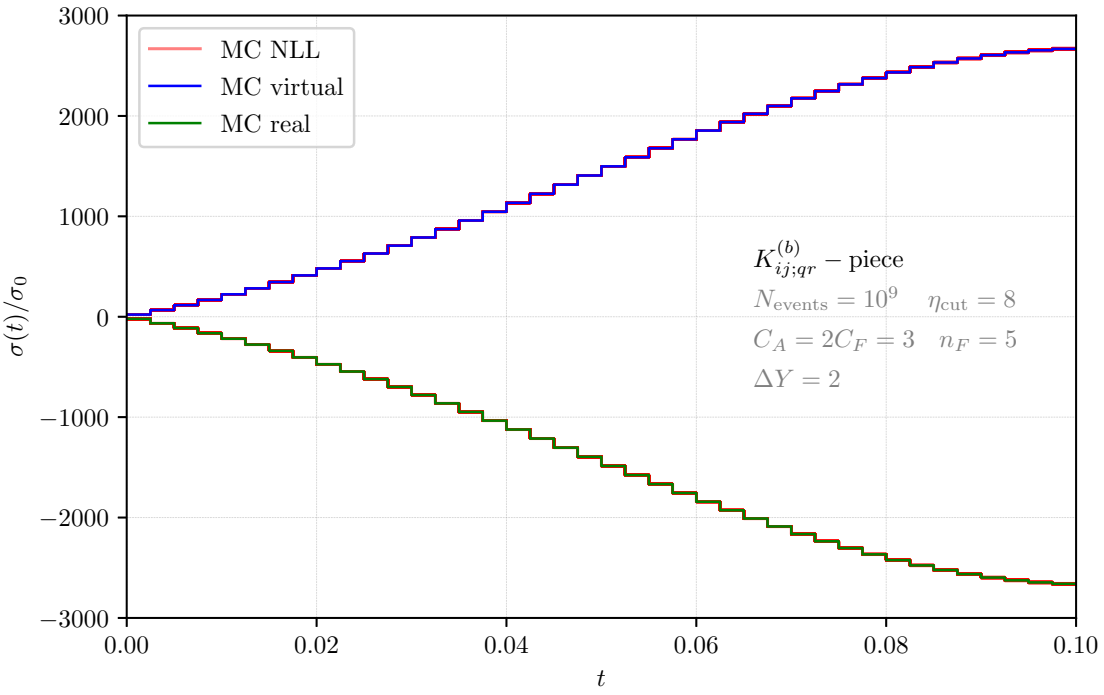

(a) Separated real and virtual contributions for $K^{(b)}_{ij;qr}$.

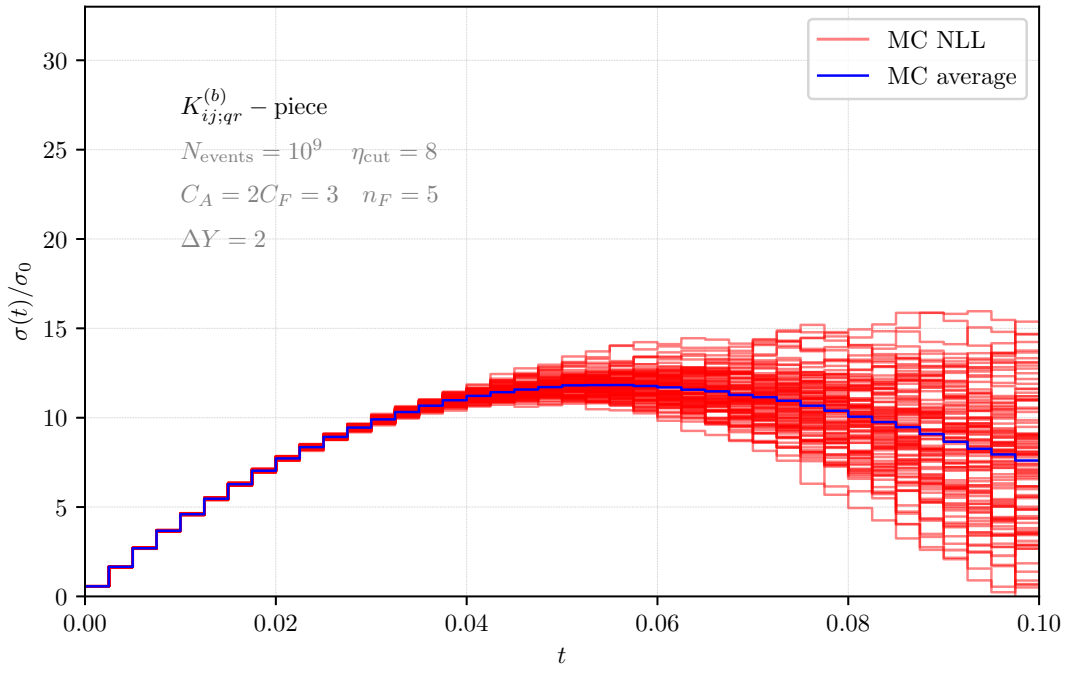

(b) Sum of real and virtual contributions for $K^{(b)}_{ij;qr}$.

Figure 3.13: Separate shower result for double-real (green) and real-virtual (blue) corrections of the $K^{(b)}_{ij;qr}$-piece. A cut of $\eta_{\text{cut}} = 8$ was used. Red histograms represent one numerical evaluation with 10^9 events. In total, 100 separate evaluations of real and virtual corrections were carried out. The lower figure represents the sum of real and virtual contributions.

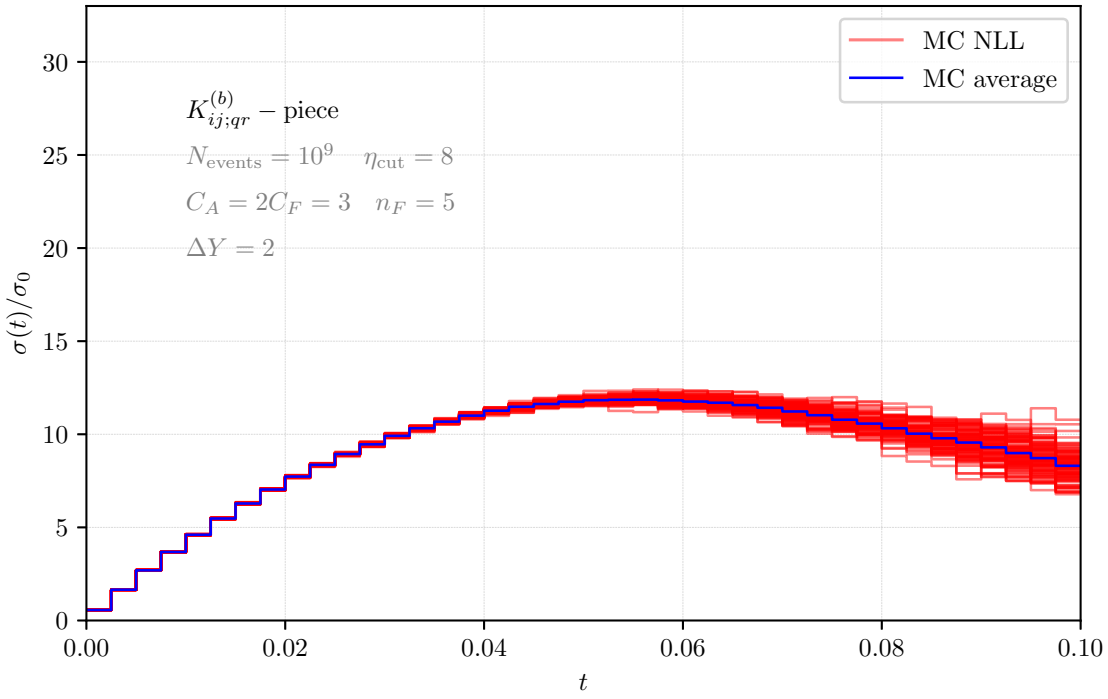

Figure 3.14: Numerical result for the $K^{(b)}_{ij;qr}$-piece of the anomalous dimension. Red histograms represent one numerical evaluation with 10^9 events. In total, 100 separate evaluations of $K^{(b)}_{ij;qr}$ were carried out. Here, real-virtual and double-real corrections were directly combined.

The terms in the double-emission contribution $\boldsymbol{d}_m$ proportional to n_F describe the splitting of a gluon into a quark-antiquark pair. The large-N_c structure of this contribution differs from the remaining terms in $\boldsymbol{\Gamma}^{(2)}$ describing the emission of two gluons. To account for this in our shower, the insertion of $\boldsymbol{d}_m$ is split up according to

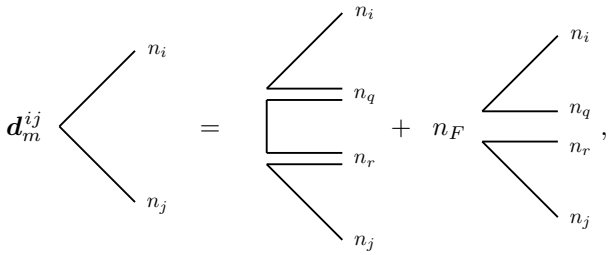

(3.105)

where the lines indicate the dipole structure after the insertion. The evolution after the insertion in (2.102) is then performed separately for the two parts, according to their dipole structure. On a technical level, it is convenient to treat n_q and n_r as an additional dipole with $V_{qr} = 0$ in the n_F part, i.e. as a dipole that never radiates.

3.4 Validation

This section thoroughly assesses the implementation of the two-loop anomalous dimension within our large-N_c parton shower framework Marzili. Since the numerical shower evolution is quite involved, robust consistency tests are necessary to ensure that the implementation is correct. We divide the validation in two sections. First, we conduct internal consistency checks in Section 3.4.1. Our shower successfully passes all internal tests.

Second, we compare our full NLL prediction for the energy flow in a rapidity slice to the results from Gnole [148] and PanScales [142]. All frameworks are able to resum the NLL non-global logarithms using a different approach. While every formalism has its own advantages, it is important to ensure that the predictions are in agreement. The details about the comparison are shown in Section 3.4.2. Generally, we find good agreement between the three entirely different frameworks. A detailed numerical analysis involving a thorough assessment of systematic uncertainties is part of a forthcoming publication [210].

3.4.1 Internal consistency checks

In this section, we verify two essential properties of our shower. As a first analysis, we exponentiate terms proportional to γ_1^{cusp} and verify whether expanding these numerically yields the same results as our insertion algorithm. In addition, we reproduce fixed-order results from [123] using the shower to demonstrate that the angular functions have been implemented correctly.

The simplest contributions of $\mathbf{\Gamma}^{(2)}$ are given by terms proportional to γ_1^{cusp}. Isolating these real-virtual and double-virtual contributions in (3.90)

$$\begin{aligned} \boldsymbol{r}_m &= +\frac{\gamma_1^{\text{cusp}}}{4} \cdot 4N_c\, W_{ij}^q\, \theta_{\text{in}}(n_q)\,, \\ \boldsymbol{v}_m &= -\frac{\gamma_1^{\text{cusp}}}{4} \cdot 4N_c \int \left[d^2\Omega_q\right] W_{ij}^q\,, \end{aligned} \tag{3.106}$$

we see that they are exactly proportional to the one-loop anomalous dimension. As a result, we can exponentiate the γ_1^{cusp} contributions by redefining the shower time in (2.97)

$$\int_{\mu_s}^{\mu_h} \frac{d\mu}{\mu}\, \mathbf{\Gamma} = \int_{\alpha_s(\mu_h)}^{\alpha_s(\mu_s)} d\alpha_s\, \frac{1}{2\beta_0\alpha_s} \left(\mathbf{\Gamma}^{(1)} + \frac{\alpha_s}{4\pi}\left(\mathbf{\Gamma}^{(2)} - \frac{\beta_1}{\beta_0}\mathbf{\Gamma}^{(1)}\right)\right) \tag{3.107}$$

$$= \int_{\alpha_s(\mu_h)}^{\alpha_s(\mu_s)} d\alpha_s\, \frac{1}{2\beta_0\alpha_s} \left(1 + \frac{\alpha_s}{4\pi}\frac{\gamma_1^{\text{cusp}}}{4}\right) \mathbf{\Gamma}^{(1)} + \cdots \tag{3.108}$$

$$= \int_{t_0}^{t} d\tilde{t}\, \mathbf{\Gamma}^{(1)}\,, \tag{3.109}$$

where the ellipsis denotes non-cusp terms and we inserted the γ_1^{cusp} contribution from (3.106) for $\mathbf{\Gamma}^{(2)}$ from the first to the second line. We omitted β_1-terms because they are remnants of corrections to the running of α_s and not directly related to γ_1^{cusp}-pieces. Finally, we introduced a modified shower time

$$\tilde{t} = t - \frac{\alpha_s(\mu_h)}{4\pi}\frac{\gamma_1^{\text{cusp}}}{4}\frac{1}{2\beta_0}\left(1 - e^{2\beta_0 t}\right)\,, \tag{3.110}$$

capturing the γ_1^{cusp} contributions. The variable $t = \frac{1}{2\beta_0}\ln\left(\frac{\alpha_s(\mu_s)}{\alpha_s(\mu_h)}\right)$ is the shower time we introduced before. This implies that we can exponentiate terms proportional to γ_1^{cusp} by simply

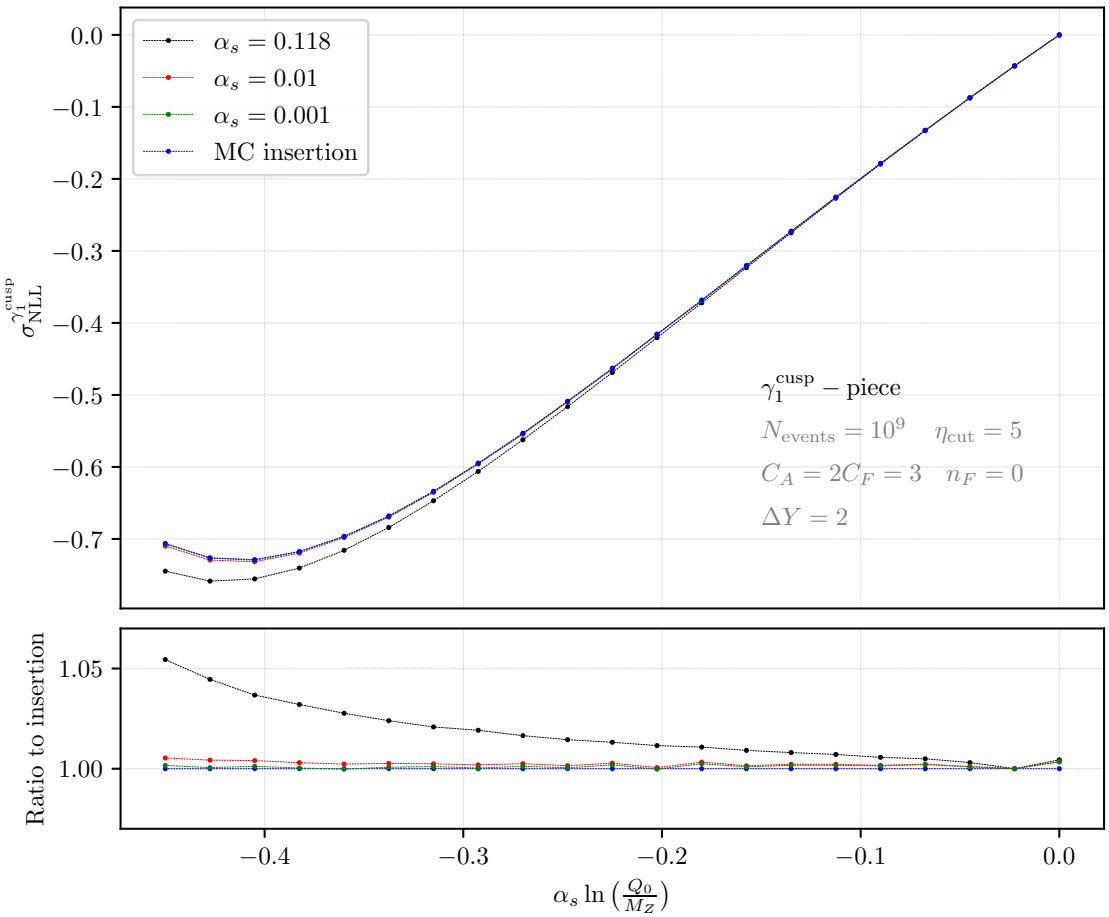

Figure 3.15: Results for one insertion of γ_1^{cusp}. The single insertion according to (3.91) is shown in blue, while the other curves are numerical extractions of the single insertion from the exponentiated result.

changing the definition of the shower time from $t \mapsto \tilde{t}$. Subsequently, we expand to isolate the pure NLL term $\sigma_{\text{NLL}}^{\gamma_1^{\text{cusp}}}$ by taking the limit

$$\lim_{\alpha_s \to 0} \frac{1}{\alpha_s} \ln \frac{\sigma_{\text{LL}}^{\gamma_1^{\text{cusp}}} + \alpha_s \, \sigma_{\text{NLL}}^{\gamma_1^{\text{cusp}}} + \alpha_s^2 \, \sigma_{\text{NNLL}}^{\gamma_1^{\text{cusp}}} + \cdots}{\sigma_{\text{LL}}^{\gamma_1^{\text{cusp}}}} = \sigma_{\text{NLL}}^{\gamma_1^{\text{cusp}}} + \mathcal{O}(\alpha_s) \, . \tag{3.111}$$

This is delicate since we have to numerically take the limit of $\alpha_s \to 0$ in order to suppress NNLL γ_1^{cusp} terms. After taking the limit we compare to the result with one insertion of the anomalous dimension. Results are shown in Figure 3.15. We see from the relative comparison between the black and blue curve that the results differ. By decreasing the value of the coupling at the hard scale α_s – while keeping the product $\alpha_s \ln \frac{Q_0}{M_Z}$ constant – we obtain full agreement between the direct insertion and the expansion. Therefore, we conclude from Figure 3.15 that our implementation of the insertion is correct.

It is more difficult to test the remaining parts of (3.90) which involve the angular functions $K_{ij;qr}$ and $M_{ij;qr}$. An important test is that our numerical code reproduces the analytical integrals over these expressions which arise in the NNLO correction of the interjet energy flow at small Q_0 given

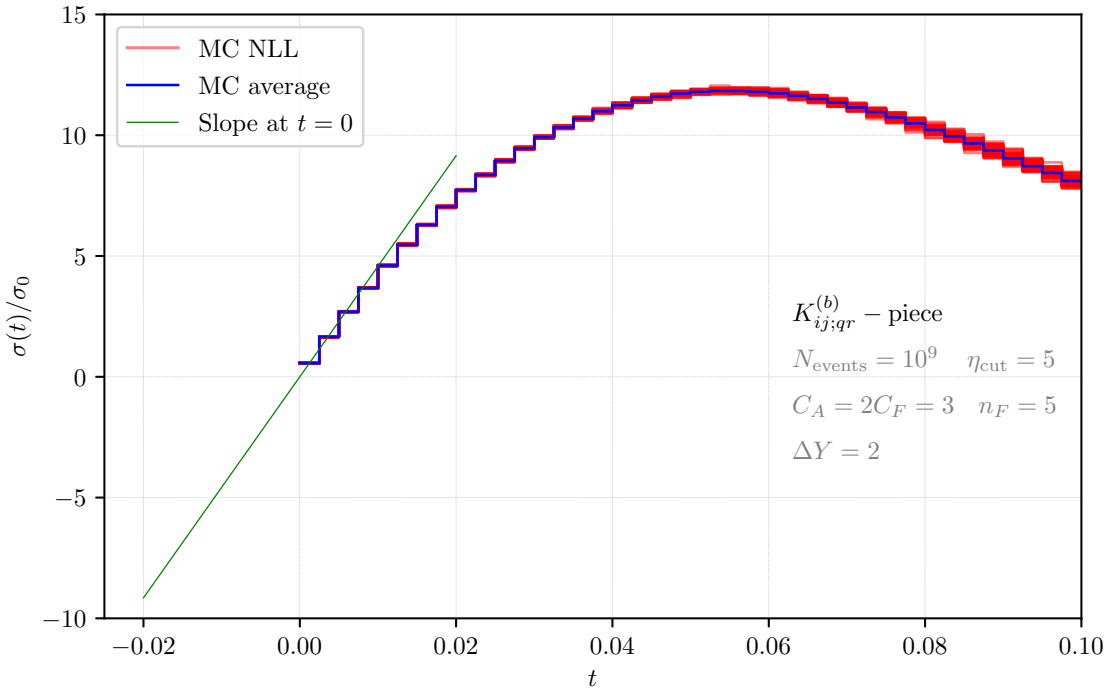

Figure 3.16: Numerical result for the $K^{(b)}_{ij;qr}$-piece of the anomalous dimension. Red histograms represent one numerical evaluation with 10^9 events. In total, 100 separate evaluations of $K^{(b)}_{ij;qr}$ were carried out. In green, we show the slope at $t = 0$. The amount of color flavors was set to $n_F = 5$ within the running correction β_0, however, purely fermionic terms inside $K^{(b)}_{ij}$ are set to 0.

in [123], for example the combination

$$\int \left[d^2\Omega_r\right] \int \left[d^2\Omega_q\right] \left(K^{(b)}_{12;qr} + K^{(b)}_{21;qr}\right) \theta_{\text{in}}(n_q)\, \theta_{\text{out}}(n_r)\,. \tag{3.112}$$

This quantity can be calculated with our shower since this value corresponds to the slope at $t = 0$ for the showered result of $K^{(b)}_{ij;qr}$. The result is illustrated in Figure 3.16. We extracted the slope by fitting a linear function to the derivative of the shower result. We find a slope $m_0 = 457.61$, which is in full agreement with the analytical value of $m_{\text{analytical}} = 457.79$, see Section 6 in [123]. We performed this fixed-order test with the remaining parts of $K_{ij;qr}$ as well as for $M_{ij;qr}$. In all cases, the integration converges to the analytical result. Together with the validation of our implementation of the single insertion of $\mathbf{\Gamma}^{(2)}$ using the γ_1^{cusp}-piece, this provides a strong consistency check on our shower code.

3.4.2 Comparison to Gnole and PanScales

It is not apparent how the more complicated parts of $\mathbf{\Gamma}^{(2)}$ map between Gnole, PanScales and our parton shower framework. The Gnole or PanScales approach works with full four-vectors instead of directions and to obtain the mapping analytically, one would have to integrate out the energies of the generated partons.

Since the three formalisms are genuinely different, numerical agreement is a strong cross-check and a good indication that the NLL are captured correctly in the three frameworks. This section will carefully outline the three-way comparison between Marzili, Gnole and PanScales. The

observable we consider is the energy flow in a rapidity slice for dijet production in e^+e^- annihilation. Particles are inside the veto region, i.e. outside of the jet cones, if their angle relative to the thrust axis is larger than $\cos\alpha = 0.761594$, which corresponds to a rapidity gap of $\Delta Y = 2$, see Figure 2.3. We calculate the gap fraction

$$R(Q_0) \equiv \frac{1}{\sigma_{\text{tot}}} \int_0^{Q_0} dE_T \, \frac{d\sigma}{dE_T} \,, \tag{3.113}$$

which is the fraction of events with transverse energy E_T in the gap below Q_0. We can directly apply the factorization theorem (2.11) to the gap fraction $R(Q_0)$. To obtain the full NLL corrections, we calculate matching corrections and contributions due to the insertion of the two-loop anomalous dimension. We follow the aforementioned approach, as outlined in Sections 3.3.1 – 3.3.3.

While our framework is based on RG-improved perturbation theory, where large logarithms are resummed and the remaining parts are expressed through the coupling at the respective scale $\alpha_s(\mu_h)$ or $\alpha_s(\mu_s)$ respectively, the situation is different for GNOLE and PanScales. Their results are expanded in terms of a power series in $\alpha_s(\mu_h)$ while keeping $\lambda \equiv \alpha_s(\mu_h) \ln \frac{\mu_s}{\mu_h}$ constant. We carry out the comparison for the default scales $\mu_h = M_Z$ and $\mu_s = Q_0$. To compare to PanScales and GNOLE, it is necessary to trade the dependence on $\alpha_s(\mu_s)$ for λ. To do so, we use for the running of the coupling [211]

$$\alpha_s(\mu_s) = \frac{\alpha_s(\mu_h)}{\ell} \left(1 - \frac{\alpha_s(\mu_h)}{4\pi} \frac{\beta_1}{\beta_0} \frac{\ln \ell}{\ell} + \cdots \right) , \tag{3.114}$$

with $\ell = 1 + \frac{\beta_0}{2\pi} \alpha_s(\mu_h) \ln \frac{\mu_s}{\mu_h} \equiv 1 + \frac{\beta_0}{2\pi} \lambda$. Inserting (3.114) into our definition of the shower time and expanding in terms of $\alpha_s(\mu_h)$ we get

$$t = \frac{1}{2\beta_0} \ln \frac{\alpha_s(\mu_s)}{\alpha_s(\mu_h)} = t_{\text{LL}} + \frac{\alpha_s(\mu_h)}{4\pi} \frac{\beta_1}{\beta_0} \, t_{\text{LL}} \, e^{2\beta_0 \, t_{\text{LL}}} + \cdots \,, \tag{3.115}$$

where we introduced the leading contribution to the shower time

$$t_{\text{LL}} = -\frac{\ln\left(1 + \frac{\beta_0}{2\pi} \lambda\right)}{2\,\beta_0} \,. \tag{3.116}$$

As a result, inserting (3.115) into the LL correction leads to

$$\sigma_{\text{LL}}\,(t) = \sigma_{\text{LL}}(t_{\text{LL}}) + \frac{\alpha_s(\mu_h)}{4\pi} \, t_{\text{LL}} \, \frac{\beta_1}{\beta_0} \, e^{2\beta_0 \, t_{\text{LL}}} \, \sigma'_{\text{LL}}(t_{\text{LL}}) + \cdots \,, \tag{3.117}$$

where the second term represents the running correction and depends on the derivative σ'_{LL} of the LL result. We implemented the derivative separately in our MC framework since taking numerically the derivative of σ_{LL} is delicate. The derivative can be obtained by slightly modifying the LL algorithm outlined in Section 3.2 [106]. It is further necessary to expand $\frac{1}{\sigma_{\text{tot}}}$ in (3.113)

$$\frac{1}{\sigma_{\text{tot}}} = \frac{1}{\sigma_{\text{LO}}} \left(1 - C_F \, \frac{\alpha_s(\mu_h)}{4\pi} \, 3\right) + \mathcal{O}\left(\alpha_s^2\right) \,, \tag{3.118}$$

as a correction to the normalization. Adding the corrections due to the normalization as well as the running, we obtain our final result for the NLL corrections, which we normalize by dividing out $\alpha_s(\mu_h)\sigma_{\text{LL}}(t_{\text{LL}})$. Using this normalization, the dependence on $\alpha_s(\mu_h)$ completely drops out.

We performed two dedicated simulations, with $n_F = 5$ and $n_F = 0$. The results, including fermionic corrections, are shown in Figure 3.17, whereas the ones without are illustrated in Figure 3.18. Since every formalism involves a slightly different implementation of the shower cutoff(s)

η_c, η_{cut} and η_{slice}, we expect the predictions to agree only once the cutoff dependence has been completely removed. In practice, this means that it is necessary to decrease the cutoffs to $\eta_c = \eta_{\text{cut}} = \eta_{\text{slice}} = 8$ in our framework. Therefore, to guarantee reliable results, we significantly increased the amount of statistics which severely affected the running time. From Figures 3.17 and 3.18, we conclude that the predictions are in good agreement. We would like to remind the reader that the results shown in Figures 3.17 and 3.18 are preliminary. A detailed numerical comparison will be addressed in the forthcoming publication [210]. The main focus will be on investigating systematic uncertainties such as the cutoff-dependence η_{cut} or the extrapolation $\alpha_s \to 0$ to isolate the NLL contribution.

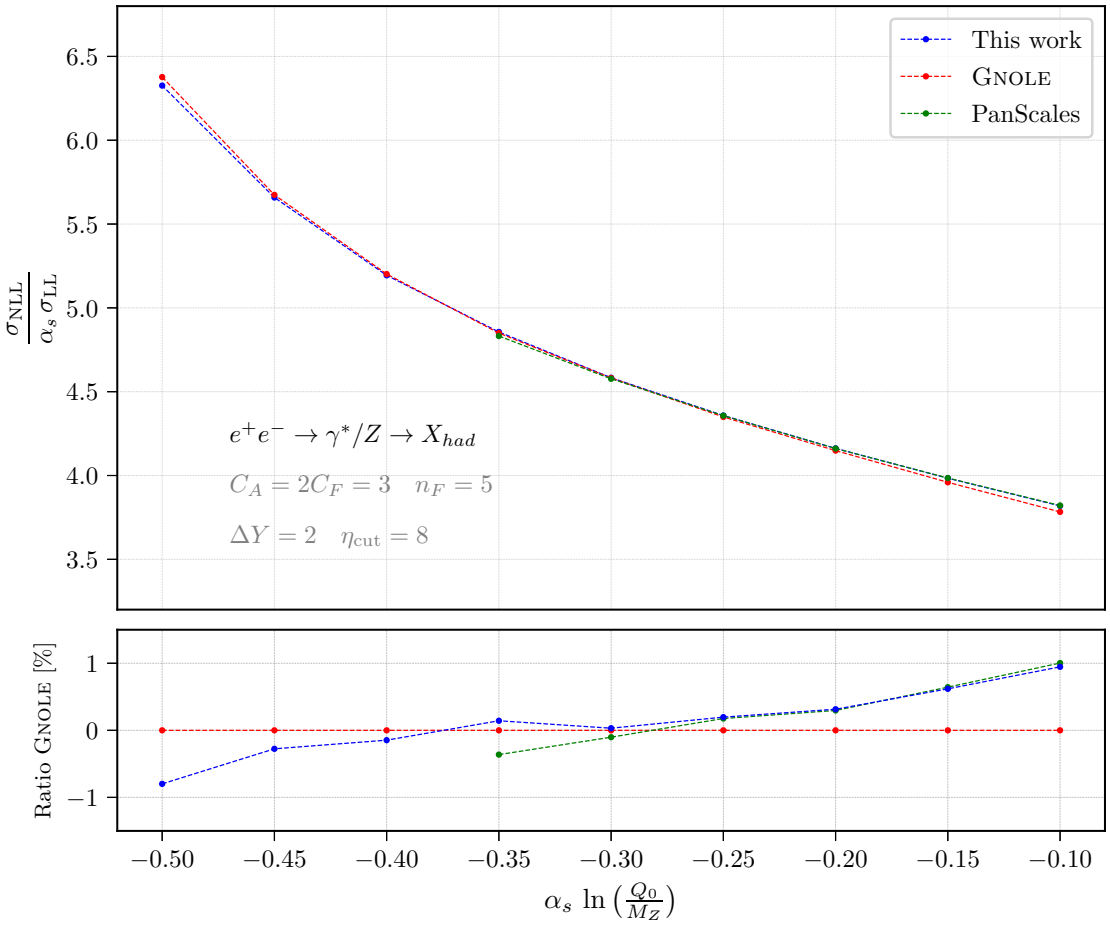

Figure 3.17: Preliminary comparison for the gap fraction including the full fermionic corrections for $n_F = 5$.

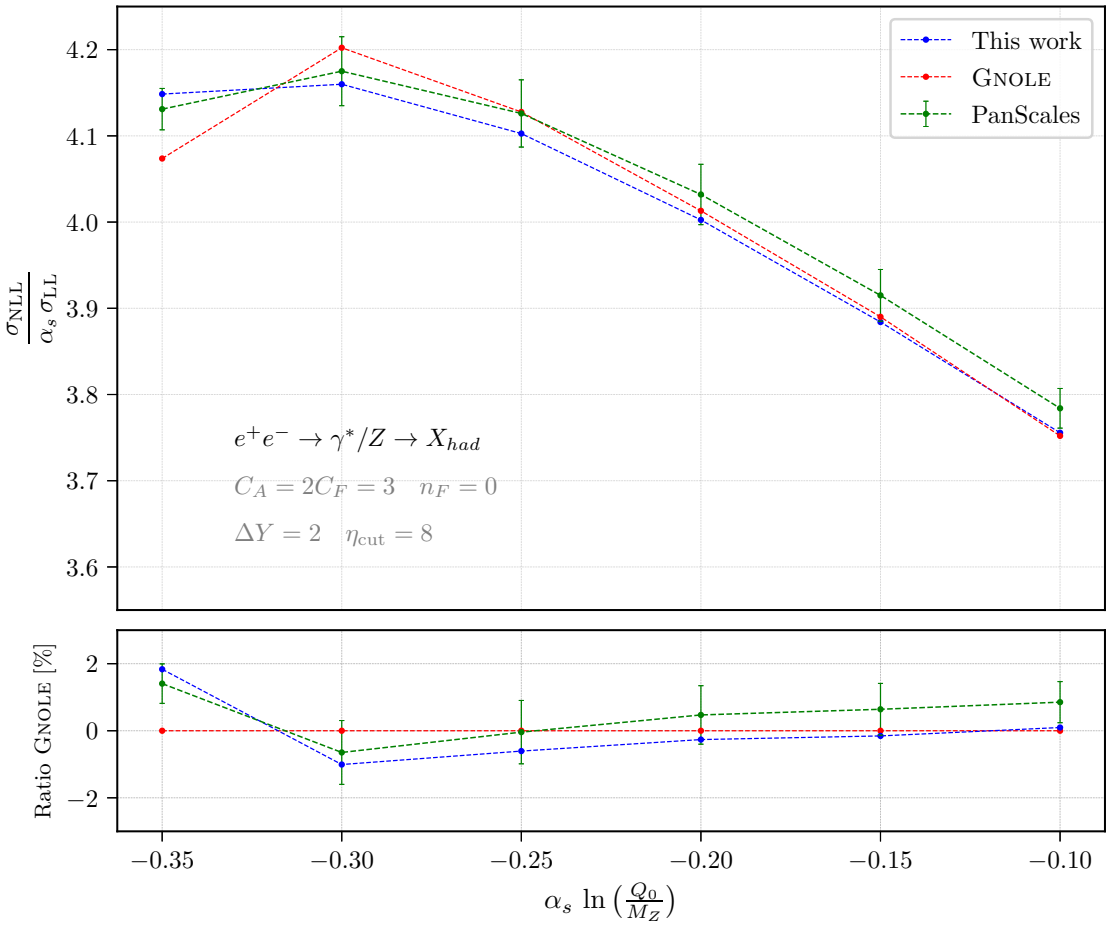

Figure 3.18: Preliminary comparison for the gap fraction setting $n_F = 0$.

3.5 Summary

In this chapter, we have precisely outlined how we implement the one- and two-loop anomalous dimensions in the large-N_c parton shower framework MARZILI (Monte-cArlo for the RenormaliZation group Improved calculation of non-global LogarIthms).

Starting from RG equations in (3.1) for the hard functions, we find an iterative solution by taking into account the explicit form of the one-loop anomalous dimension. This iterative solution naturally relates our effective field theory approach with parton showers since the solution (3.9) is precisely a parton shower algorithm. We implemented this algorithm and carried out a qualitative study at LL accuracy for gaps between jets. We find that neglecting NGLs overestimates the cross section. Additionally, we also explained that even the leading NGLs do not exponentiate – in contrast to the global ones.

To capture hard matching corrections, we rely on a calculation in the full theory to obtain the matrix elements. Once either a real or a virtual emission has been generated, the particle configuration is subsequently showered. A subtlety one needs to carefully take into account is that real contributions contain a priori +-distributions acting on $\widehat{\boldsymbol{\mathcal{S}}}_3$ which cannot be evaluated directly in the MC. The simplest way to circumvent this issue is to introduce a slicing scheme.

The soft matching corrections are obtained by inserting the (soft) weight of the final emission into a histogram. In this context, the final emission is the first emission inside the veto region and the corresponding weight is given in (3.57). At NLL accuracy, this is the only ingredient that is sensitive whether we restrict the energy or its transverse component, see (3.60).

The most complicated correction at subleading accuracy is the insertion of the two-loop anomalous dimension. Fortunately, to isolate the pure NLL correction, it is sufficient to insert it exactly once. We obtain a concise form of the two-loop anomalous dimension in the large-N_c limit involving ϵ-terms. We find that ϵ-terms nicely combine with $\boldsymbol{\Gamma}^{(2)}$ – in fact, ϵ-terms restore Lorentz invariance. The final result for the anomalous dimension in the large-N_c limit is presented in (3.90). Crucially, the invariance allows us to generate additional emissions in the back-to-back frame of the emitting dipole, which is the most efficient way to sample the angular integrals. In practice, we carry out the insertion by starting a LL shower $\boldsymbol{U}_{kl}(t_0, t')$ at t_0, which evolves until t', where we evaluate $\boldsymbol{\Gamma}^{(2)}$, and then we restart a LL shower.

Finally, we carried out a series of tests to validate our implementation. Most importantly, we find good agreement between our predictions, PanScales and GNOLE within statistical and systematic uncertainties.

In the next section, we will apply our formalism to non-global observables at hadron colliders, focusing on the difference between fixed-order and resummed predictions.

Chapter 4

Phenomenological predictions for non-global observables

In this chapter, we will present phenomenological results for gap fractions in dijet production from e^+e^- annihilation and in Z-boson production. The full set of NLL contributions was initially obtained in [1]. While first results at NLL accuracy for the interjet energy flow in e^+e^- were obtained in [147, 148], using our parton shower framework MARZILI, we were able to obtain first results for a gap-between-jets observable at hadron colliders.

4.1 Gap fraction in e^+e^-

For our cross section computations, we work at center-of-mass energy $\sqrt{s} = M_Z$ with $\alpha_s(M_Z) = 0.119$ and use two-loop running for α_s. We calculate the gap fraction exactly as defined in (3.113). To include power corrections beyond the factorization theorem (2.11), we match to the fixed-order prediction at order α_s. In other words, we add perturbative corrections to the resummed result and subtract the pieces already included, which are precisely the soft pieces. The power-suppressed matching corrections ΔR are included through additive matching

$$\Delta R(Q_0) = \frac{1}{\sigma_{\text{tot}}} \int_0^{Q_0} dE_T \left(\frac{d\sigma}{dE_T} - \frac{d\sigma}{dE_T}\bigg|_{E_T \to 0} \right) , \tag{4.1}$$

where the second term corresponds to the singular limit of the full distribution, which is the same as using the factorization theorem without evolution. Specifically, we obtain the matching corrections by subtracting the soft contributions from real emissions within the gap. These soft contributions are precisely captured by the soft function, which is already accounted for in the resummation. We use profile functions [29] to continuously switch off resummation once the power-suppressed terms become relevant. The shape of the curve at larger Q_0 values is affected by this choice. We use the functions introduced in [107]. On the left side of Figure 4.1 we show our numerical results for the gap fraction of the interjet energy flow in e^+e^-. The bands arise from varying the soft scale μ_s since this effect dominates over the μ_h variation. The LL (red curve) in Figure 4.1 is taken from [85] at finite $N_c = 3$. These results at full color were obtained using a conformal transformation, relating the BMS equation to the Balitsky-JIMWLK [212–218] equation. The corresponding numerical solutions include full color dependence. After adding the NLL corrections computed from our shower (blue curve), we obtain a resummed result that is only missing subleading color contributions at NLL. These effects are expected to contribute at the percent level or below. We want to emphasize two properties of our result. First, the large

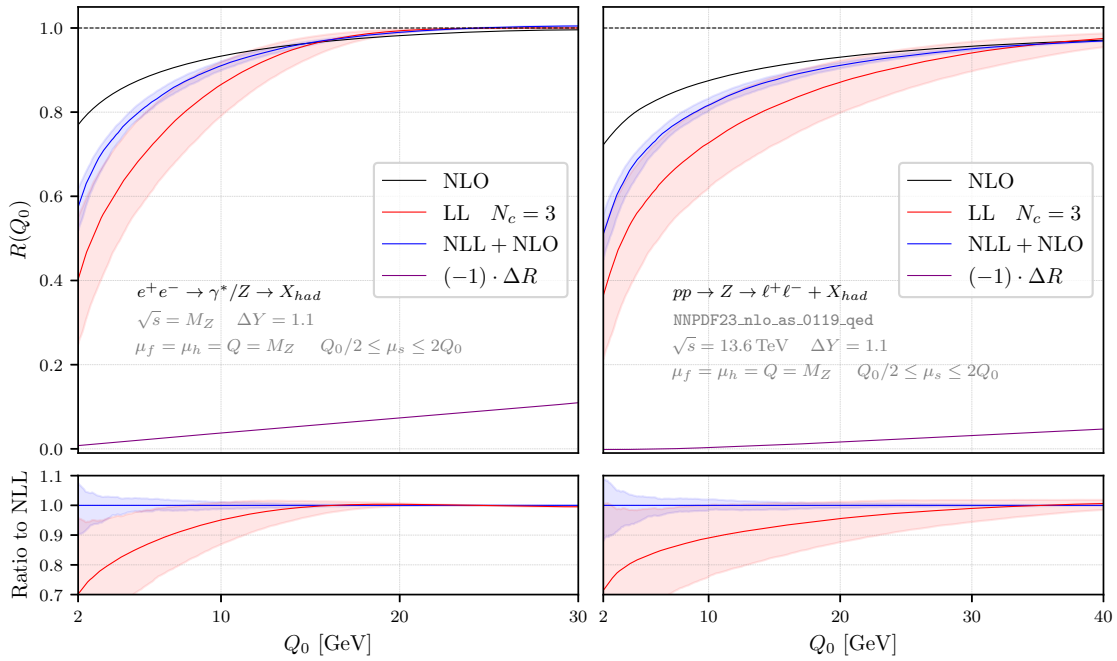

Figure 4.1: Gap-between-jets cross sections at lepton (left) and hadron colliders (right) using $Q = M_Z$. The statistical fluctuations visible in the results are due to the $N_c = 3$ LL result.

logarithms significantly reduce the gap fraction $R(Q_0)$ in the low-energy regime in comparison to the fixed-order prediction (black line). Secondly, after including the NLL corrections, the width of the scale uncertainty band decreases by a factor of two, which represents a significant increase in precision.

4.2 Gap fraction in Z production

As a first hadron-collider application, we consider $pp \to Z \to \ell^+\ell^-$ [219] and compute the cross section for a gap around the incoming beam, centered at the rapidity of the electroweak boson, as considered in [115]. The hadron-collider analog of factorization formula (2.11) was given in [106,110]

$$\sigma(Q, Q_0) = \sum_{i,j=q,\bar{q},g} \int dx_1 dx_2 \sum_{m=m_0}^{\infty} \left\langle \boldsymbol{\mathcal{H}}_m(\{\underline{n}\}, Q, \mu) \otimes \boldsymbol{\mathcal{W}}_m(\{\underline{n}\}, Q_0, x_1, x_2, \mu) \right\rangle \tag{4.2}$$

where the hard function is the same as (2.10) describing the hard interaction initiated by the partons i and j. The quantity $\boldsymbol{\mathcal{W}}_m$ is the low-energy matrix element encoding all soft and collinear dynamics. The longitudinal momentum fractions are denoted by x_1 and x_2 and the sum over m takes into account the different partonic channels. In the large-N_c limit $\boldsymbol{\mathcal{W}}_m$ factorizes into parton distribution functions[5] (PDFs) convoluted with the partonic cross section and soft Wilson lines for the m partons. Therefore, most ingredients for the resummation carry over from the e^+e^- case. In

[5]Non-global hadron-collider cross sections at finite N_c involve super-leading logarithms due to Glauber phases [90, 110]. One might wonder whether the Glauber effects would lead to a breakdown of PDF factorization. Indeed, the papers [220, 221] suggest that even global observables (e.g. jet vetoes) would suffer from factorization-breaking effects due to Glauber gluons. Whether PDF factorization holds beyond inclusive Drell-Yan is an important open question for all of hadron collider physics, but beyond the scope of the present work.

particular, the RG evolution and the one-loop soft function can be directly obtained from our MC code. The only new elements are the hard real-emission corrections $\boldsymbol{\mathcal{H}}_3^{(1)}$. The hard functions are simply the partonic cross sections with their infrared singularities subtracted in the $\overline{\text{MS}}$ scheme, which are well known [222–224]. However, the literature assumes that an infrared safe observable is computed and simplifies the cross section results by integrating soft terms over the full angular region. These simplifications do not apply to the hard functions because the angular constraint in (2.10) restricts hard partons to the jet region, while contributions with partons inside the gap are part of the soft function. To avoid double counting, we need to restore the terms that were dropped in [222–224]. We will perform this calculation in the next section and provide explicit expressions for the hard functions in all partonic channels.

4.2.1 Hard matching corrections for Z production

In this section we derive the radiative corrections to the hard functions $\boldsymbol{\mathcal{H}}_3^{(1)}, \boldsymbol{\mathcal{H}}_2^{(1)}$ which can be obtained by a standard NLO QCD calculation [222–224] for the Drell-Yan process [219]. The production of a (virtual) color-singlet boson with invariant mass Q in hadron-hadron collisions at center-of-mass energy $\sqrt{s}$ occurs through the annihilation of quarks. More precisely, we study the process $N_1 + N_2 \to Z + X_{\text{had}}$, where N_1 and N_2 are the colliding hadrons (protons at the LHC) and X_{had} is an arbitrary hadronic final state. The hadron collider cross section can be expressed as a convolution of the partonic cross sections $\frac{d\hat{\sigma}_{ij}}{dQ^2}$ with PDFs $f_{i/N}(x,\mu_f)$

$$\frac{d\sigma}{dQ^2} = \sum_{i,j=q,\bar{q},g} \int dx_1 \int dx_2\, f_{i/N_1}(x_1,\mu_f)\, f_{j/N_2}(x_2,\mu_f)\, \sigma_0^q\, \frac{d\hat{\sigma}_{ij}}{dQ^2}\,. \tag{4.3}$$

For convenience, we have split off a prefactor

$$\sigma_0^q = \frac{4\pi^2\alpha}{N_c s} \sum_q \frac{|g_L^q|^2 + |g_R^q|^2}{2}\,, \tag{4.4}$$

which absorbs the electromagnetic coupling α as well as the left- and right-handed couplings $g_{L,R}$ of the Z to fermions. At NLO, each partonic channel only involves a single (anti-)quark flavor q. The explicit form of the couplings for different electroweak bosons can be found in [30]; for simplicity, we only consider Z production in the present work. The PDFs $f_{i/N}(x,\mu_f)$ are related to the probability of finding a parton i inside the hadron N with momentum fraction x, and μ_f is the factorization scale. In the center-of-mass frame, we parametrize the incoming hadron-momenta as $P_{1,2} = \frac{\sqrt{s}}{2}(1,0,0,\pm 1)$ which translates to, as usual, $p_1 = x_1 P_1$ and $p_2 = x_2 P_2$ at the partonic level. We find it useful to introduce the variables (see e.g. [25])

$$\tau = \frac{Q^2}{s}\,, \qquad z = \frac{Q^2}{\hat{s}} = \frac{\tau}{x_1 x_2}\,, \tag{4.5}$$

where $\hat{s} = (p_1+p_2)^2 = x_1 x_2 s$ denotes the center-of-mass energy squared in the partonic system. In addition, we also introduce the Mandelstam variable $\hat{t} = (p_1 - k)^2$, where k is the momentum of the final-state gluon or quark at NLO. Factoring out the electroweak prefactors as in (4.3), the partonic cross section can be written in terms of hard scattering kernels C_{ij}

$$\frac{d\hat{\sigma}_{ij}}{dQ^2} = \int \mathrm{d}\Pi_f\, |\mathcal{M}_{ij}|^2\, \delta\Big(z - \tfrac{Q^2}{\hat{s}}\Big) = \int_\tau^1 dz \int_0^1 dy\, C_{ij}(z,y,Q,\mu_f)\, \delta\Big(z - \tfrac{Q^2}{\hat{s}}\Big)\,, \tag{4.6}$$

with $y = 1 + \frac{\hat{t}}{\hat{s}+Q^2}$, which is related to the scattering angle θ in the partonic center-of-mass frame through $\cos\theta = 2y - 1$. We have written the phase space of the final-state particles $\mathrm{d}\Pi_f$ in terms of

y, z and Q. The hard scattering kernels C_{ij} are expanded perturbatively in α_s. At leading order, i.e. α_s^0, only the $q\bar{q}$ channel contributes. In contrast, at NLO the inelastic qg channel opens up (of course, together with the directly related $\bar{q}q$, $\bar{q}g$, gq and $g\bar{q}$ channels). After combining real and virtual corrections and performing the collinear factorization, we obtain the LO and NLO hard scattering kernels in the $\overline{\text{MS}}$ scheme

$$\begin{aligned}
C_{q\bar{q}} &= \delta(1-z)\,\tfrac{\delta(y)+\delta(1-y)}{2}\left[1+\frac{\alpha_s}{4\pi}\,C_F\left(8\zeta_2-16-6\ln\tfrac{\mu_f^2}{Q^2}\right)\right] \\
&\quad+\frac{\alpha_s}{4\pi}\,C_F\left[2\big(\delta(y)+\delta(1-y)\big)\left(4\Big[\tfrac{\ln(1-z)}{1-z}\Big]_+-2\,(1+z)\ln(1-z)-\tfrac{(1+z^2)}{1-z}\ln(z)\right.\right. \\
&\qquad\left.+1-z-(1+z^2)\Big[\tfrac{1}{1-z}\Big]_+\ln\tfrac{\mu_f^2}{Q^2}\right) \\
&\qquad\left.+2\left((1+z^2)\Big[\tfrac{1}{1-z}\Big]_+\left(\Big[\tfrac{1}{y}\Big]_+-\Big[\tfrac{1}{1-y}\Big]_+\right)-2\,(1-z)\right)\right] \\
&\quad+\frac{\alpha_s}{4\pi}\,C_F\,\delta(1-z)\left[2\zeta_2\,\big(\delta(y)+\delta(1-y)\big)+2\left(\tfrac{\ln(1-y)}{y}+\tfrac{\ln(y)}{1-y}+\Big[\tfrac{\ln(y)}{y}\Big]_+-\Big[\tfrac{\ln(1-y)}{1-y}\Big]_+\right)\right. \\
&\qquad\left.-2\ln\tfrac{\mu_h^2}{Q^2}\left(\Big[\tfrac{1}{y}\Big]_+-\Big[\tfrac{1}{1-y}\Big]_+\right)\right], \qquad (4.7)
\end{aligned}$$

$$\begin{aligned}
C_{qg} &= \frac{\alpha_s}{4\pi}\,T_F\left[2\,\delta(y)\,\left(\big(z^2+(1-z)^2\big)\ln\Big(\tfrac{(1-z)^2}{z}\Big)+2z(1-z)-\big(z^2+(1-z)^2\big)\ln\tfrac{\mu_f^2}{Q^2}\right)\right. \\
&\qquad\left.+2\left(\big(z^2+(1-z)^2\big)\Big[\tfrac{1}{y}\Big]_+-2z(1-z)+(1-z)^2\,y\right)\right]. \qquad (4.8)
\end{aligned}$$

The remaining channels can be reconstructed from these results. Using the fact that (4.3) is independent on the factorization scale, we may derive the dependence on μ_f in (4.7) and (4.8), since the PDFs obey the DGLAP evolution equations [225–227]. As pointed out in the main text, the expressions for partonic cross sections are usually simplified by integrating soft contributions over all angles. In our case, this concerns the terms in the last two lines of (4.7), which can be written in compact form as

$$\Delta\hat{\sigma}_{q\bar{q}}=\frac{C_F\,\alpha_s}{2\pi}\,\delta(1-z)\left\{\Big[\tfrac{\ln((1-y)\,y)}{(1-y)\,y}\Big]_+-\ln\tfrac{\mu_h^2}{Q^2}\Big[\tfrac{1}{(1-y)\,y}\Big]_+\right\}. \qquad (4.9)$$

These terms were omitted in [223] since they integrate to zero in perturbative predictions for infrared-safe observables. However, we use the partonic cross section to construct the hard functions (2.10) in the factorization theorem and due to the restriction $\Theta_{\text{in}}(\{\underline{n}\})$ in (2.10) also the $\delta(1-z)$ terms are only integrated over the jet region. The part of the cross section where the gluon is inside the gap is included in the soft function and integrating the terms (4.9) in the hard function over the full angle would lead to a double counting. The terms in the last line of (4.7) depend on the renormalization scale which we denote by μ_h, since the above partonic cross sections will be part of the hard function. For the same reason, the coupling $\alpha_s \equiv \alpha_s(\mu_h)$ is evaluated at this scale.

We now want to use the results (4.7) and (4.8) for the calculation of the angular convolutions of the hard and soft functions. This is done in close analogy to the dijet case. For the hard

matching corrections, we need the one-loop corrections to the hard function $\boldsymbol{\mathcal{H}}_2$, together with the leading-order hard function $\boldsymbol{\mathcal{H}}_3$ in the combination

$$\frac{\alpha_s}{4\pi}\Delta^{(1)} = \frac{\alpha_s}{4\pi}\big\langle \boldsymbol{\mathcal{H}}_2^{(1)} \otimes \boldsymbol{\mathcal{S}}_2^{\mathrm{LL}}(t) + \boldsymbol{\mathcal{H}}_3^{(1)} \otimes \boldsymbol{\mathcal{S}}_3^{\mathrm{LL}}(t)\big\rangle\,, \tag{4.10}$$

where the LL soft functions include the evolution from the hard to the soft scale

$$\boldsymbol{\mathcal{S}}_m^{\mathrm{LL}}(t) = \sum_k \boldsymbol{U}_{mk}(t_0 = 0, t) \hat{\otimes} \mathbf{1}\,, \tag{4.11}$$

and the leading-order soft functions are trivial. The symbol $\hat{\otimes}$ indicates the integration over the directions of the additional partons generated during the evolution.

For the hard function $\boldsymbol{\mathcal{H}}_2$, the angular convolution in (4.10) is trivial since the two incoming partons are along the beam directions. For the function $\boldsymbol{\mathcal{H}}_3$, a single nontrivial angular integral remains, corresponding to the angle of the emitted final-state particle with respect to the beam axis. We parameterize this angle in the variable y so that we have

$$\begin{aligned}\Delta^{(1)} &= \big\langle \boldsymbol{\mathcal{H}}_2^{(1)}(z)\, \boldsymbol{\mathcal{S}}_2(t) + \int_0^1 dy\, \boldsymbol{\mathcal{H}}_3^{(1)}(y,z)\, \boldsymbol{\mathcal{S}}_3(y,t)\big\rangle \\ &= \int_0^1 dy \left[\tfrac{\delta(y)+\delta(1-y)}{2}\, \boldsymbol{\mathcal{H}}_2^{(1)}(z) + \boldsymbol{\mathcal{H}}_3^{(1)}(y,z)\right] \boldsymbol{\mathcal{S}}_3(y,t)\,,\end{aligned} \tag{4.12}$$

where we use that the soft function $\boldsymbol{\mathcal{S}}_3(y,t)$ reduces to the two-parton soft function when the emitted parton is along the beam direction, i.e. $\boldsymbol{\mathcal{S}}_3(1,t) = \boldsymbol{\mathcal{S}}_3(0,t) = \boldsymbol{\mathcal{S}}_2(t)$. The soft functions $\boldsymbol{\mathcal{S}}_3(y,t)$ are computed by starting the LL shower with an appropriate three-parton configuration.

The advantage of combining the real and virtual corrections in (4.12) is that the combined hard functions are directly related to the partonic amplitudes given above. For example, for the $q\bar{q}$ channel, we have

$$\tfrac{\delta(y)+\delta(1-y)}{2}\, \boldsymbol{\mathcal{H}}_{2,q\bar{q}}(z) + \boldsymbol{\mathcal{H}}_{3,q\bar{q}}(y,z) = \sigma_0^q\, C_{q\bar{q}}(z,y)\, \Theta_{\mathrm{in}}(y,z)\,, \tag{4.13}$$

where we express the in-jet constraint $\Theta_{\mathrm{in}}(y,z)$ through the partonic variables y and z. For a gap around the rapidity of the Z-boson, we have

$$\Theta_{\mathrm{in}}(y,z) = \theta\Big(|Y| - Y_{\mathrm{max}}\Big)\,, \tag{4.14}$$

where

$$Y = \frac{1}{2}\ln\frac{\hat{y}}{1-\hat{y}}\,, \qquad \text{with} \qquad \hat{y} = \frac{y(y(1-z)+z)}{1-2(1-y)y(1-z)}\,. \tag{4.15}$$

The quark-gluon channel is not present at the lowest order, so that

$$\boldsymbol{\mathcal{H}}_{3,qg}(y,z) = \sigma_0^q\, C_{qg}(z,y)\, \Theta_{\mathrm{in}}(y,z)\,. \tag{4.16}$$

For this process, we calculate the soft functions $\boldsymbol{\mathcal{S}}_3^{qg}(y,t), \boldsymbol{\mathcal{S}}_3^{q\bar{q}}(y,t)$ numerically via LL evolution for a grid of y values. In practice, we generate a value of y, corresponding to a three-particle event where the real emission is inside the jet cones, and shower this configuration. Repeating this procedure for multiple values of y we obtain a grid. We then interpolate linearly in both variables y, t and evaluate the convolution with the partonic amplitudes. The integrations in y, z as well as x_i are performed using VEGAS [228, 229]. To simplify the matching to fixed order, we compute the order α_s corrections to the hard and soft functions for $N_c = 3$. This approach is different than the slicing scheme we used in the dijet case. The main advantage of using interpolation

grids it to avoid a dependence on the slicing parameter, thus preventing potentially large power corrections on the slicing parameter. However, as soon as one changes a parameter, for example the gap size, it is necessary to create a new grid which is cumbersome. In the future, it seems that the most convenient choice would be to introduce a subtraction scheme so that each real event is automatically associated with its counter-event, thus regularising the IR divergences from real emissions.

4.2.2 Numerical results

In the right plot of Figure 4.1 we show our numerical results for the gap fraction (3.113). We work at $\sqrt{s} = 13.6$ TeV and use the NNPDF23_nlo_as_0119_qed [230] set and associated α_s. We again use the LL results of [85] at full color and match to fixed order. We note that the result of [85] does not account for complex phase terms in the anomalous dimension (2.55). These cancel for e^+e^- but are present for hadron colliders and lead to double logarithms at higher orders [90]. However, for Z production the effect of these so-called super-leading logarithms is strongly suppressed and numerically below the percent level [110]. For the same gap size $\Delta Y = \ln(3) \approx 1.1$, we see a similar behavior as in the e^+e^- case, see Figure 4.1. To study the effect of large logarithms on the fixed-order expansion, we increase the center-of-mass energy Q to 1 TeV and the gap size $\Delta Y = 2$. Once the hierarchy between Q and Q_0 is large, it is unclear how the renormalization and factorization scales μ_r and μ_f should be chosen in the fixed-order result. In the left plot of Figure 4.2 we compare the perturbative predictions for a high value $\mu = \mu_f = \mu_r = 1\,\text{TeV}$ (solid black line) and for the choice $\mu = Q_0$ (dashed black line). The difference in the two predictions is an inherent uncertainty in the fixed-order result. The dynamical scale $\mu = Q_0$ leads to better overall agreement with the resummed result, but also to an unphysical negative cross section at low Q_0. In our effective field theory approach, each part is evaluated at its natural scale. On the right side of Figure 4.2 we show the LL as well as the NLL results, both obtained in the large-N_c limit. In all cases, we observe that at low Q_0 the NLL effects are around 20% and are within the large LL uncertainty band. As expected, the scale uncertainty is greatly reduced at NLL.

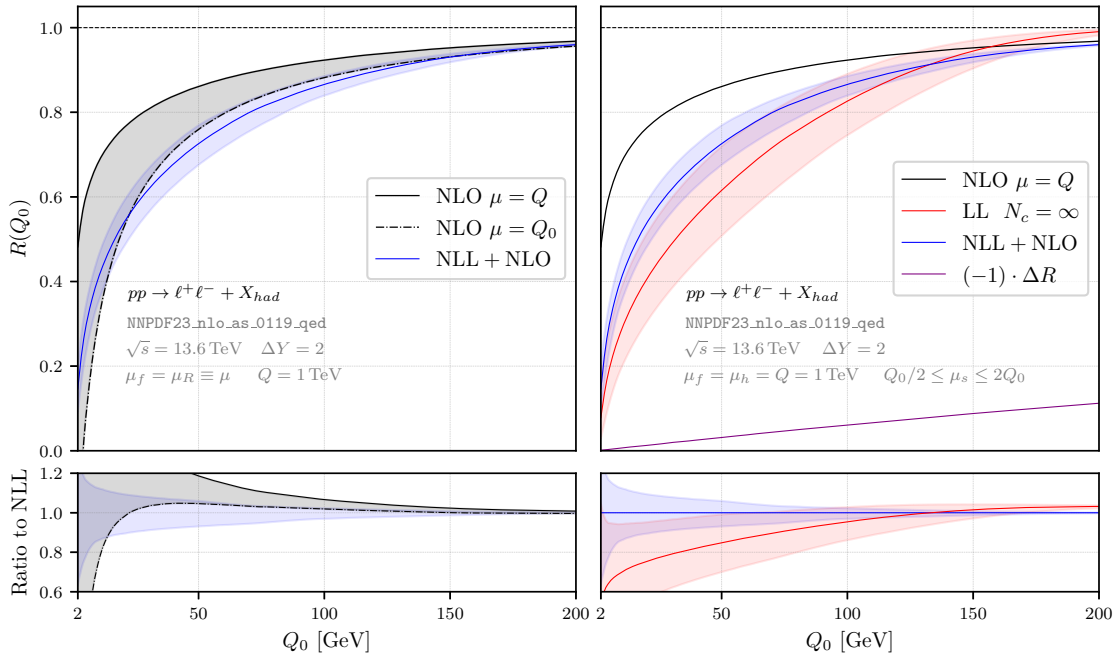

Figure 4.2: Fixed-order predictions for different scale choices (left) and resummed results at LL and NLL (right) for the value $Q = 1\,\text{TeV}$.

Chapter 5

Conclusions and outlook

This project is very easy [...] all you need to do is the Monte Carlo implementation.

— Thomas Becher, *an optimistic supervisor*

Starting from a factorization theorem obtained in soft-collinear effective theory and its associated RG equations, the objective of this thesis was to resum non-global logarithms at NLL accuracy. According to the factorization formula (2.11), there are three distinct contributions at subleading accuracy that are necessary to resum the full set of NLL corrections. Hard and soft matching corrections as well as contributions from the two-loop anomalous dimension to the running.

While first results for matching corrections were available in [107], the inclusion of the two-loop anomalous dimension in the renormalization-group evolution only became conceivable once analytical results for this quantity were presented in [123]. An earlier result for this quantity [97] contained many ingredients but not in the $\overline{\text{MS}}$ scheme relevant to our case. The main achievement of this thesis is the implementation of the two-loop anomalous dimension into the dedicated large-N_c parton shower framework Marzili. In practice, we augment the LL implementation [106, 108] with precisely one insertion of the two-loop anomalous dimension. A single insertion of $\mathbf{\Gamma}^{(2)}$ is sufficient since contributions from $\mathbf{\Gamma}^{(2)}$ are supressed by α_s. More precisely, we start a LL shower from a certain particle configuration which runs until an intermediate scale, where we evaluate $\mathbf{\Gamma}^{(2)}$, and subsequently restart a LL shower. Throughout the evolution, additional particles are generated. In this way, we are able to resum the full set of next-to-leading non-global logarithms for jet observables, such as the interjet energy flow in dijet production at lepton colliders.

We validate our implementation by comparing predictions for the energy flow into a rapidity slice around the thrust axis with results from Gnole [148] and PanScales [142]. The results, independently obtained using entirely different frameworks, are in agreement within statistical and systematic uncertainties. This provides a strong cross-check on our implementation.

As a first hadron collider application, we resum the next-to-leading non-global logarithms in $pp \to Z \to l^+l^-$. We veto radiation in a gap outside the beam region. The gap is centered around the rapidity of the electroweak boson. The shower evolution is the same as for e^+e^-, the only additional ingredients to the resummation are the relevant NLO hard functions, which we extract analytically. In the future, these should be extracted from existing fixed-order codes. The simple non-global observables computed here can serve as benchmark results for the development of general-purpose parton showers at subleading, i.e. (N)NLL, accuracy [127–132]. On the experimental side, it would be interesting to measure a gap fraction in Z-boson production to study how large non-global logarithms turn out to be for fiducial phase-space constraints. Experimentally, it is problematic to

decrease the veto energy Q_0 for the leading jet in the gap below 20 GeV. This is due to an increase of the background noise and a lower detector sensitivity. As a result, the ratio between the soft and hard scale might not be large enough for non-global effects to become manifestly dominant. A possibility to increase this scale ratio would be to explore Drell-Yan events at high center-of-mass energies. In addition, it would be interesting to see how widely used general-purpose parton showers, e.g. Pythia [124], which do not capture non-global logarithms entirely [231], compare to our theoretical prediction and experimental data.

Our result is a first step concerning the resummation of non-global observables at hadron colliders and there are several interesting extensions of this work. Moving forward, it would be interesting to insert the two-loop anomalous dimension a second time during the evolution, as a first step towards exponentiation. In principle, this is possible with the current implementation since we would modify the second LL shower in (2.102) to also contain an insertion of $\mathbf{\Gamma}^{(2)}$. Since these corrections are suppressed by $\alpha_s(\mu_h)$, they are expected to be numerically small in comparison to the results we obtained in this work. One concern when increasing the number of insertions of the two-loop anomalous dimension is the numerical stability of the angular integrals. Increasing the statistics to obtain a stable result may be necessary, which would require a more efficient implementation. It seems plausible that porting some parts of the code onto GPUs to make use of the highly concurrent infrastructure would achieve a significant speed-up [232].

Another interesting line of research would be to apply our framework to the invariant-mass distribution of jets and extend previously obtained results [107] to full NNLL accuracy. The jet mass distribution has been measured at the Large Electron-Positron collider, however, the typical jet mass is relatively low which means that the distribution is sensitive to hadronic contributions. Nevertheless, it is an interesting observable to study, since it may be used at hadron colliders to extract α_s [233]. The factorization theorem for this observable is known [98] and the matching corrections can be obtained by slightly modifying our implementation for the interjet energy flow [107]. While for the gap fraction only soft logarithms arise, the situation is more complicated for the distribution of the jet mass because collinear emissions are another source of large logarithms. On the technical side, it will be necessary to subtract collinear contributions from the anomalous dimension and exponentiate these separately. The collinear logarithm yields a double-logarithmic contribution so that the leading non-global logarithms start at NLL accuracy. Therefore, by including the two-loop anomalous dimension in the evolution, one will obtain NNLL results. Our formalism is well-suited to address this problem.

An observable of phenomenological interest with sensitivity to non-global logarithms is photon production [234]. To distinguish experimentally between photons produced in hard scattering processes and photons originating from other sources, it is necessary to isolate photons. In practice, this is done similarly as in the gap fraction, but instead of restricting the energy in a central region, the energy of additional radiation inside a cone around photons is restricted to a fraction ϵ_γ of the photon energy. As a consequence of these isolation requirements, a twofold pattern of logarithms arises. We obtain enhancements proportional to $\ln \epsilon_\gamma$ and $\ln R$, where R is the opening radius of the isolation cone. The logarithms in $\ln \epsilon_\gamma$ are non-global and can be resummed using the parton shower framework presented in this thesis. One of the missing analytical ingredients to resum subleading logarithms are the NLO corrections in α_s to the jet function. These contributions can be extracted by studying higher-order splitting functions, representing the analog to hard matching corrections in gap fractions. The logarithms $\ln R$ are obtained by solving a DGLAP-like evolution equation for the fragmentation function. To improve the resummation accuracy regarding the $\ln R$ terms, it is necessary to calculate higher-order splitting kernels. We believe that these can be extracted from the corresponding QCD splitting functions. Once the subleading logarithms in R

and ϵ_γ have been resummed, the result should be matched to existing state-of-the-art fixed-order NNLO computations for photon production with realistic isolation criteria [235].

Phenomenologically interesting examples of more complicated observables include $H+\text{jets}$ production with a veto on additional jets in $pp \to H \to W^+W^-$. Experimental analyses typically divide the data into exclusive jet bins because the background-to-signal ratio changes considerably with the number of jets present. The jet veto is imposed to reduce the background from top-quark pair production with subsequent decay into bottom jets. Since the p_T^{veto} cut is very stringent, large logarithms in terms of $\ln \frac{m_H}{p_T^{\text{veto}}}$ deteriorate the cross section. While non-global logarithms are power-suppressed in the zero-jet bin [106], as soon as one distinct jet is present jet-veto cross sections are genuinely non-global. Treating the zero-jet bin as a global observable, the large logarithms have been resummed up to N^3LL [34–36, 43, 44]. Starting from the one-jet bin, there is a non-global $\ln \frac{p_T^{\text{jet}}}{p_T^{\text{veto}}}$ logarithm present, which should be resummed even though its size was estimated in [236] to be at the level of a few percent. However, this estimate is not based on a full factorization theorem for $H+\text{jets}$, hence, it should be used with caution.

Higgs-boson production from vector-boson fusion with a jet veto for central rapidities is another process where non-global logarithms should definitely be investigated. To suppress background, experiments impose large rapidity gaps which implies that the final-state jets are widely separated and in different hemispheres. By imposing a veto on the energy of additional radiation in the central region between the final-state jets, we anticipate sizable non-global contributions, in particular to the gluon-induced background. The main challenge to resum subleading logarithms is the calculation of the hard functions. To get the hard functions for VBF, we would use the structure-function approach [237]. Having analytical expressions would help to investigate the possibility of extracting hard functions from existing fixed-order codes, e.g. MadGraph [238] or MCFM [239], thereby automating the calculation of the hard functions. As the first application of this automatized extraction procedure, we would calculate the hard functions for the gluon-induced background. Combined with one-loop corrections to the soft function and contributions due to the running of the two-loop anomalous dimension, we would get the subleading non-global logarithms.

A limitation in our framework is the strict large-N_c limit. As a result, we are unable to capture contributions due to Glauber exchanges in non-global observables. While these so-called super-leading logarithms [90] vanish in e^+e^- initiated processes, they may become relevant for $2 \to 2$ scattering processes at hadron colliders [110, 193]. An open problem is to account for multiple soft emissions which build up the non-global nature. It is certainly possible to perform multiple insertions of the anomalous dimension numerically at full color, however, higher-order insertions are only feasible numerically. Even though there are efforts to develop a parton shower at finite color [199] and first numerical results exist [88], so far Glauber contributions have not been implemented. Perhaps the most promising approach would be to include the Glauber exchanges at full color in our framework and treat subsequent soft emissions using our large-N_c parton shower. We believe that our formalism is suitable to obtain the leading contributions numerically and we are looking forward to working on that.

To conclude, this monograph represents an important milestone concerning the resummation of jet observables using effective field theory techniques. More than two decades after the leading non-global logarithms have been resummed, we finally achieved NLL accuracy, the new state-of-the-art for non-global observables. This accomplishment culminates nearly a decade of work [94, 95, 106–108, 123], demonstrating the significant development made in this field. The results and insights obtained here, pave the way for future precision studies at colliders.

Bibliography

[1] T. Becher, N. Schalch and X. Xu, *Resummation of Next-to-Leading Nonglobal Logarithms at the LHC*, *Phys. Rev. Lett.* **132** (2024) 081602 [2307.02283].

[2] S.L. Glashow, *Partial Symmetries of Weak Interactions*, *Nucl. Phys.* **22** (1961) 579.

[3] S. Weinberg, *A Model of Leptons*, *Phys. Rev. Lett.* **19** (1967) 1264.

[4] A. Salam, *Weak and Electromagnetic Interactions*, *Conf. Proc. C* **680519** (1968) 367.

[5] G. 't Hooft and M.J.G. Veltman, *Regularization and Renormalization of Gauge Fields*, *Nucl. Phys. B* **44** (1972) 189.

[6] F. Englert and R. Brout, *Broken Symmetry and the Mass of Gauge Vector Mesons*, *Phys. Rev. Lett.* **13** (1964) 321.

[7] P. Higgs, *Broken symmetries, massless particles and gauge fields*, *Physics Letters* **12** (1964) 132.

[8] P.W. Higgs, *Broken Symmetries and the Masses of Gauge Bosons*, *Phys. Rev. Lett.* **13** (1964) 508.

[9] P.W. Anderson, *Plasmons, Gauge Invariance, and Mass*, *Phys. Rev.* **130** (1963) 439.

[10] G.S. Guralnik, C.R. Hagen and T.W.B. Kibble, *Global Conservation Laws and Massless Particles*, *Phys. Rev. Lett.* **13** (1964) 585.

[11] T.W.B. Kibble, *Symmetry breaking in non-abelian gauge theories*, *Phys. Rev.* **155** (1967) 1554.

[12] CDF collaboration, *High-precision measurement of the W boson mass with the CDF II detector*, *Science* **376** (2022) 170.

[13] Muon g-2 collaboration, *Measurement of the Positive Muon Anomalous Magnetic Moment to 0.20 ppm*, *Phys. Rev. Lett.* **131** (2023) 161802 [2308.06230].

[14] T. Aoyama, N. Asmussen, M. Benayoun, J. Bijnens, T. Blum, M. Bruno et al., *The anomalous magnetic moment of the muon in the Standard Model*, *Phys. Rept.* **887** (2020) 1 [2006.04822].

[15] D.J. Gross and F. Wilczek, *Ultraviolet Behavior of Nonabelian Gauge Theories*, *Phys. Rev. Lett.* **30** (1973) 1343.

[16] H.D. Politzer, *Reliable Perturbative Results for Strong Interactions?*, *Phys. Rev. Lett.* **30** (1973) 1346.

[17] A. Banfi, G.P. Salam and G. Zanderighi, *Principles of general final-state resummation and automated implementation*, *JHEP* **03** (2005) 073 [hep-ph/0407286].

[18] S. Catani, G. Turnock, B.R. Webber and L. Trentadue, *Thrust distribution in e^+e^- annihilation*, *Phys. Lett. B* **263** (1991) 491.

[19] A. Banfi, H. McAslan, P.F. Monni and G. Zanderighi, *A general method for the resummation of event-shape distributions in e^+e^- annihilation*, *JHEP* **05** (2015) 102

[1412.2126].

[20] A. Banfi, H. McAslan, P.F. Monni and G. Zanderighi, *The two-jet rate in e^+e^- at next-to-next-to-leading-logarithmic order*, *Phys. Rev. Lett.* **117** (2016) 172001 [1607.03111].

[21] A. Banfi, B.K. El-Menoufi and P.F. Monni, *The Sudakov radiator for jet observables and the soft physical coupling*, *JHEP* **01** (2019) 083 [1807.11487].

[22] G. Bozzi, S. Catani, D. de Florian and M. Grazzini, *The q_T spectrum of the Higgs boson at the LHC in QCD perturbation theory*, *Phys. Lett. B* **564** (2003) 65 [hep-ph/0302104].

[23] T. Becher and M. Neubert, *Threshold resummation in momentum space from effective field theory*, *Phys. Rev. Lett.* **97** (2006) 082001 [hep-ph/0605050].

[24] T. Becher, M. Neubert and B.D. Pecjak, *Factorization and Momentum-Space Resummation in Deep-Inelastic Scattering*, *JHEP* **01** (2007) 076 [hep-ph/0607228].

[25] T. Becher, M. Neubert and G. Xu, *Dynamical Threshold Enhancement and Resummation in Drell-Yan Production*, *JHEP* **07** (2008) 030 [0710.0680].

[26] T. Becher and M.D. Schwartz, *A precise determination of α_s from LEP thrust data using effective field theory*, *JHEP* **07** (2008) 034 [0803.0342].

[27] V. Ahrens, T. Becher, M. Neubert and L.L. Yang, *Renormalization-Group Improved Prediction for Higgs Production at Hadron Colliders*, *Eur. Phys. J. C* **62** (2009) 333 [0809.4283].

[28] C.F. Berger, C. Marcantonini, I.W. Stewart, F.J. Tackmann and W.J. Waalewijn, *Higgs Production with a Central Jet Veto at NNLL+NNLO*, *JHEP* **04** (2011) 092 [1012.4480].

[29] R. Abbate, M. Fickinger, A.H. Hoang, V. Mateu and I.W. Stewart, *Thrust at N^3LL with Power Corrections and a Precision Global Fit for $\alpha_s(m_Z)$*, *Phys. Rev. D* **83** (2011) 074021 [1006.3080].

[30] T. Becher and M. Neubert, *Drell-Yan Production at Small q_T, Transverse Parton Distributions and the Collinear Anomaly*, *Eur. Phys. J. C* **71** (2011) 1665 [1007.4005].

[31] I.W. Stewart, F.J. Tackmann and W.J. Waalewijn, *The Beam Thrust Cross Section for Drell-Yan at NNLL Order*, *Phys. Rev. Lett.* **106** (2011) 032001 [1005.4060].

[32] A. Banfi, M. Dasgupta and S. Marzani, *QCD predictions for new variables to study dilepton transverse momenta at hadron colliders*, *Phys. Lett. B* **701** (2011) 75 [1102.3594].

[33] T. Becher, C. Lorentzen and M.D. Schwartz, *Resummation for W and Z production at large p_T*, *Phys. Rev. Lett.* **108** (2012) 012001 [1106.4310].

[34] A. Banfi, G.P. Salam and G. Zanderighi, *NLL+NNLO predictions for jet-veto efficiencies in Higgs-boson and Drell-Yan production*, *JHEP* **06** (2012) 159 [1203.5773].

[35] T. Becher and M. Neubert, *Factorization and NNLL Resummation for Higgs Production with a Jet Veto*, *JHEP* **07** (2012) 108 [1205.3806].

[36] A. Banfi, P.F. Monni, G.P. Salam and G. Zanderighi, *Higgs and Z-boson production with a jet veto*, *Phys. Rev. Lett.* **109** (2012) 202001 [1206.4998].

[37] T. Becher, C. Lorentzen and M.D. Schwartz, *Precision Direct Photon and W-Boson Spectra at High p_T and Comparison to LHC Data*, *Phys. Rev. D* **86** (2012) 054026 [1206.6115].

[38] H.X. Zhu, C.S. Li, H.T. Li, D.Y. Shao and L.L. Yang, *Transverse-momentum resummation for top-quark pairs at hadron colliders*, *Phys. Rev. Lett.* **110** (2013) 082001 [1208.5774].

[39] T. Becher and G. Bell, *NNLL Resummation for Jet Broadening*, *JHEP* **11** (2012) 126 [1210.0580].

[40] T. Becher, M. Neubert and D. Wilhelm, *Higgs-Boson Production at Small Transverse*

Momentum, *JHEP* **05** (2013) 110 [1212.2621].

[41] Z.-B. Kang, X. Liu, S. Mantry and J.-W. Qiu, *Probing nuclear dynamics in jet production with a global event shape*, *Phys. Rev. D* **88** (2013) 074020 [1303.3063].

[42] D. Kang, C. Lee and I.W. Stewart, *Using 1-Jettiness to Measure 2 Jets in DIS 3 Ways*, *Phys. Rev. D* **88** (2013) 054004 [1303.6952].

[43] T. Becher, M. Neubert and L. Rothen, *Factorization and N^3LL_p+NNLO predictions for the Higgs cross section with a jet veto*, *JHEP* **10** (2013) 125 [1307.0025].

[44] I.W. Stewart, F.J. Tackmann, J.R. Walsh and S. Zuberi, *Jet p_T resummation in Higgs production at NNLL'+NNLO*, *Phys. Rev. D* **89** (2014) 054001 [1307.1808].

[45] T. Becher, G. Bell, C. Lorentzen and S. Marti, *Transverse-momentum spectra of electroweak bosons near threshold at NNLO*, *JHEP* **02** (2014) 004 [1309.3245].

[46] Z.-B. Kang, X. Liu and S. Mantry, *1-jettiness DIS event shape: NNLL+NLO results*, *Phys. Rev. D* **90** (2014) 014041 [1312.0301].

[47] S. Catani, M. Grazzini and A. Torre, *Transverse-momentum resummation for heavy-quark hadroproduction*, *Nucl. Phys. B* **890** (2014) 518 [1408.4564].

[48] A.H. Hoang, D.W. Kolodrubetz, V. Mateu and I.W. Stewart, *C-parameter distribution at N^3LL' including power corrections*, *Phys. Rev. D* **91** (2015) 094017 [1411.6633].

[49] T. Becher, R. Frederix, M. Neubert and L. Rothen, *Automated NNLL + NLO resummation for jet-veto cross sections*, *Eur. Phys. J. C* **75** (2015) 154 [1412.8408].

[50] S. Alioli, C.W. Bauer, C. Berggren, F.J. Tackmann and J.R. Walsh, *Drell-Yan production at NNLL'+NNLO matched to parton showers*, *Phys. Rev. D* **92** (2015) 094020 [1508.01475].

[51] T. Becher, X. Garcia i Tormo and J. Piclum, *Next-to-next-to-leading logarithmic resummation for transverse thrust*, *Phys. Rev. D* **93** (2016) 054038 [1512.00022].

[52] C. Frye, A.J. Larkoski, M.D. Schwartz and K. Yan, *Precision physics with pile-up insensitive observables*, 1603.06375.

[53] M.A. Ebert, J.K.L. Michel and F.J. Tackmann, *Resummation Improved Rapidity Spectrum for Gluon Fusion Higgs Production*, *JHEP* **05** (2017) 088 [1702.00794].

[54] W. Bizon, P.F. Monni, E. Re, L. Rottoli and P. Torrielli, *Momentum-space resummation for transverse observables and the Higgs $p_\perp$ at N^3LL+NNLO*, *JHEP* **02** (2018) 108 [1705.09127].

[55] Z. Tulipánt, A. Kardos and G. Somogyi, *Energy–energy correlation in electron–positron annihilation at NNLL + NNLO accuracy*, *Eur. Phys. J. C* **77** (2017) 749 [1708.04093].

[56] J.K.L. Michel, P. Pietrulewicz and F.J. Tackmann, *Jet Veto Resummation with Jet Rapidity Cuts*, *JHEP* **04** (2019) 142 [1810.12911].

[57] W. Bizoń, X. Chen, A. Gehrmann-De Ridder, T. Gehrmann, N. Glover, A. Huss et al., *Fiducial distributions in Higgs and Drell-Yan production at N^3LL+NNLO*, *JHEP* **12** (2018) 132 [1805.05916].

[58] M. Procura, W.J. Waalewijn and L. Zeune, *Joint resummation of two angularities at next-to-next-to-leading logarithmic order*, *JHEP* **10** (2018) 098 [1806.10622].

[59] X. Chen, T. Gehrmann, E.W.N. Glover, A. Huss, Y. Li, D. Neill et al., *Precise QCD Description of the Higgs Boson Transverse Momentum Spectrum*, *Phys. Lett. B* **788** (2019) 425 [1805.00736].

[60] T. Becher and M. Hager, *Event-Based Transverse Momentum Resummation*, *Eur. Phys. J. C* **79** (2019) 665 [1904.08325].

[61] G. Lustermans, J.K.L. Michel, F.J. Tackmann and W.J. Waalewijn, *Joint two-dimensional resummation in q_T and 0-jettiness at NNLL*, *JHEP* **03** (2019) 124 [1901.03331].

[62] W. Bizon, A. Gehrmann-De Ridder, T. Gehrmann, N. Glover, A. Huss, P.F. Monni et al., *The transverse momentum spectrum of weak gauge bosons at $N^3LL+NNLO$*, *Eur. Phys. J. C* **79** (2019) 868 [1905.05171].

[63] S. Alioli, A. Broggio, S. Kallweit, M.A. Lim and L. Rottoli, *Higgsstrahlung at $NNLL'+NNLO$ matched to parton showers in GENEVA*, *Phys. Rev. D* **100** (2019) 096016 [1909.02026].

[64] M.A. Ebert, J.K.L. Michel, I.W. Stewart and F.J. Tackmann, *Drell-Yan q_T resummation of fiducial power corrections at N^3LL*, *JHEP* **04** (2021) 102 [2006.11382].

[65] T. Becher and T. Neumann, *Fiducial q_T resummation of color-singlet processes at $N^3LL+NNLO$*, *JHEP* **03** (2021) 199 [2009.11437].

[66] M.A. Ebert, B. Mistlberger and G. Vita, *The Energy-Energy Correlation in the back-to-back limit at N^3LO and N^3LL'*, *JHEP* **08** (2021) 022 [2012.07859].

[67] S. Alioli, A. Broggio, A. Gavardi, S. Kallweit, M.A. Lim, R. Nagar et al., *Next-to-next-to-leading order event generation for Z boson pair production matched to parton shower*, *Phys. Lett. B* **818** (2021) 136380 [2103.01214].

[68] G. Billis, B. Dehnadi, M.A. Ebert, J.K.L. Michel and F.J. Tackmann, *Higgs p_T Spectrum and Total Cross Section with Fiducial Cuts at Third Resummed and Fixed Order in QCD*, *Phys. Rev. Lett.* **127** (2021) 072001 [2102.08039].

[69] S. Camarda, L. Cieri and G. Ferrera, *Drell-Yan lepton-pair production: q_T resummation at N^3LL accuracy and fiducial cross sections at N^3LO*, *Phys. Rev. D* **104** (2021) L111503 [2103.04974].

[70] T. Neumann, *The diphoton q_T spectrum at $N^3LL'+NNLO$*, *Eur. Phys. J. C* **81** (2021) 905 [2107.12478].

[71] S. Alioli, A. Broggio and M.A. Lim, *Zero-jettiness resummation for top-quark pair production at the LHC*, *JHEP* **01** (2022) 066 [2111.03632].

[72] X. Chen, T. Gehrmann, E.W.N. Glover, A. Huss, P.F. Monni, E. Re et al., *Third-Order Fiducial Predictions for Drell-Yan Production at the LHC*, *Phys. Rev. Lett.* **128** (2022) 252001 [2203.01565].

[73] C. Duhr, B. Mistlberger and G. Vita, *Four-Loop Rapidity Anomalous Dimension and Event Shapes to Fourth Logarithmic Order*, *Phys. Rev. Lett.* **129** (2022) 162001 [2205.02242].

[74] T. Neumann and J. Campbell, *Fiducial Drell-Yan production at the LHC improved by transverse-momentum resummation at $N^4LL' + N^3LO$*, *Phys. Rev. D* **107** (2023) L011506 [2207.07056].

[75] J.M. Campbell, R.K. Ellis, T. Neumann and S. Seth, *Transverse momentum resummation at $N^3LL+NNLO$ for diboson processes*, *JHEP* **03** (2023) 080 [2210.10724].

[76] S. Alioli, G. Billis, A. Broggio, A. Gavardi, S. Kallweit, M.A. Lim et al., *Double Higgs production at NNLO interfaced to parton showers in GENEVA*, *JHEP* **06** (2023) 205 [2212.10489].

[77] J.M. Campbell, R.K. Ellis, T. Neumann and S. Seth, *Jet-veto resummation at N^3LL_p+NNLO in boson production processes*, *JHEP* **04** (2023) 106 [2301.11768].

[78] S. Camarda, L. Cieri and G. Ferrera, *Drell-Yan lepton-pair production: q_T resummation at N^4LL accuracy*, *Phys. Lett. B* **845** (2023) 138125 [2303.12781].

[79] A. Gavardi, M.A. Lim, S. Alioli and F.J. Tackmann, *NNLO+PS W^+W^- production using*

jet veto resummation at NNLL′, *JHEP* **12** (2023) 069 [2308.11577].

[80] J. Campbell and T. Neumann, *Third order QCD predictions for fiducial W-boson production*, *JHEP* **11** (2023) 127 [2308.15382].

[81] S. Alioli, G. Bell, G. Billis, A. Broggio, B. Dehnadi, M.A. Lim et al., *N^3LL resummation of one-jettiness for Z-boson plus jet production at hadron colliders*, *Phys. Rev. D* **109** (2024) 094009 [2312.06496].

[82] M. Dasgupta and G.P. Salam, *Resummation of non-global QCD observables*, *Phys. Lett. B* **512** (2001) 323 [hep-ph/0104277].

[83] M. Dasgupta and G.P. Salam, *Accounting for coherence in interjet E_t flow: A Case study*, *JHEP* **03** (2002) 017 [hep-ph/0203009].

[84] A. Banfi, G. Marchesini and G. Smye, *Away from jet energy flow*, *JHEP* **08** (2002) 006 [hep-ph/0206076].

[85] Y. Hatta and T. Ueda, *Resummation of non-global logarithms at finite N_c*, *Nucl. Phys. B* **874** (2013) 808 [1304.6930].

[86] Y. Hagiwara, Y. Hatta and T. Ueda, *Hemisphere jet mass distribution at finite N_c*, *Phys. Lett. B* **756** (2016) 254 [1507.07641].

[87] Y. Hatta and T. Ueda, *Non-global logarithms in hadron collisions at $N_c = 3$*, *Nucl. Phys. B* **962** (2021) 115273 [2011.04154].

[88] M. De Angelis, J.R. Forshaw and S. Plätzer, *Resummation and Simulation of Soft Gluon Effects beyond Leading Color*, *Phys. Rev. Lett.* **126** (2021) 112001 [2007.09648].

[89] H. Weigert, *Non-global jet evolution at finite N_c*, *Nucl. Phys. B* **685** (2004) 321 [hep-ph/0312050].

[90] J.R. Forshaw, A. Kyrieleis and M.H. Seymour, *Super-leading logarithms in non-global observables in QCD*, *JHEP* **08** (2006) 059 [hep-ph/0604094].

[91] J. Forshaw, J. Keates and S. Marzani, *Jet vetoing at the LHC*, *JHEP* **07** (2009) 023 [0905.1350].

[92] R.M. Duran Delgado, J.R. Forshaw, S. Marzani and M.H. Seymour, *The dijet cross section with a jet veto*, *JHEP* **08** (2011) 157 [1107.2084].

[93] M.D. Schwartz and H.X. Zhu, *Non-global logarithms at three loops, four loops, five loops, and beyond*, *Phys. Rev. D* **90** (2014) 065004 [1403.4949].

[94] T. Becher, M. Neubert, L. Rothen and D.Y. Shao, *Effective Field Theory for Jet Processes*, *Phys. Rev. Lett.* **116** (2016) 192001 [1508.06645].

[95] T. Becher, M. Neubert, L. Rothen and D.Y. Shao, *Factorization and Resummation for Jet Processes*, *JHEP* **11** (2016) 019 [1605.02737].

[96] A.J. Larkoski, I. Moult and D. Neill, *Non-Global Logarithms, Factorization, and the Soft Substructure of Jets*, *JHEP* **09** (2015) 143 [1501.04596].

[97] S. Caron-Huot, *Resummation of non-global logarithms and the BFKL equation*, *JHEP* **03** (2018) 036 [1501.03754].

[98] T. Becher, B.D. Pecjak and D.Y. Shao, *Factorization for the light-jet mass and hemisphere soft function*, *JHEP* **12** (2016) 018 [1610.01608].

[99] D. Neill, *The Asymptotic Form of Non-Global Logarithms, Black Disc Saturation, and Gluonic Deserts*, *JHEP* **01** (2017) 109 [1610.02031].

[100] S. Caron-Huot and M. Herranen, *High-energy evolution to three loops*, *JHEP* **02** (2018) 058 [1604.07417].

[101] A.J. Larkoski, I. Moult and D. Neill, *The Analytic Structure of Non-Global Logarithms: Convergence of the Dressed Gluon Expansion*, *JHEP* **11** (2016) 089 [1609.04011].

[102] Y. Hatta, E. Iancu, A.H. Mueller and D.N. Triantafyllopoulos, *Resumming double non-global logarithms in the evolution of a jet*, *JHEP* **02** (2018) 075 [1710.06722].

[103] T. Becher, R. Rahn and D.Y. Shao, *Non-global and rapidity logarithms in narrow jet broadening*, *JHEP* **10** (2017) 030 [1708.04516].

[104] R. Ángeles Martínez, M. De Angelis, J.R. Forshaw, S. Plätzer and M.H. Seymour, *Soft gluon evolution and non-global logarithms*, *JHEP* **05** (2018) 044 [1802.08531].

[105] D. Neill, *Non-Global and Clustering Effects for Groomed Multi-Prong Jet Shapes*, *JHEP* **02** (2019) 114 [1808.04897].

[106] M. Balsiger, T. Becher and D.Y. Shao, *Non-global logarithms in jet and isolation cone cross sections*, *JHEP* **08** (2018) 104 [1803.07045].

[107] M. Balsiger, T. Becher and D.Y. Shao, *NLL′ resummation of jet mass*, *JHEP* **04** (2019) 020 [1901.09038].

[108] M. Balsiger, T. Becher and A. Ferroglia, *Resummation of non-global logarithms in cross sections with massive particles*, *JHEP* **09** (2020) 029 [2006.00014].

[109] S. Caletti, O. Fedkevych, S. Marzani, D. Reichelt, S. Schumann, G. Soyez et al., *Jet angularities in Z+jet production at the LHC*, *JHEP* **07** (2021) 076 [2104.06920].

[110] T. Becher, M. Neubert and D.Y. Shao, *Resummation of Super-Leading Logarithms*, *Phys. Rev. Lett.* **127** (2021) 212002 [2107.01212].

[111] F.A. Dreyer, G.P. Salam and G. Soyez, *The Lund Jet Plane*, *JHEP* **12** (2018) 064 [1807.04758].

[112] M. Dasgupta, F.A. Dreyer, K. Hamilton, P.F. Monni, G.P. Salam and G. Soyez, *Parton showers beyond leading logarithmic accuracy*, *Phys. Rev. Lett.* **125** (2020) 052002 [2002.11114].

[113] K. Hamilton, R. Medves, G.P. Salam, L. Scyboz and G. Soyez, *Colour and logarithmic accuracy in final-state parton showers*, *JHEP* **03** (2021) 041 [2011.10054].

[114] M. van Beekveld, S. Ferrario Ravasio, G.P. Salam, A. Soto-Ontoso, G. Soyez and R. Verheyen, *PanScales parton showers for hadron collisions: formulation and fixed-order studies*, *JHEP* **11** (2022) 019 [2205.02237].

[115] M. van Beekveld, S. Ferrario Ravasio, K. Hamilton, G.P. Salam, A. Soto-Ontoso, G. Soyez et al., *PanScales showers for hadron collisions: all-order validation*, *JHEP* **11** (2022) 020 [2207.09467].

[116] M. van Beekveld and S.F. Ravasio, *Next-to-leading-logarithmic PanScales showers for Deep Inelastic Scattering and Vector Boson Fusion*, 2305.08645.

[117] C.W. Bauer, S. Fleming and M.E. Luke, *Summing Sudakov logarithms in $B \to X_s\gamma$ in effective field theory.*, *Phys. Rev. D* **63** (2000) 014006 [hep-ph/0005275].

[118] C.W. Bauer, S. Fleming, D. Pirjol and I.W. Stewart, *An Effective field theory for collinear and soft gluons: Heavy to light decays*, *Phys. Rev. D* **63** (2001) 114020 [hep-ph/0011336].

[119] C.W. Bauer, D. Pirjol and I.W. Stewart, *Soft collinear factorization in effective field theory*, *Phys. Rev. D* **65** (2002) 054022 [hep-ph/0109045].

[120] C.W. Bauer, S. Fleming, D. Pirjol, I.Z. Rothstein and I.W. Stewart, *Hard scattering factorization from effective field theory*, *Phys. Rev. D* **66** (2002) 014017 [hep-ph/0202088].

[121] M. Beneke, A.P. Chapovsky, M. Diehl and T. Feldmann, *Soft collinear effective theory and*

heavy to light currents beyond leading power, *Nucl. Phys. B* **643** (2002) 431 [hep-ph/0206152].

[122] M. Beneke and T. Feldmann, *Multipole expanded soft collinear effective theory with non-abelian gauge symmetry*, *Phys. Lett. B* **553** (2003) 267 [hep-ph/0211358].

[123] T. Becher, T. Rauh and X. Xu, *Two-loop anomalous dimension for the resummation of non-global observables*, *JHEP* **08** (2022) 134 [2112.02108].

[124] C. Bierlich, S. Chakraborty, N. Desai, L. Gellersen, I. Helenius, P. Ilten et al., *A comprehensive guide to the physics and usage of PYTHIA 8.3*, *SciPost Phys. Codeb.* **2022** (2022) 8 [2203.11601].

[125] T. Gleisberg, S. Hoeche, F. Krauss, M. Schonherr, S. Schumann, F. Siegert et al., *Event generation with SHERPA 1.1*, *JHEP* **02** (2009) 007 [0811.4622].

[126] M. Bähr, S. Gieseke, M.A. Gigg, D. Grellscheid, K. Hamilton, O. Latunde-Dada et al., *Herwig++ Physics and Manual*, *Eur. Phys. J. C* **58** (2008) 639 [0803.0883].

[127] J.R. Forshaw, J. Holguin and S. Plätzer, *Building a consistent parton shower*, *JHEP* **09** (2020) 014 [2003.06400].

[128] Z. Nagy and D.E. Soper, *Summations of large logarithms by parton showers*, *Phys. Rev. D* **104** (2021) 054049 [2011.04773].

[129] Z. Nagy and D.E. Soper, *Summations by parton showers of large logarithms in electron-positron annihilation*, 2011.04777.

[130] F. Herren, S. Höche, F. Krauss, D. Reichelt and M. Schoenherr, *A new approach to color-coherent parton evolution*, *JHEP* **10** (2023) 091 [2208.06057].

[131] S. Höche, F. Krauss and D. Reichelt, *The Alaric parton shower for hadron colliders*, 2404.14360.

[132] C.T. Preuss, *A partitioned dipole-antenna shower with improved transverse recoil*, 2403.19452.

[133] M. Dasgupta, F.A. Dreyer, K. Hamilton, P.F. Monni and G.P. Salam, *Logarithmic accuracy of parton showers: a fixed-order study*, *JHEP* **09** (2018) 033 [1805.09327].

[134] D. Anderle, M. Dasgupta, B.K. El-Menoufi, J. Helliwell and M. Guzzi, *Groomed jet mass as a direct probe of collinear parton dynamics*, *Eur. Phys. J. C* **80** (2020) 827 [2007.10355].

[135] A. Karlberg, G.P. Salam, L. Scyboz and R. Verheyen, *Spin correlations in final-state parton showers and jet observables*, *Eur. Phys. J. C* **81** (2021) 681 [2103.16526].

[136] M. Dasgupta and B.K. El-Menoufi, *Dissecting the collinear structure of quark splitting at NNLL*, *JHEP* **12** (2021) 158 [2109.07496].

[137] K. Hamilton, A. Karlberg, G.P. Salam, L. Scyboz and R. Verheyen, *Soft spin correlations in final-state parton showers*, *JHEP* **03** (2022) 193 [2111.01161].

[138] R. Medves, A. Soto-Ontoso and G. Soyez, *Lund and Cambridge multiplicities for precision physics*, *JHEP* **10** (2022) 156 [2205.02861].

[139] R. Medves, A. Soto-Ontoso and G. Soyez, *Lund multiplicity in QCD jets*, *JHEP* **04** (2023) 104 [2212.05076].

[140] K. Hamilton, A. Karlberg, G.P. Salam, L. Scyboz and R. Verheyen, *Matching and event-shape NNDL accuracy in parton showers*, *JHEP* **03** (2023) 224 [2301.09645].

[141] M. van Beekveld and S. Ferrario Ravasio, *Next-to-leading-logarithmic PanScales showers for Deep Inelastic Scattering and Vector Boson Fusion*, *JHEP* **02** (2024) 001 [2305.08645].

[142] S. Ferrario Ravasio, K. Hamilton, A. Karlberg, G.P. Salam, L. Scyboz and G. Soyez,

Parton Showering with Higher Logarithmic Accuracy for Soft Emissions, *Phys. Rev. Lett.* **131** (2023) 161906 [2307.11142].

[143] M. van Beekveld, M. Dasgupta, B.K. El-Menoufi, J. Helliwell and P.F. Monni, *Collinear fragmentation at NNLL: generating functionals, groomed correlators and angularities*, *JHEP* **05** (2024) 093 [2307.15734].

[144] M. van Beekveld, M. Dasgupta, B.K. El-Menoufi, S. Ferrario Ravasio, K. Hamilton, J. Helliwell et al., *Introduction to the PanScales framework, version 0.1*, *SciPost Physics Codebases* (2024) [2312.13275].

[145] M. van Beekveld, M. Dasgupta, B.K. El-Menoufi, J. Helliwell, A. Karlberg and P.F. Monni, *Two-loop anomalous dimensions for small-R jet versus hadronic fragmentation functions*, 2402.05170.

[146] M. van Beekveld, M. Dasgupta, B.K. El-Menoufi, S.F. Ravasio, K. Hamilton, J. Helliwell et al., *A new standard for the logarithmic accuracy of parton showers*, 2406.02661.

[147] A. Banfi, F.A. Dreyer and P.F. Monni, *Next-to-leading non-global logarithms in QCD*, *JHEP* **10** (2021) 006 [2104.06416].

[148] A. Banfi, F.A. Dreyer and P.F. Monni, *Higher-order non-global logarithms from jet calculus*, *JHEP* **03** (2022) 135 [2111.02413].

[149] G. Sterman and S. Weinberg, *Jets from quantum chromodynamics*, *Phys. Rev. Lett.* **39** (1977) 1436.

[150] M. Dasgupta and G.P. Salam, *Event shapes in e+ e- annihilation and deep inelastic scattering*, *J. Phys. G* **30** (2004) R143 [hep-ph/0312283].

[151] P.E.L. Rakow and B.R. Webber, *Transverse Momentum Moments of Hadron Distributions in QCD Jets*, *Nucl. Phys. B* **191** (1981) 63.

[152] S. Catani, G. Turnock and B.R. Webber, *Jet broadening measures in e^+e^- annihilation*, *Phys. Lett. B* **295** (1992) 269.

[153] M. Stahlhofen. Private Communication, 2023.

[154] S. Catani, Y.L. Dokshitzer, M.H. Seymour and B.R. Webber, *Longitudinally invariant K_t clustering algorithms for hadron hadron collisions*, *Nucl. Phys. B* **406** (1993) 187.

[155] S.D. Ellis and D.E. Soper, *Successive combination jet algorithm for hadron collisions*, *Phys. Rev. D* **48** (1993) 3160 [hep-ph/9305266].

[156] M. Cacciari, G.P. Salam and G. Soyez, *The anti-k_t jet clustering algorithm*, *JHEP* **04** (2008) 063 [0802.1189].

[157] Y.L. Dokshitzer, G.D. Leder, S. Moretti and B.R. Webber, *Better jet clustering algorithms*, *JHEP* **08** (1997) 001 [hep-ph/9707323].

[158] M. Wobisch and T. Wengler, *Hadronization corrections to jet cross-sections in deep inelastic scattering*, in *Workshop on Monte Carlo Generators for HERA Physics (Plenary Starting Meeting)*, pp. 270–279, 4, 1998 [hep-ph/9907280].

[159] T. Becher and J. Haag, *Factorization and resummation for sequential recombination jet cross sections*, *JHEP* **01** (2024) 155 [2309.17355].

[160] S. Catani and L. Trentadue, *Resummation of the QCD perturbative series for hard processes*, *Nuclear Physics B* **327** (1989) 323.

[161] S. Catani, B. Webber and G. Marchesini, *QCD coherent branching and semi-inclusive processes at large χ*, *Nuclear Physics B* **349** (1991) 635.

[162] R.J. Hill and M. Neubert, *Spectator interactions in soft collinear effective theory*, *Nucl.*

Phys. B **657** (2003) 229 [hep-ph/0211018].

[163] T. Becher, A. Broggio and A. Ferroglia, *Introduction to Soft-Collinear Effective Theory*, vol. 896, Springer (2015), 10.1007/978-3-319-14848-9, [1410.1892].

[164] S. Catani and M.H. Seymour, *A General algorithm for calculating jet cross-sections in NLO QCD*, *Nucl. Phys. B* **485** (1997) 291 [hep-ph/9605323].

[165] R.N. Lee, A. von Manteuffel, R.M. Schabinger, A.V. Smirnov, V.A. Smirnov and M. Steinhauser, *Quark and Gluon Form Factors in Four-Loop QCD*, *Phys. Rev. Lett.* **128** (2022) 212002 [2202.04660].

[166] S. Catani, *The Singular behavior of QCD amplitudes at two loop order*, *Phys. Lett. B* **427** (1998) 161 [hep-ph/9802439].

[167] N. Kidonakis, G. Oderda and G.F. Sterman, *Evolution of color exchange in QCD hard scattering*, *Nucl. Phys. B* **531** (1998) 365 [hep-ph/9803241].

[168] G.F. Sterman and M.E. Tejeda-Yeomans, *Multiloop amplitudes and resummation*, *Phys. Lett. B* **552** (2003) 48 [hep-ph/0210130].

[169] R. Bonciani, S. Catani, M.L. Mangano and P. Nason, *Sudakov resummation of multiparton QCD cross-sections*, *Phys. Lett. B* **575** (2003) 268 [hep-ph/0307035].

[170] Y.L. Dokshitzer and G. Marchesini, *Soft gluons at large angles in hadron collisions*, *JHEP* **01** (2006) 007 [hep-ph/0509078].

[171] S.M. Aybat, L.J. Dixon and G.F. Sterman, *The Two-loop soft anomalous dimension matrix and resummation at next-to-next-to leading pole*, *Phys. Rev. D* **74** (2006) 074004 [hep-ph/0607309].

[172] L.J. Dixon, L. Magnea and G.F. Sterman, *Universal structure of subleading infrared poles in gauge theory amplitudes*, *JHEP* **08** (2008) 022 [0805.3515].

[173] T. Becher and M. Neubert, *Infrared singularities of scattering amplitudes in perturbative QCD*, *Phys. Rev. Lett.* **102** (2009) 162001 [0901.0722].

[174] E. Gardi and L. Magnea, *Factorization constraints for soft anomalous dimensions in QCD scattering amplitudes*, *JHEP* **03** (2009) 079 [0901.1091].

[175] T. Becher and M. Neubert, *On the Structure of Infrared Singularities of Gauge-Theory Amplitudes*, *JHEP* **06** (2009) 081 [0903.1126].

[176] L.J. Dixon, *Matter Dependence of the Three-Loop Soft Anomalous Dimension Matrix*, *Phys. Rev. D* **79** (2009) 091501 [0901.3414].

[177] L.J. Dixon, E. Gardi and L. Magnea, *On soft singularities at three loops and beyond*, *JHEP* **02** (2010) 081 [0910.3653].

[178] V. Del Duca, C. Duhr, E. Gardi, L. Magnea and C.D. White, *The Infrared structure of gauge theory amplitudes in the high-energy limit*, *JHEP* **12** (2011) 021 [1109.3581].

[179] S. Caron-Huot, *When does the gluon reggeize?*, *JHEP* **05** (2015) 093 [1309.6521].

[180] V. Ahrens, M. Neubert and L. Vernazza, *Structure of Infrared Singularities of Gauge-Theory Amplitudes at Three and Four Loops*, *JHEP* **09** (2012) 138 [1208.4847].

[181] O. Almelid, C. Duhr and E. Gardi, *Three-loop corrections to the soft anomalous dimension in multileg scattering*, *Phys. Rev. Lett.* **117** (2016) 172002 [1507.00047].

[182] O. Almelid, C. Duhr, E. Gardi, A. McLeod and C.D. White, *Bootstrapping the QCD soft anomalous dimension*, *JHEP* **09** (2017) 073 [1706.10162].

[183] T. Becher and M. Neubert, *Infrared singularities of QCD amplitudes with massive partons*, *Phys. Rev. D* **79** (2009) 125004 [0904.1021].

[184] A. Ferroglia, M. Neubert, B.D. Pecjak and L.L. Yang, *Two-loop divergences of scattering amplitudes with massive partons*, *Phys. Rev. Lett.* **103** (2009) 201601 [0907.4791].

[185] A. Ferroglia, M. Neubert, B.D. Pecjak and L.L. Yang, *Two-loop divergences of massive scattering amplitudes in non-abelian gauge theories*, *JHEP* **11** (2009) 062 [0908.3676].

[186] A. Mitov, G.F. Sterman and I. Sung, *The Massive Soft Anomalous Dimension Matrix at Two Loops*, *Phys. Rev. D* **79** (2009) 094015 [0903.3241].

[187] A. Mitov, G.F. Sterman and I. Sung, *Computation of the Soft Anomalous Dimension Matrix in Coordinate Space*, *Phys. Rev. D* **82** (2010) 034020 [1005.4646].

[188] Z.L. Liu and N. Schalch, *Infrared Singularities of Multileg QCD Amplitudes with a Massive Parton at Three Loops*, *Phys. Rev. Lett.* **129** (2022) 232001 [2207.02864].

[189] J.M. Henn, C. Milloy and K. Yan, *A new method for calculating the soft anomalous dimension matrix for massive particle scattering*, *JHEP* **04** (2024) 117 [2310.10145].

[190] S. Catani and M. Grazzini, *The soft gluon current at one loop order*, *Nucl. Phys. B* **591** (2000) 435 [hep-ph/0007142].

[191] C. Duhr and T. Gehrmann, *The two-loop soft current in dimensional regularization*, *Phys. Lett. B* **727** (2013) 452 [1309.4393].

[192] L.J. Dixon, E. Herrmann, K. Yan and H.X. Zhu, *Soft gluon emission at two loops in full color*, *JHEP* **05** (2020) 135 [1912.09370].

[193] T. Becher, M. Neubert, D.Y. Shao and M. Stillger, *Factorization of non-global LHC observables and resummation of super-leading logarithms*, *JHEP* **12** (2023) 116 [2307.06359].

[194] E. Remiddi and J.A.M. Vermaseren, *Harmonic polylogarithms*, *Int. J. Mod. Phys. A* **15** (2000) 725 [hep-ph/9905237].

[195] D. Maitre, *HPL, a mathematica implementation of the harmonic polylogarithms*, *Comput. Phys. Commun.* **174** (2006) 222 [hep-ph/0507152].

[196] D. Maitre, *Extension of HPL to complex arguments*, *Comput. Phys. Commun.* **183** (2012) 846 [hep-ph/0703052].

[197] C. Runge, *Über die numerische Auflösung von Differentialgleichungen*, *Mathematische Annalen* **46** (1895) 167.

[198] W. Kutta, *Beitrag zur Näherungsweisen Integration totaler Differentialgleichungen*, *Z. Math. Phys.* **46** (1901) .

[199] S. Plätzer and M. Sjodahl, *Subleading N_c improved Parton Showers*, *JHEP* **07** (2012) 042 [1201.0260].

[200] Z. Nagy and D.E. Soper, *Parton shower evolution with subleading color*, *JHEP* **06** (2012) 044 [1202.4496].

[201] Z. Nagy and D.E. Soper, *Effects of subleading color in a parton shower*, *JHEP* **07** (2015) 119 [1501.00778].

[202] S. Plätzer, M. Sjodahl and J. Thorén, *Color matrix element corrections for parton showers*, *JHEP* **11** (2018) 009 [1808.00332].

[203] Z. Nagy and D.E. Soper, *Parton showers with more exact color evolution*, *Phys. Rev. D* **99** (2019) 054009 [1902.02105].

[204] J.R. Forshaw, J. Holguin and S. Plätzer, *Parton branching at amplitude level*, *JHEP* **08** (2019) 145 [1905.08686].

[205] S. Höche and D. Reichelt, *Numerical resummation at subleading color in the strongly*

ordered soft gluon limit, *Phys. Rev. D* **104** (2021) 034006 [2001.11492].

[206] J. Holguin, J.R. Forshaw and S. Plätzer, *Comments on a new 'full colour' parton shower*, 2003.06399.

[207] J. Holguin, J.R. Forshaw and S. Plätzer, *Improvements on dipole shower colour*, *Eur. Phys. J. C* **81** (2021) 364 [2011.15087].

[208] A.S. Householder, *Unitary triangularization of a nonsymmetric matrix*, *J. ACM* **5** (1958) 339–342.

[209] M. Cacciari, F.A. Dreyer, A. Karlberg, G.P. Salam and G. Zanderighi, *Fully Differential Vector-Boson-Fusion Higgs Production at Next-to-Next-to-Leading Order*, *Phys. Rev. Lett.* **115** (2015) 082002 [1506.02660].

[210] T. Becher, P. Monni and N. Schalch, *A comparison of formalisms for non-global evolution,* in preparation, .

[211] S. Catani, D. de Florian, M. Grazzini and P. Nason, *Soft gluon resummation for Higgs boson production at hadron colliders*, *JHEP* **07** (2003) 028 [hep-ph/0306211].

[212] I. Balitsky, *Operator expansion for high-energy scattering*, *Nucl. Phys. B* **463** (1996) 99 [hep-ph/9509348].

[213] J. Jalilian-Marian, A. Kovner, A. Leonidov and H. Weigert, *The BFKL equation from the Wilson renormalization group*, *Nucl. Phys. B* **504** (1997) 415 [hep-ph/9701284].

[214] J. Jalilian-Marian, A. Kovner, A. Leonidov and H. Weigert, *The Wilson renormalization group for low x physics: Towards the high density regime*, *Phys. Rev. D* **59** (1998) 014014 [hep-ph/9706377].

[215] A. Kovner, J.G. Milhano and H. Weigert, *Relating different approaches to nonlinear QCD evolution at finite gluon density*, *Phys. Rev. D* **62** (2000) 114005 [hep-ph/0004014].

[216] E. Iancu, A. Leonidov and L.D. McLerran, *Nonlinear Gluon Evolution in the Color Glass Condensate: I*, *Nucl. Phys. A* **692** (2001) 583 [hep-ph/0011241].

[217] E. Iancu, A. Leonidov and L.D. McLerran, *The Renormalization Group Equation for the Color Glass Condensate*, *Phys. Lett. B* **510** (2001) 133 [hep-ph/0102009].

[218] E. Ferreiro, E. Iancu, A. Leonidov and L. McLerran, *Nonlinear Gluon Evolution in the Color Glass Condensate: II*, *Nucl. Phys. A* **703** (2002) 489 [hep-ph/0109115].

[219] S.D. Drell and T.-M. Yan, *Massive Lepton Pair Production in Hadron-Hadron Collisions at High-Energies*, *Phys. Rev. Lett.* **25** (1970) 316.

[220] J.R. Gaunt, *Glauber Gluons and Multiple Parton Interactions*, *JHEP* **07** (2014) 110 [1405.2080].

[221] M. Zeng, *Drell-Yan process with jet vetoes: breaking of generalized factorization*, *JHEP* **10** (2015) 189 [1507.01652].

[222] G. Altarelli, R.K. Ellis and G. Martinelli, *Large Perturbative Corrections to the Drell-Yan Process in QCD*, *Nucl. Phys. B* **157** (1979) 461.

[223] C. Anastasiou, L.J. Dixon, K. Melnikov and F. Petriello, *Dilepton rapidity distribution in the Drell-Yan process at NNLO in QCD*, *Phys. Rev. Lett.* **91** (2003) 182002 [hep-ph/0306192].

[224] C. Anastasiou, L.J. Dixon, K. Melnikov and F. Petriello, *High precision QCD at hadron colliders: Electroweak gauge boson rapidity distributions at NNLO*, *Phys. Rev. D* **69** (2004) 094008 [hep-ph/0312266].

[225] V.N. Gribov and L.N. Lipatov, e^+e^- *pair annihilation and deep inelastic ep scattering in*

perturbation theory, *Sov. J. Nucl. Phys.* **15** (1972) 675.

[226] Y.L. Dokshitzer, *Calculation of the Structure Functions for Deep Inelastic Scattering and e^+e^- Annihilation by Perturbation Theory in Quantum Chromodynamics*, *Sov. Phys. JETP* **46** (1977) 641.

[227] G. Altarelli and G. Parisi, *Asymptotic Freedom in Parton Language*, *Nucl. Phys. B* **126** (1977) 298.

[228] G.P. Lepage, *A New Algorithm for Adaptive Multidimensional Integration*, *J. Comput. Phys.* **27** (1978) 192.

[229] G.P. Lepage, *Adaptive multidimensional integration: VEGAS enhanced*, *J. Comput. Phys.* **439** (2021) 110386 [2009.05112].

[230] A. Buckley, J. Ferrando, S. Lloyd, K. Nordström, B. Page, M. Rüfenacht et al., *LHAPDF6: parton density access in the LHC precision era*, *Eur. Phys. J. C* **75** (2015) 132 [1412.7420].

[231] A. Banfi, G. Corcella and M. Dasgupta, *Angular ordering and parton showers for non-global QCD observables*, *JHEP* **03** (2007) 050 [hep-ph/0612282].

[232] M.H. Seymour and S. Sule, *An Algorithm to Parallelise Parton Showers on a GPU*, 2403.08692.

[233] H.S. Hannesdottir, A. Pathak, M.D. Schwartz and I.W. Stewart, *Prospects for strong coupling measurement at hadron colliders using soft-drop jet mass*, *JHEP* **04** (2023) 087 [2210.04901].

[234] T. Becher, S. Favrod and X. Xu, *QCD anatomy of photon isolation*, *JHEP* **01** (2023) 005 [2208.01554].

[235] X. Chen, T. Gehrmann, E.W.N. Glover, M. Höfer, A. Huss and R. Schürmann, *Single photon production at hadron colliders at NNLO QCD with realistic photon isolation*, *JHEP* **08** (2022) 094 [2205.01516].

[236] X. Liu and F. Petriello, *Reducing theoretical uncertainties for exclusive Higgs-boson plus one-jet production at the LHC*, *Phys. Rev. D* **87** (2013) 094027 [1303.4405].

[237] T. Han, G. Valencia and S. Willenbrock, *Structure function approach to vector boson scattering in p p collisions*, *Phys. Rev. Lett.* **69** (1992) 3274 [hep-ph/9206246].

[238] J. Alwall, R. Frederix, S. Frixione, V. Hirschi, F. Maltoni, O. Mattelaer et al., *The automated computation of tree-level and next-to-leading order differential cross sections, and their matching to parton shower simulations*, *JHEP* **07** (2014) 079 [1405.0301].

[239] J. Campbell and T. Neumann, *Precision Phenomenology with MCFM*, *JHEP* **12** (2019) 034 [1909.09117].

Acknowledgments

First and foremost, I would like to express my gratitude to my supervisor, Thomas Becher, for giving me the opportunity to work on this PhD project. Despite the numerous challenges we encountered, you always remained patient and motivated. I also thank you for letting me supervise Michael, who will become my successor. I am looking forward to continuing to collaborate with both of you. Most importantly, I am counting on you as a ski buddy during the next Moriond conference, don't forget that we still need to prepare a talk!

I would like to extend my gratitude to Pier Monni for engaging in a detailed comparison between our results. The two months you agreed to host me at CERN were a fantastic experience. Without you, the results presented in this thesis would still be utterly wrong.

I wish to thank all my collaborators for the countless discussions about particle physics during my PhD. In particular, thank you to Tim Engel, Sebastian Jaskiewicz, Ze Long Liu, Thomas Rauh, Yannick Ulrich, and Xiaofeng Xu for your patience and emotional support whenever needed.

I also thank Simone Alioli for accepting the position of external examiner of my thesis and Mikko Laine for chairing my defense.

Spending the last three and a half years at the Institute for Theoretical Physics at the University of Bern has been a pleasure. I am grateful to my fellow PhD students Sebastian Burri, Martina Cottini, Samuel Favrod, Simona Procacci and Elnaz Zyaee for the time spent together outside of the university. Special thanks should be given to Samuel Favrod, with whom I had the honor to share the journey.

I also thank my current office mates Dominik and Julian for the nice company. The GS building will remain forever in my memories.

To my friends from ETH, Bern and Les Paccots, thank you for the time we spent together either on holidays, climbing, skiing or playing the alphorn.

Finally, my heartfelt thanks go to my family for their unconditional support. To my parents, sister, and girlfriend, thank you for your understanding, patience, and encouragement throughout this long and challenging endeavor.

Declaration of consent

on the basis of Article 18 of the PromR Phil.-nat. 19

Name/First Name:	Schalch Nicolas François
Registration Number:	15-922-594
Study program:	Theoretical Physics, PhD
	Bachelor ☐ Master ☐ Dissertation ☒
Title of the thesis:	Resummation of Next-to-Leading Non-Global Logarithms
Supervisor:	Prof. Dr. Thomas Becher

I declare herewith that this thesis is my own work and that I have not used any sources other than those stated. I have indicated the adoption of quotations as well as thoughts taken from other authors as such in the thesis. I am aware that the Senate pursuant to Article 36 paragraph 1 litera r of the University Act of September 5th, 1996 and Article 69 of the University Statute of June 7th, 2011 is authorized to revoke the doctoral degree awarded on the basis of this thesis.
For the purposes of evaluation and verification of compliance with the declaration of originality and the regulations governing plagiarism, I hereby grant the University of Bern the right to process my personal data and to perform the acts of use this requires, in particular, to reproduce the written thesis and to store it permanently in a database, and to use said database, or to make said database available, to enable comparison with theses submitted by others.

Place/Date: Bern, 13.08.2024 Signature

Schalch Nicolas François